Dark matter indirect detection in gamma-rays

Celine Combet

Communauté
UNIVERSITÉ Grenoble Alpes

Mémoire

présenté pour obtenir le diplôme d'

HABILITATION À DIRIGER LES RECHERCHES

Spécialité : **Physique**

Présentée par

Céline COMBET

Docteur de l'Université de Paris XI
Chercheuse CNRS

préparée au **Laboratoire de Physique Subatomique et de Cosmologie**
École doctorale de physique

Dark matter indirect detection in γ-rays

HDR soutenue publiquement le 19/06/2018,
devant le jury composé de :

Pierre Antilogus
Directeur de recherche, Rapporteur
Corinne Bérat
Directrice de recherche, Examinatrice
Fiorenza Donato
Professeur, Rapporteur
Olivier Perdereau
Directeur de recherche, Rapporteur
Pierre Salati
Professeur, Président

Contents

Remerciements

Tout d'abord, un grand merci à Pierre Antilogus, Fiorenza Donato et Olivier Perdereau d'avoir rapporté cette HDR. Je remercie également chaleureusement Corinne Bérat d'avoir accepté de faire partie du jury et Pierre Salati de l'avoir présidé avec sa classe habituelle.

Au fil des années, beaucoup de personnes m'ont apporté soutien et gentillesse et ont contribué au fait que je présente aujourd'hui cette HDR. Je vais rester sur un registre professionnel, donc les amis, la famille, ne m'en voulez pas de ne pas apparaitre ici, mais je pense bien à vous aussi !

Merci à Jonathan pour son soutien et sa disponibilité depuis mon passage en ATER au LAOG et pour n'avoir jamais rechigné à envoyer des lettres de recommandation pour les concours, année après année, même en pleines vacances de Noël. For the same reasons, a big thank you to Graham, with whom I worked during my postdoc in Leicester. I'm also very grateful to the Theoretical Astrophysics Group at the University of Leicester for the freedom I was allowed there to start the work presented in this manuscript.

Je remercie très chaleureusement toute l'équipe Planck/NIKA du LPSC que j'ai rejointe à mon retour d'Angleterre. On aura rarement vu d'équipe plus bienveillante vis-à-vis de "ses jeunes" et j'ai eu beaucoup beaucoup de chance d'en faire partie. Une mention très spéciale pour Juan, le Jefe... Merci de ta gentillesse, de m'avoir formée à l'analyse de données (je partais vraiment de zéro !), de m'avoir poussée à présenter au Core Team HFI autant que possible et m'avoir permis d'avoir cette visibilité, si indispensable, au sein d'une grande collaboration. Un grand merci à Jean-Loup pour sa confiance et son soutien qui ont aussi beaucoup joué.

Depuis deux ans, je suis embarquée dans l'aventure LSST, toujours au LPSC ; je remercie chaleureusement notre directeur, Arnaud, d'avoir soutenu cette affectation avec enthousiasme. J'ai la chance de travailler avec des personnes aussi agréables que motivées : Dominique, Nicolas, Mariana, Cécile, Myriam, Aurélien, merci à vous ! Et merci à Laurent de sa grande sagesse et de nous avoir gentillement acceptées, moi et mes plantes, dans son bureau.

Avant de conclure, une petite mention spéciale pour Vincent et Moritz, tous deux doctorants sur la période 2013-2016. Ce fut un très grand plaisir de travailler avec eux autour du développement du code CLUMPY. De nombreux résultats présentés dans ce document n'ont été possibles que grâce à leur dur travail toujours effectué dans la bonne humeur ! Un grand merci à vous deux !

Et enfin un gigantesque merci à David, présent sur tous les fronts, sans qui la vie serait juste vachement moins bien. Merci pour tout.

Background information

This document focusses on the question of dark matter indirect detection, before opening on observational cosmology with LSST; I would first like to put this choice of topic into the general context of my research career and activities since my PhD defence. From a thematic point of view, I have followed anything but a linear path, with studies on various topics often led in parallel. While I value this diversity, which has given me a very broad view of the astronomy, astroparticle and cosmology communities and approaches, it also makes things a bit harder, especially when having to wrap everything up in fifty or so pages [1].

Research topics and selection for this document

I did my PhD at the Dublin Institute for Advanced Studies (DIAS) where the primary topic I pursued was that of the early stages of star formation. Cosmic-ray physics was also a topic of interest at DIAS and I also started, in parallel, a study of the ultra-heavy cosmic rays (UHCR), thanks to a European Ulysses/EGIDE grant we were awarded for exchanges between the Institut d'Astrophysique de Paris and DIAS.

After my PhD defence in 2006, I moved back to France, for a one-year research-teaching position (ATER) at the Laboratoire d'Astrophysique de l'Observatoire de Grenoble. I started working on the accretion-ejection process in TTauri stars, and more specifically on the structure of jet-emitting accretion discs and how it may affect subsequent planet formation. I then joined the Theoretical Astrophysics Group at the University of Leicester in 2007, to study the accretion-ejection process in another type of systems, namely X-ray binary stars. I worked on numerical simulations of this type of objects but also on evaluating the impact that a primordial population of high-mass X-ray binaries could have had on the reionization of the universe. It is during my time in Leicester that I also started getting involved in the topic of dark matter indirect detection (around 2010), a topic I still pursue today and the one I selected for this HDR. At that point, I had essentially been working on theoretical astrophysics topics, and dark matter indirect detection was a first shift towards the astroparticle community.

A second change came in 2011, when I moved back to Grenoble, for a postdoctoral position at the Laboratoire de Physique Subatomique et de Cosmologie (LPSC) where I joined the *Planck* group. It was a time of rush, with data pouring in and the collaboration getting ready for the first data release. Despite being a newbie, I was able to contribute to the 2013 results and data release, in great part thanks to the very favourable environment at LPSC. I focussed on component separation and diffuse foreground emission, working in particular on *internal linear combination* approaches. I was in charge of producing, validating and delivering the carbon monoxide (CO) map products. Later and finally more acquainted with the *Planck* data, I also largely contributed to the *Planck* polarisation release in 2015, while still coordinating and updating the CO-related results. A main feature of the 2015 polarisation release was a systematic effect termed intensity-to-polarisation leakage; any mismatch between detectors (zero level, gain, bandpass) translated into a fake polarisation signal during the map-making procedure. I was very involved in the team aiming at assessing and mitigating this spurious signals, and produced the leakage correction maps

1. Actually, I think this a very good thing that UGA suggests this limited number of pages for the manuscript!

that were eventually released among the 2015 *Planck* products. During that time, I also kept my involvement in DM indirect detection, although I was less 'elbow deep' in the subject as most of my time was dedicated to the *Planck* data analysis.

Finally, since my recruitment at CNRS in 2014 and the release of the 2015 *Planck* results, I have kept working on a few projects linked with indirect detection but also joined, around mid-2016, the 'LSST Dark Energy Science Collaboration'; this definitely is a new challenge. The LSST survey will start in 2021 and is scheduled to last ten years. While I have welcome the various changes of topics that have paced my academic career, part of it was circumstantial, driven by moving places every few years and adapting to whatever situation was there to be found. With LSST and my new-found stability, I now really look forward to contributing over the long run to such an exciting project but also to supervising PhD students willing to work in this field; I am hoping to do so within the next 2 years and this is the reason why I am presenting this HDR.

Interactions with undergraduate and graduate students

I have never had the official title of supervisor or co-supervisor of a PhD student. However I have had several opportunities to work directly with some PhD students, often providing directions and advices; I summarize these interactions below.

When I arrived in Leicester, Patrick Deegan (supervised by Graham Wynn) was starting his second year on the topic of X-ray binaries and accretion onto stellar mass black holes. After getting up to speed with this topic, that was central to my postdoctoral position there, I actively worked with Patrick, helped him in organising and writing his first paper and also played an active role when he wrote his dissertation, reading and correcting his manuscript. A year before I left, Gillian James started her PhD in the group, also under the supervision of Graham Wynn, I contributed in getting her started in her project.

During my time at LPSC, I have worked closely with Vincent Bonnivard who was doing his PhD (under the supervision of David Maurin) on DM indirect detection in dwarf spheroidal galaxies, following up on the work my collaborators and I initiated when I was in Leicester. Working with Vincent was a great experience and beyond our scientific collaboration and discussing directions for his work, I advised him on a day-to-day basis (e.g., writing articles, presentations, talk rehearsals). During that time, we also started working with Moritz Hütten, a PhD student at DESY (supervised by Gernot Maier), who was first interested in using the code we had developed for DM indirect detection, and with whom David Maurin and myself are still actively working. Aside from our collaboration *per se*, I (remotely) helped Moritz in prioritising his research, and also provided feedback and advices on article writing, presentations and job seeking.

In 2016, I supervised the end-of-year project of a master's student (M1), Antoine Lacroix, on a topic also linked to DM indirect detection. This was a 4 month project and even though it cannot compare to the investment, on both the student and supervisor's part, required for a PhD, this at least gave me a flavour of what it was to have the sole responsibility of someone's progress. I believe it was a good experience for the both of us, partly due to the fact that he was a remarkable student, learning fast and showing a lot of initiative, something quite rare at this level.

I have recently attended a 4-day class entitled "Management : cycle directeur de thèse", the goal of which is to provide us with the communication and support tools for successful PhD supervision. While I am very aware of the gap that may arise between theory and practice, I believe that having a set of good practice guidelines can only be beneficial.

Organisation of the document

The first outline of this document featured both indirect detection and *Planck*. However, trying to do so, it became quickly apparent that I could not do justice to both DM indirect detection and CMB cosmology in fifty pages. Then why choose DM indirect detection over CMB cosmology? The answer is twofold. First, as hinted above, my work in Planck was linked to quite technical topics, namely diffuse foreground component separation and to the control of the systematic effects in polarisation. While both are essential to extract the cosmological information from the Planck data, I thought they would make a more technical and drier read than indirect detection. Second, and more importantly, my somewhat longer experience in DM indirect detection means I have had more time to interact with and advise undergraduate and PhD students on this topic. This being a HDR, aimed at allowing me to supervise students in the future, this choice was the most relevant.

In the first part, I give an overview of the dark matter indirect detection in gamma-ray studies we have undertaken. After introducing the topic and some experimental highlights, I present the main features of the CLUMPY code, a code we have developed over the years for such studies and used to produce results in a variety of indirect detection targets. The latter include dark Galactic clumps, dwarf spheroidal galaxies, galaxy clusters and extragalactic emission that are discussed in turns. I close this first part with some perspectives on the modelling and experimental fronts.

The second part of the document is dedicated to my recent activity as part of the LSST/DESC collaboration. After briefly presenting the LSST project and its science goals and cosmological probes, I focus on cluster cosmology and my current involvement and work in the Clusters working group of the collaboration

After consideration, I opted for writing this document in English. There is no other reason than trying to speedup the writing process. I have already written a lot of material in English on the topic of dark matter indirect detection and would have found a translation exercise into French pointless.

Part I

Dark matter indirect detection in γ-rays

1

Introduction and the CLUMPY toolbox

Contents

Understanding the nature of dark matter is one of the main scientific challenges of contemporary physics. To that end, DM searches are performed on every possible fronts as scientists explore the possibility of: i) finding Beyond the Standard Model (BSM) physics and new particles at the Large Hadron Collider (LHC) facility at CERN (see, e.g., section 5 of Klasen et al. 2015); ii) witnessing the interaction of a DM particle with a nucleus of an underground detector for direct detection experiments (Agnese et al. 2015; Akerib et al. 2016); or iii) detecting the stable standard model particles produced by DM annihilation or decay as an excess over the expected astrophysical fluxes for indirect detection experiments.

The latter was pioneered by Gunn et al. (1978); Stecker (1978); Silk and Srednicki (1984); Silk and Bloemen (1987) who laid the foundations of DM indirect detection, being the first to establish that DM annihilation or decay could contribute to the measured fluxes of γ-rays and anti-protons. In the last thirty years, indirect detection has been developed in three different experimental flavours, depending on the end product under scrutiny:

- Anti-particles (anti-protons, anti-deuterons and positrons) constitute the indirect detection channels of charged cosmic-ray experiments such as PAMELA (Boezio et al. 2009) or AMS-02 (`http://www.ams02.org`). Let's mention the PAMELA positron excess (Adriani et al. 2009), confirmed since by the AMS-02 results (Aguilar et al. 2014), which has led to a lot of excitement and yielded hundreds of DM-oriented papers. A (more?) plausible astrophysical explanation could however lie in nearby pulsars (Profumo 2012) or in the cosmic-ray acceleration process itself (Blasi 2009).
- γ-rays is the other channel of choice, investigated by instruments such as Fermi-LAT or H.E.S.S., and it will be thoroughly described in this chapter.
- With the new window opened by the ANTARES and IceCube experiments, the neutrino channel is becoming an interesting new contender (e.g., Albert et al. 2017b; The ANTARES Collaboration 2015), even though the sensitivity is not yet sufficient to reach the limits obtained by the other two approaches.

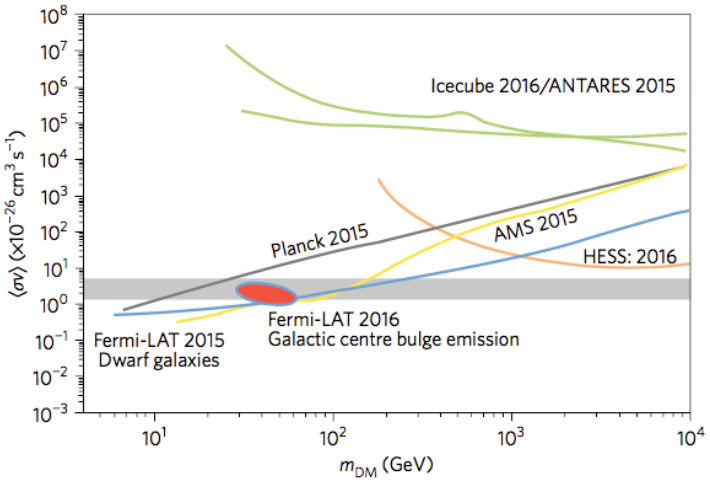

FIGURE 1.1: Current best DM indirect detection limits from the various possible DM annihilation products: i) γ-rays with *Fermi*-LAT (blue) and HESS (orange), ii) antiprotons from AMS-02 (yellow) and iii) neutrinos from IceCube and ANTARES (green). The red-filled blue ellipse corresponds to the *Fermi*-LAT Galactic centre excess when interpreted in terms of DM annihilation.The limit inferred from CMB measurements with *Planck* is also shown in dark grey. The grey band shows to the canonical value for the annihilation cross section $\langle\sigma v\rangle \approx 3 \times 10^{-26}$ cm^3 s^{-1}. See §1.1 for details. Figure taken from Conrad and Reimer (2017).

Figure 1.1, taken from the recent review by Conrad and Reimer (2017), summarises the state-of-the-art limits that are currently achieved by these various approaches, in terms of annihilation cross section versus DM candidate mass (see the formalism in §1.1.2). Below $\sim$ 100 GeV, *Fermi*-LAT γ-rays and AMS-02 antiprotons lead the race, yielding comparable limits. Above 1 TeV, γ-rays observed from the ground by H.E.S.S. give the most stringent constraints.

The figure also shows the limits obtained from the *Planck* CMB data. Indeed, DM annihilations in the primordial universe would inject energy into the plasma and impact the recombination history, leaving an imprint in the temperature and polarisation power spectra (Padmanabhan and Finkbeiner 2005). In Planck Collaboration et al. (2016b), the *Planck* temperature and polarisation data have been used, along with a cosmological model accounting for DM annihilations, to place the interesting limit shown as the grey solid line in figure 1.1. Closing this aside, the remaining of this document will focus solely on the γ-ray channel.

Indirect detection in the γ-ray channel is a topic I started to investigate in 2009-2010 during my postdoc in Leicester, in collaboration with David Maurin (working at the time in the H.E.S.S collaboration at LPNHE), Mark Wilkinson (Univ. of Leicester), and Jim Hinton who is working on the CTA project and who had just arrived in Leicester at the time. Initially a side project, this research topic has taken a larger part of my time as results and collaborations with junior and senior scientists grew. In §1.1, I first describe the formalism of indirect detection in γ-rays and give a summary of the main experimental results obtained in the last 10-15 years. Not being a member of any γ-ray experimental collaboration, my work in the field has been organised around the development of the CLUMPY code (§1.2), the goal of which is to allow for fast computations of the γ-ray exotic signal, under a wide variety of configurations. Using CLUMPY, we have studied the potential of many targets w.r.t indirect detection studies, namely dark Galactic clumps, dwarfs spheroidal galaxies, galaxy clusters and the extragalactic exotic background, that are described afterwards in §2.1, 2.2, 3.1, and 3.2.

1.1 Dark matter indirect detection in γ-rays

This entire chapter focusses on the astrophysical side of DM, i.e. on the ingredient and modelling required rather than on the DM candidates themselves; the latter are only briefly discussed in the paragraph below.

1.1.1 DM properties and candidates

Cosmological observations and structure formation and evolution studies give us the main properties that a DM candidate should have. It must be a non-baryonic collisionless fluid that interacts mainly gravitationally, and being *dark* means it cannot interact electromagnetically. A good candidate should be neutral and have a very small self-interaction cross section. It should be stable or with a lifetime at least that of the age of the universe. Finally, DM must be *cold*, i.e. non relativistic after its decoupling in the early universe, as a *hot* DM scenario yields a large DM free streaming scale that would have washed out the *small* scales density fluctuations and therefore prevented galaxy formation.

Despite its popularity and large success at explaining most observations, the CDM paradigm is somewhat challenged at subgalactic scales where observations do not match predictions of CDM simulations (missing satellite problem (Bullock 2010), too-big-to-fail problem (Boylan-Kolchin et al. 2011), core inner density profiles in dwarf spheroidal galaxies (Kaplinghat et al. 2016)). A lot of effort and cpu-hours are being spent to solve these issues by including baryonic physics into the simulations. Alternatively, the concept of self-interacting DM (SIDM) has raised the attention of the community in the last years as a possible solution (see Tulin and Yu 2017 for a review). In contrast to warm DM (WDM) made of sub-MeV particles also invoked in this context, SIDM could solve these tensions while at the same time preserving the remarkable successes of CDM. In any case, no known particle is a good DM candidate and alternatives are therefore being sought for in Beyond the Standard Model (BSM) theories.

To date, the most popular DM candidates are the WIMPs (Weakly Interacting Massive Particles) which naturally arise in supersymmetric extensions of the standard model (SUSY) or in extra dimension theories. WIMP candidates interact with standard matter through the weak force and gravity only, have typical masses in the $\sim$10 GeV – 10 TeV range, are naturally produced in the early universe, and after decoupling, yield the right amount of relic DM as measured today [1]. Given the typical WIMP masses, the photons produced from their annihilation or decay fall into the energy range covered by γ-ray astronomy (see §1.2.2.3). Non-WIMP DM candidates, such as axions or sterile neutrinos, have also been proposed and may be investigated in the X-ray regime instead.

1.1.2 Formalism

The expected exotic differential γ-ray flux at energy E from DM annihilation or decay, in the direction $\vec{k} = (\psi, \vartheta)$ and per solid angle $d\Omega$ reads

$$\frac{d\Phi}{dE\, d\Omega}(E, \vec{k}) = \frac{d\Phi^{\rm PP}}{dE}(E) \times \frac{dJ}{d\Omega}(\vec{k})\,. \tag{1.1}$$

1. This is often referred to as the *WIMP miracle*.

The particle physics term depends on whether the DM candidate annihilates or decays:

$$\frac{\mathrm{d}\Phi^{\mathrm{PP}}}{\mathrm{d}E}(E) = \frac{1}{4\pi}\sum_f \frac{dN^f_{\gamma,\nu}}{dE} B_f \times \begin{cases} \dfrac{\langle\sigma v\rangle}{m_\chi^2 \delta} & \text{(annihilation)} \\ \dfrac{1}{\tau\, m_\chi} & \text{(decay)}, \end{cases} \tag{1.2}$$

where m_χ is the mass of the DM particle, $\langle\sigma v\rangle$ is the velocity-averaged annihilation cross-section, τ is the decay lifetime, and dN^f_γ/dE and B_f correspond to the spectrum and branching ratio of annihilation channel f. The parameter δ is $\delta = 2$ for a Majorana and $\delta = 4$ for a Dirac particle. We will only consider the so-called *prompt* γ-ray emission that is produced at the location of the annihilation/decay process [2] from either i) the hadronization and subsequent decay of the reaction products yielding a γ-ray emission continuum; or ii) the direct $\gamma\gamma$ channel yielding a distinctive emission line (see §1.2.2.3). If detected, such a line would constitute a *smoking-gun* signature of DM annihilation/decay, but it comes from a one-loop process and is therefore suppressed.

The second term in Eq. (1.1) is the astrophysical factor J and is generically written as

$$J(\vec{k}) = \int_0^{2\pi}\int_0^{\theta_{\mathrm{int}}}\int_{\mathrm{l.o.s}} \begin{cases} \rho^2(\vec{k};\, l,\, \theta,\, \phi) dl\, \sin\theta\, d\theta\, d\phi & \text{(annihilation)} \\ \rho(\vec{k};\, l,\, \theta,\, \phi) dl\, \sin\theta\, d\theta\, d\phi & \text{(decay)}\ , \end{cases} \tag{1.3}$$

where the DM density ρ is integrated along the line of sight (l.o.s.), and up to a maximum angular distance θ_{int}. Its evaluation depends on the more or less informed choice one can make for the DM distribution, and this question is central to the work my collaborators and I have been pursuing.

Inverting Eq. (1.1) allows us to express $\langle\sigma v\rangle$ or τ as a function of the DM particle mass. In the absence of a γ-ray signal, and after estimating the J-factor and choosing the annihilation (resp. decay) channels, exclusion limits in the $\langle\sigma v\rangle - m_\chi$ (resp. $\tau - m_\chi$) plane may be determined. For DM annihilation, these upper limits are generally compared to the canonical value $\langle\sigma v\rangle \approx 3\times10^{-26}$ cm^3 s^{-1} that would explain the DM relic density observed today (e.g, figure 1.1). This procedure is at the core of the indirect detection approach but requires several important prerequisites to yield robust limits on the DM candidates:

- a thorough understanding of instrumental sensitivity, effects and systematics;
- a careful estimation of the astrophysical (i.e. non-exotic) γ-ray background in the target, if such background is expected;
- a robust determination of the J-factors of the target.

All three points are equally important but handled differently by the various research teams and it is therefore not unusual to find conflicting results or interpretations in the literature. This is exemplified in the next section, which presents an overview of experimental results to date.

1.1.3 Experimental highlights in the last decade

In the last ten years or so, γ-ray astronomy has known two great advances with the Large Area Telescope (LAT) on-board the *Fermi* space telescope (Atwood et al. 2009), direct successor of EGRET (Hartman et al. 1992), and the opening of the TeV window thanks to ground-based

2. Added to the prompt emission, electrons and positrons from DM annihilation will produce multi-wavelength emissions through a variety of processes (synchrotron, Bremsstrahlung, etc.), including hard X-ray/soft γ-ray emission from inverse Compton scattering of the ambient radiation field (CMB, star light). We have not included this component in our calculations so far, but are considering it as a future development of the CLUMPY code (§1.2).

Imaging Atmospheric Cherenkov Telescopes (IACTs) such as H.E.S.S. (Hinton and the HESS Collaboration 2004), MAGIC (Cortina et al. 2009) or VERITAS (Holder et al. 2006). While *Fermi*-LAT provides a fullsky survey of the γ-ray emission in the 20 MeV−300 GeV energy range, IACTs operate typically between $\sim$ 100 GeV and 100 TeV and rely on pointed observations.

Gamma-rays (and neutrinos) propagate in straight lines. This brings to the forth the notion of targets for indirect detection [3]. Given that the exotic annihilation γ-ray flux roughly goes as the DM density squared over the distance squared, the best targets are dense and/or close by. Ideally, they would also be free of astrophysical background to ease the exotic interpretation of a signal. In this context, the Galactic centre, dwarf spheroidal galaxies (dSphs) orbiting the Milky Way, dark Galactic clumps and galaxy clusters have been widely studied by the aforementioned instruments and collaborations. I have organised the overview of experimental results in the last few years around these targets, ordered from the smallest to the largest structures.

Dark Galactic clumps. These are the DM halos at the lower end of the mass range, with masses as low as 10^{-11} – 10^{-6} $M_\odot$ (Green et al. 2004; Bringmann 2009), and are expected to be present throughout the Milky Way's DM halo. Not massive enough to have retained gas and formed stars (hence *dark*), they are not expected to possess any astrophysical γ-ray emission and could therefore be identified as sources of exotic γ-rays, with no counterpart at other wavelengths. *Fermi*-LAT data have been used by various authors to perform such analyses. The Fermi collaboration, in 2012, using the first LAT source catalogue (1FGL), reported $\langle\sigma v\rangle \lesssim 10^{-24}$ cm^{-3} s^{-1} for 100 GeV WIMP candidate annihilating in the $b\bar{b}$ channel (Ackermann et al. 2012). Recent studies, using the latest 3FGL catalogue typically find $\langle\sigma v\rangle \lesssim 10^{-26} - 10^{-25}$ cm^{-3} s^{-1} (Bertoni et al. 2015; Schoonenberg et al. 2016; Mirabal et al. 2016) for the same channel. Current IACTs are pointed instruments and, in this context, can only perform follow-up observations of LAT-discovered unassociated sources (e.g., Nieto Castaño 2011). This could change with the extragalactic survey envisioned for the future Cherenkov Telescope Array (CTA) (Dubus et al. 2013), that would allow us to place limits from dark clumps (non-)detection, similarly to what has already been done with *Fermi*-LAT data; this is what I will further describe in §2.1.

Dwarf spheroidal galaxies. Conversely to dark clumps, these DM halos are massive enough to have formed stars and be identified as dwarf galaxies orbiting the MW. They are among the prime targets for indirect detection thanks to i) their significant DM content as suggested by the dynamics of member stars, ii) the absence of γ-ray astrophysical background and iii) their proximity to Earth (with typical distances between 20-100s kpc). Dwarf spheroidal galaxies have been widely studied using both *Fermi*-LAT data and IACTs. To date, the best limits come from stacked dSph analyses, such as performed by the *Fermi*-LAT collaboration, reaching $\langle\sigma v\rangle \lesssim 3 \times 10^{-26}$ cm^3 s^{-1} below 100 GeV for the $b\bar{b}$ channel (Ackermann et al. 2014b). IACTs have targeted several dSphs (Acciari et al. 2010; Abramowski et al. 2014b; Aleksić et al. 2014; MAGIC collaboration 2016), the most popular being Segue I (located 23 kpc away only) but for which estimation of the J-factor is still actively debated in the community (e.g., Bonnivard et al. 2015a, 2016b; Hayashi et al. 2016; Chiappo et al. 2016). In 2015, a lot of excitement surrounded the DES-discovered Reticulum II dSph galaxy (Bechtol et al. 2015), for which Geringer-Sameth et al. (2015b) reported γ-ray detection from *Fermi*-LAT Pass 7 data. This emission was unfortunately not confirmed by the joint *Fermi*-DES analysis, using the improved Pass 8 data (Drlica-Wagner et al. 2015).

3. This is not the case of charged cosmic rays that diffuse of magnetic inhomogeneities in the Galaxy, resulting in (almost) isotropic fluxes.

The Galactic centre region. The centre of the Milky Way is possibly the most interesting target, as it is both very close (~8.5 kpc away) and dense, yielding the highest J-factors. The GC has drawn a lot of attention in the recent years. In 2012, the analysis of Weniger (2012) suggested the existence of a 130 GeV emission line in the *Fermi*-LAT data, yielding hundreds of subsequent DM-oriented interpretations; the line was however not confirmed by the *Fermi* collaboration's analysis using Pass 8 data (Ackermann et al. 2015a). The *Fermi*-LAT data also shows an *excess* of diffuse emission up to 10° away from the Galactic centre (Ajello et al. 2016; Daylan et al. 2016). This excess is still very debated, being interpreted in terms of DM candidates of 10 – 100 GeV or missing components in the modelling of the astrophysical background, such as unresolved millisecond pulsars (e.g., Gordon and Macías 2013; Boehm et al. 2014; Abazajian et al. 2014; Kaplinghat et al. 2015; Daylan et al. 2016). At higher energy, the Galactic centre also provides the best constraints on annihilation DM for IACTs, with $\langle\sigma v\rangle \lesssim 2\times10^{-26}$ cm^3 s^{-1} at 1 TeV in the $\tau^+\tau^-$ channel, as recently obtained by the H.E.S.S collaboration (Lefranc et al. 2016). Despite a challenging astrophysical γ-ray background estimation, regions close to the Galactic centre ($|b| > 0.3°$) are, to date, the most constraining targets for DM indirection detection in γ-rays for IACTs.

Clusters of galaxies. They correspond to the last stage of hierarchical structure formation and are the largest reservoirs of DM in the universe, with masses ranging between 10^{14} – 10^{15}M$_\odot$, at the other end of the mass spectrum. The main appeal comes from their huge DM content and the fact that substructures in galaxy clusters could boost the signal, potentially yielding similar J-factors to closer targets such as dSph galaxies (the Virgo cluster is the closest and is located 18 Mpc from us). Difficulties come from the fact that i) the boost factors are affected by large uncertainties (see §3.1) and ii) astrophysical γ-ray emission from CR propagation in the intracluster medium is expected[4]. VERITAS observations of the Perseus clusters and HESS observation of the Fornax cluster typically yield $\langle\sigma v\rangle \lesssim 10^{-20}-10^{-21}$ cm^3 s^{-1} in the TeV range (Arlen et al. 2012; Abramowski et al. 2012, 2014a). More stringent limits have been obtained at lower energies from *Fermi*-LAT, with $\langle\sigma v\rangle \lesssim 10^{-24}$ – 10^{-25} cm^3 s^{-1} below 100 GeV, exploring various substructures configurations (Ackermann et al. 2010). Galaxies clusters have briefly attracted the spotlight when a possible emission line at 110-130 GeV was reported to be seen in the *Fermi*-LAT data (Hektor et al. 2013), similarly to the Galactic centre (see below), but an exotic origin of this line is now ruled-out by the *Fermi*-LAT collaboration (Ackermann et al. 2013). Clusters have drawn more attention at lower energy, in the X-ray regime, where a 3.5 keV line was first detected by Bulbul et al. (2014) in the stacked XMM-Newton spectrum of 73 clusters and tentatively interpreted as the decay of a ~7 keV sterile neutrino or axion (e.g., Lee et al. 2014).

1.2 CLUMPY – a public code for DM indirect detection

As mentioned before, my work in the field of DM indirect detection in γ-rays has started with the writing of the CLUMPY code, first made public in 2012 (Charbonnier et al. 2012) and upgraded in 2015 to become a far more complete tool (Bonnivard et al. 2016a). The first version was developed in collaboration with David Maurin and Aldée Charbonnier, while Vincent Bonnivard, Moritz Hütten and Emmanuel Nezri joined us for the second release. CLUMPY is regularly used to publish results from experimental collaborations e.g., HAWC (Albert et al. 2017a), ANTARES

4. Although not directly detected yet (Ackermann et al. 2014a), a positive cross-correlation signal was recently found between *Fermi*-LAT data and several cluster catalogs (Branchini et al. 2017). A recent study (not yet accepted for publication) from Xi et al. (2017) also claims a 6σ detection in the Coma cluster, using *Fermi*-LAT data.

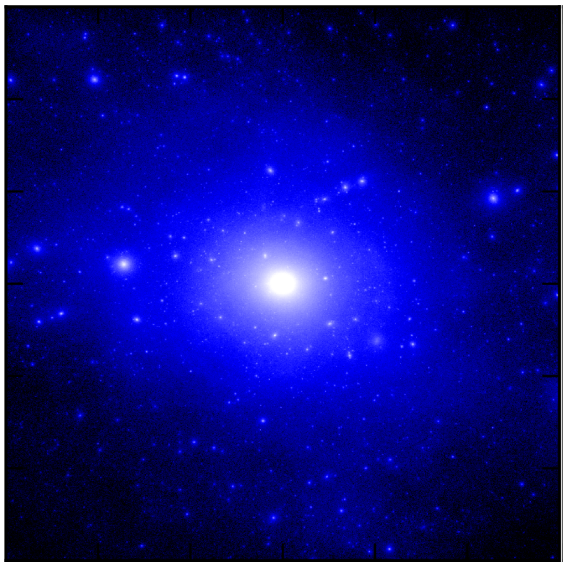

FIGURE 1.2: Projected DM surface density of a MW-like galaxy from the 'DM+gas' run of the Latte simulation at $z = 0$ (Wetzel et al. 2016).

(The ANTARES Collaboration 2015; Albert et al. 2017b), or independent research teams (e.g., Nichols et al. 2014; Genina and Fairbairn 2016; Balázs et al. 2017; Campos et al. 2017.) We also regularly receive help requests from a variety of users all over the globe and provide as much user support as possible.

After mentioning how CLUMPY came to be (§1.2.1), I will discuss the key ingredients included in the code (§1.2.2), both in term of particle physics and DM halo properties; the latter sections provide all the required quantities to compute J-factors. In §1.2.3, I will finally give a brief, and non-exhaustive, overview of the main features of the code.

1.2.1 Rationale

In the ΛCDM hierarchical structure formation scenario, small structures collapse first, then merge into larger structures, therefore becoming *substructures* of this larger halo. Structure formation and evolution on cosmological scales, and properties of DM halos on smaller scales, are being studied using numerical simulations. The latter type of simulations use zoom-in techniques on the former to provide a detailed view of the DM distribution at the galactic or galaxy cluster scales. In the last 20 years, the increase of computational power and the improvement of algorithms have allowed for more refined simulations, both in terms of mass resolution (more simulated particles of smaller mass in the simulation volume) and physical processes at play (see Kuhlen et al. 2012 for a nice review). State-of-the-art galactic scale simulations now include both gravity and complex baryonic sub-grid physics (star formation, supernovae and AGN feedback, radiative cooling; see fig. 1.2). These baryonic effects affect the structural properties of DM (sub)halos (see, e.g., Brooks and Zolotov 2014; Mollitor et al. 2015; Chan et al. 2015; Zhu et al. 2016; Wetzel et al. 2016). Those simulations, such as Aquarius (Springel et al. 2008) and Via Lactea (Diemand et al. 2008) for DM-only simulations, or APOSTLE (Sawala et al. 2016) and Latte (Wetzel et al. 2016) for 'DM+gas' simulations, are indispensable to parameterise the properties of DM halos (§1.2.2.1). However, after millions of cpu-hours, these impressive runs are limited in terms of mass resolution, and provide *only* a single realisation of the DM distribution for a given set of choices regarding cosmology and subgrid physics.

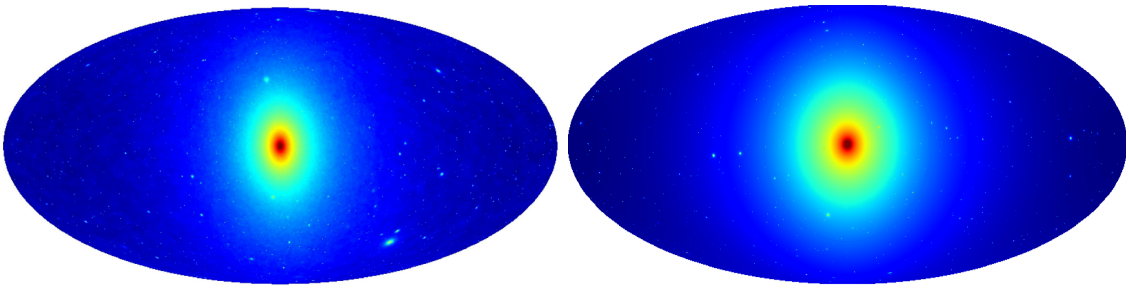

FIGURE 1.3: Differential J-factor $dJ/d\Omega$ over the all sky, including substructures, obtained from the Aquarius-A1 simulation (left, adapted from Springel et al. 2008) or from a CLUMPY run (right). Arbitrary units.

The initial idea behind the writing of CLUMPY was to have a flexible code that would simulate quickly the γ-ray skymap from DM annihilation or decay, as if computed directly from the end-product of these DM-only or 'DM+gas simulations'. The code would allow to both extend the results below the mass resolution of the DM simulations and easily explore how the results are affected when changing the properties of the DM halos. Figure 1.3 (left) shows the differential J-factor $dJ/d\Omega$ as computed directly from the Aquarius-A1 run in fig. 1.2, while a similar map obtained in 7 hours only with CLUMPY is given in the right panel.

From such skymaps, we can, for example, explore a wide variety of DM substructure configurations and explore the sensitivity of γ-ray instruments to DM substructures in the Milky Way (§2.1). CLUMPY can also be used on a per object basis, providing J-factors of individual objects such as dwarf spheroidal galaxies (§2.2) or galaxy clusters (§3.1). It will soon also include the extragalactic contribution to the exotic γ-ray flux, as described in §3.2.

1.2.2 Ingredients

The following briefly describes the backbone on which CLUMPY relies, in terms of astrophysical properties and particle physics spectra. I have chosen to give the minimal information required to follow what will be presented afterwards, regarding our studies of Galactic clumps (Hütten et al. 2016), dSph galaxies (Charbonnier et al. 2011; Walker et al. 2011; Bonnivard et al. 2015a,b,c) and galaxy clusters (Combet et al. 2012; Nezri et al. 2012; Maurin et al. 2012); the reader should be advised that any of the *ingredients* cited hereafter is the subject of active research and cannot be reduced to the few lines I dedicate to the matter.

1.2.2.1 Key properties of a single DM halo

As seen from fig. 1.2, the overall DM density of a galactic DM halo in Eq. (1.3) may be decomposed into a smooth component $\rho_{\rm sm}$ and a substructure contribution $\rho^{\rm tot}_{\rm subs}$ such as $\rho = \rho_{\rm sm} + \rho^{\rm tot}_{\rm subs}$. The ingredients required to account for these two components in CLUMPY come from the results of numerical simulations, and are described below in a generic manner only. The specificities of the various types of halos (dark clumps, dwarf spheroidal galaxies and galaxy clusters) will be discussed in their corresponding sections (§2.1, 2.2, and 3.1).

Halo DM profile. Although simulations show DM halo to be triaxial structures, spherical symmetry is generally assumed and DM profiles parameterised as a function of the distance r to the halo centre. Two standard parameterisations are the Zhao (a.k.a generalised NFW) and Einasto

descriptions (Zhao 1996; Springel et al. 2008),

$$\rho_{\rm Zhao}(r) = \frac{\rho_s}{(r/r_s)^\gamma\ [1+(r/r_s)^\alpha]^{(\beta-\gamma)/\alpha}}\ , \tag{1.4}$$

and

$$\rho_{\rm Einasto}(r) = \rho_s \exp\left\{-\frac{2}{\alpha_{\rm E}}\left[\left(\frac{r}{r_s}\right)^{\alpha_{\rm E}} - 1\right]\right\}\ . \tag{1.5}$$

When ignoring baryonic effects, halos are characterised by cuspy profiles, with two standard parameterisations being the Navarro-Frenk-White ($\rho_{\rm NFW} = \rho_{\rm Zhao}$ with $[\alpha,\beta,\gamma] = [1,3,1]$) and Einasto (with $\alpha_{\rm E} = 0.17$) descriptions (Navarro et al. 1996; Einasto and Haud 1989). For a given halo of mass M_Δ enclosed in R_Δ [5], the normalisation and scale radius of the DM inner profile are obtained from the mass-concentration relation $c_\Delta(M_\Delta, z) \equiv R_\Delta/r_s$, further discussed in the next paragraph.

Mass-concentration parameterisation $c_\Delta - M_\Delta$. Once the parameterisation of the DM profile is chosen, its structural parameters (normalisation and scale radius) are fully determined from its mass M_Δ and concentration-mass $c_\Delta - M_\Delta$ relation. For a given mass, the latter depends on the redshift and whether the halo is a field halo or subhalo. In case of a subhalo, the concentration also depends on the distance to the centre of host halo, i.e., $c_\Delta(M_\Delta, z) \to c_\Delta(M_\Delta, z, r)$, as tidal effects enter the game. Several parameterisations, based on the results of numerical simulations have been proposed and are implemented in CLUMPY (e.g., Bullock et al. 2001; Duffy et al. 2008; Giocoli et al. 2012; Sánchez-Conde and Prada 2014; Correa et al. 2015). The most recent studies suggest a flattening of the relation at low masses and a higher concentration of subhalos compared to field halos (see fig. 1.4, Sánchez-Conde and Prada 2014; Correa et al. 2015). The latter effect was shown to yield an extra ~ 5 boost factor (Bartels and Ando 2015; Zavala and Afshordi 2016; Moliné et al. 2017) on $J^{\rm tot}_{\rm subs}$ compared to previous calculations.

1.2.2.2 Accounting for DM substructures

The two above characteristics suffice to describe the DM distribution of a single smooth halo but must be supplemented by more properties to account for the contribution of a population of DM substructures, a feature characteristic of the hierarchical structure formation. Semi-analytical models as well as numerical simulations have been used to characterise the properties of these substructures down (or extrapolated down) to the smallest mass scale. Substructures in a host halo are characterised by their mass and spatial distribution, as well as the description of the DM distribution within each subhalo.

Normalisation. The number of halos $N_{\rm calib}$ in a given mass range is used as a calibration for the total number of subhalos in MW-like halos. ΛCDM simulations of Milky-Way size halos predict an overabundance of high-mass subhalos compared to the currently known satellite galaxies; this is the so-called 'missing satellites' problem (Bullock 2010). Baryonic feedback onto the cusps of DM subhalos could possibly solve this tension (Del Popolo et al. 2014; Maxwell et al. 2015). Indeed, hydrodynamical simulations roughly show half as many high-mass subhalos as DM only simulations, with about $100-150$ objects above $10^8\ {\rm M}_\odot$ (Mollitor et al. 2015; Sawala et al. 2016).

5. Here, M_Δ is the mass enclosed in R_Δ, where the latter corresponds to the radius within which the average density in Δ times the critical density of the universe. The values $\Delta = 200$ or $\Delta = 500$ are generally considered in the literature.

Coupled to a mass distribution, this defines the fraction of the parent halo mass under the form of subhalos. Alternatively, one may choose to fix this mass fraction and the mass distribution to obtain the normalisation; this is the approach chosen for non-MW halos.

Mass distribution. The DM halo mass distribution is well described as $\mathrm{d}\mathcal{P}_M/\mathrm{d}M \propto M^{-\alpha_m}$, with $\alpha_m = 1.9$ a typical value found from numerical simulations of Milky Way-like halos (Springel et al. 2008; Madau et al. 2008). Together with $N_{\rm calib}$, the choice of α_m determines the total number of clumps $N_{\rm tot}$ and their total mass $M_{\rm sub}^{\rm tot}$ (see Charbonnier et al. 2012 for details).

Spatial distribution of Galactic substructures $\mathrm{d}\mathcal{P}_V/\mathrm{d}V$. The fraction of mass bound into substructures is expected to decrease towards the Galactic centre (*anti-biaised* behaviour), as subhalos are tidally disrupted by the strong gradient of the gravitational potential. This is discussed in detail in Han et al. (2016), where the authors argue that this is the result of a selection effect of 'evolved' subhalos (suffering from tidal stripping), the 'unevolved' distribution following the host smooth distribution (*biased* distribution). CLUMPY includes both type of behaviour for the spatial distribution of subahlos, the *anti-biased* description being generally preferred to mimic the end-product of numerical simulations (Springel et al. 2008; Madau et al. 2008).

Width of the mass-concentration distribution, σ_c. Rather than assuming a single concentration for a given halo mass from the mean parameterisations implemented in CLUMPY, the concentration of each subhalo is drawn from a log-normal distribution of width σ_c around the mean value

$$\frac{\mathrm{d}\mathcal{P}_c}{\mathrm{d}c}(M,c) = \frac{\exp -\left[\dfrac{\ln c - \ln(\bar{c}(M))}{\sqrt{2}\sigma_c(M)}\right]^2}{\sqrt{2\pi}\ c\ \sigma_c(M)}. \tag{1.6}$$

This is incorporated in CLUMPY to account for the intrinsic scatter of the $c_\Delta - M_\Delta$ relation found in numerical simulations as illustrated by the grey-shaded area in fig. 1.4 (Sánchez-Conde and Prada 2014; Wechsler et al. 2002).

1.2.2.3 Particle physics ingredients

CLUMPY relies on the tabulated spectra of existing PYTHIA simulations, PPPC4DMID and PPPC4DMν (Cirelli et al. 2011; Baratella et al. 2014), including or not EW corrections (Ciafaloni et al. 2011) to provide the gamma and neutrino spectra [6] from dark matter annihilation and decay. Twenty-eight primary channels, including e^+e^-, $\mu^+\mu^-$, $\tau^+\tau^-$, $b\bar{b}$, $\gamma\gamma$, $\nu_e\nu_e$, $\nu_\mu\nu_\mu$, $\nu_\tau\nu_\tau$, may be combined through as many branching ratios.

PPPC4DMν provides neutrino production spectra only. For distant astrophysical sources, the journey in vacuum and transition between the different flavour states should be accounted for. This can be described by average oscillations (Bilenky and Petcov 1987):

$$P(\nu_l \to \nu_{l'}) = P(\bar{\nu}_l \to \bar{\nu}_{l'}) = \sum_{k=1}^{3} |U_{l'k}|^2 |U_{lk}|^2 \tag{1.7}$$

6. Although this document focuses on the γ-ray channel only, the neutrino channel formalism is the same and is also included in CLUMPY.

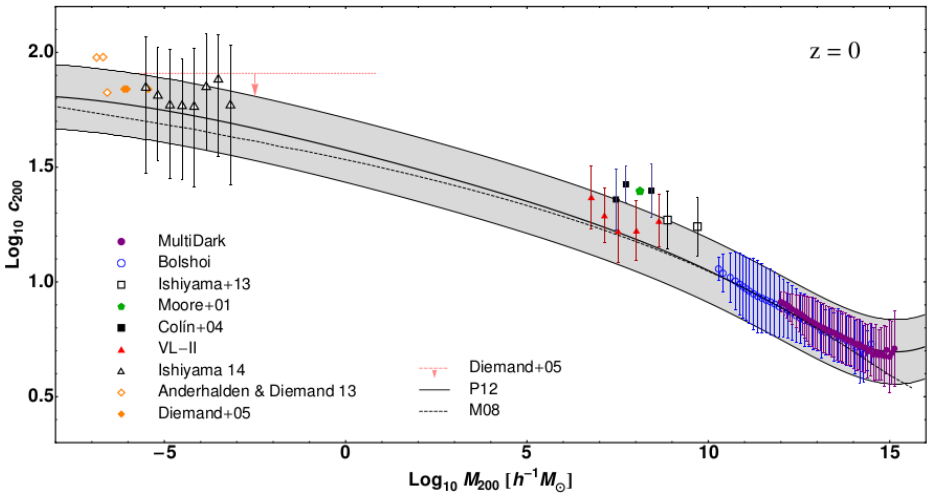

FIGURE 1.4: Overview of the mass-concentration constraints obtained from various numerical simulations (symbols) spanning a large halo mass range. The grey band is a typical $1-\sigma$ scatter centred on the P12 model. Figure taken from Sánchez-Conde and Prada (2014).

where U is the neutrino mixing matrix and $k = 1, 2, 3$ for the 3 mass eigenstates. The default values for the mixing angles $\{\theta_{12}, \theta_{23}, \theta_{13}\} = \{34°, 49°, 9°\}$, are taken from Forero et al. (2014) and the code gives the resulting ν_e, ν_μ or ν_τ fluxes.

1.2.3 Advertising CLUMPY

In this section, I describe the main features of the code, without entering into the details; some will be given when addressing the specifics of each type of targets (in §2.1, 2.2, 3.1, and 3.2), and in any case, all there is to know about the code may be found at `https://lpsc.in2p3.fr/clumpy/`.

1.2.3.1 General

User-friendliness. With the idea of making the code a public tool, we have from the start made a lot of effort in making CLUMPY as user-friendly as possible. In that respect, the three main features are i) a detailed `Doxygen` documentation, automatically generated with the code, ii) an easy-to-use text-based user interface, including run examples, iii) a quick visualisation of the results with the automatic generation of various figures. These nice features require that the user has indeed managed to compile CLUMPY; this is were we provide the most user-support as compilation of the current version is a bit intricate. We are currently working at removing some dependencies that will make the next version much easier to compile. For the 2018 code release, the code will be distributed from a git repository, that will also simplify the interactions with the users who will be able to directly raise issues and comments.

Flexibility. From a single parameter file, the user selects all the DM properties, both in terms of astrophysics (see §1.2.2.1) or particle physics (annihilation/decay channels, branching ratios, see §1.2.2.3). This is done through a set of keywords corresponding to the various predefined parameterisations. In the forthcoming release, the use of this (large) parameter file will be much simplified for the user's benefit.

Speed and accuracy. We have optimised the code whenever possible to speed up the runs. When generating a skymap of the Galactic exotic signal, this means drawing the minimum number of substructures that meets a user-defined precision requirement (see §2.1.1) and interpolating between grid points. The triple integral to compute J-factors has also been optimised, to account for the sometimes complex behaviour of the DM density along the line-of-sight (e.g., triaxiality, diverging profiles).

1.2.3.2 Features

Skymap or individual halo. The code may be used to generate random realisations of the exotic γ-ray (and neutrino) sky, including several levels of substructures, as well as used for specific DM halos (such as dSph galaxies or galaxy clusters).

Galactic and (soon) extragalactic exotic contribution: The first two releases of CLUMPY have been exclusively focusing on the 'local' universe, i.e. suitable to use for the Galactic halo, subhalos, dSph galaxies and close galaxy clusters. To account for the extragalactic contribution to the exotic γ-ray signal, cosmology must be taken into account. The upcoming release will include this component, to make CLUMPY the most complete tool possible for DM indirect detection in γ-rays. Details and preliminary results on this ongoing work are given in §3.2.

Jeans analysis and MCMC. One may determine the DM profile parameters from the kinematics of tracers of the underlying gravitational potential (i.e. stars in a dSph galaxy). The so-called Jeans analysis (§2.2.1) has been widely used in the literature in that context and was implemented in the second release of the code. Coupled to the GreAT MCMC engine (Putze and Derome 2014), this module outputs the probability density distributions of the DM profile parameters, that can then be consistently propagated to the J-factors.

Triaxiality. Numerical simulations show that DM halos are not spherical. While this is often ignored in DM indirect detection searches, CLUMPY allows for a full triaxial treatment to compute the J-factors. From this, we have shown that ignoring orientation of a triaxial halo with respect to the line-of-sight yields a 30% uncertainty on the J-factors. More importantly, we have shown that applying a spherical Jeans analysis to a triaxial halo can bias the J-factor by a factor of a few (Bonnivard et al. 2015c).

2

Focus on the Galactic scale

Contents

This chapter first focuses on the DM annihilation signal expected at the Galactic scale, from the dark Galactic clumps (§2.1, based on the results we published in Hütten et al. 2016) and dSph galaxies (§2.2, summarising our studies published in Charbonnier et al. 2011; Walker et al. 2011; Bonnivard et al. 2015a,b,c).

2.1 Dark Galactic clumps

Dark clumps could provide a smoking-gun signature of DM if detected as γ-ray point sources with no counterparts at other wavelengths. One may also look for their 'statistical' imprint in the angular power spectrum (APS) over the diffuse DM background (that can be boosted by these same micro-halos). In any case, the sensitivity of γ-ray experiments to the dark halos of the MW crucially depends on the modelling of these clumps. As seen in §1.2.2.1, a significant scatter exists in the findings of the various simulations regarding, e.g., the mass-concentration relation or the spatial distribution of the subhalos.

In Hütten et al. (2016), we explored a wide variety of Galactic clumps configurations, using CLUMPY to i) identify which subhalo property is the most critical and ii) what sensitivity to dark clumps could be expected of the future CTA instrument, given the characteristics of the foreseen extragalactic survey. To do so, we used realistic survey and instrument responses and we underwent the official CTA reviewing process before submitting this work. Before summarising these results, I first briefly describe how Galactic substructures are handled in CLUMPY, a key aspect that has allowed the completion aforementioned of the study.

2.1.1 CLUMPY: accounting for the necessary number of clumps

As mentioned earlier, generating skymaps of the exotic γ-ray sky, quickly, in a flexible way and on one's own PC, was the original reason for writing CLUMPY. Galactic clumps are a major

```
  * find #clumps to draw below l_crit for each mass decade (360 x 180 deg map)

  mass decade  | #clumps (Gal) | l_crit (kpc) | <#clumps to draw> => #clumps = Poisson(<#clumps>)
-6.0 --> -5.0      5.304e+14       1.000e-03        3.220e-01    =>     0
-5.0 --> -4.0      6.677e+13       1.000e-03        4.054e-02    =>     0
-4.0 --> -3.0      8.406e+12       1.000e-03        5.104e-03    =>     0
-3.0 --> -2.0      1.058e+12       1.000e-03        6.425e-04    =>     0
-2.0 --> -1.0      1.332e+11       7.402e-03        3.280e-02    =>     0
-1.0 --> +0.0      1.677e+10       5.753e-02        1.939e+00    =>     1
+0.0 --> +1.0      2.112e+09       4.258e-01        9.899e+01    =>     111
+1.0 --> +2.0      2.658e+08       2.723e+00        3.245e+03    =>     3318
+2.0 --> +3.0      3.347e+07       1.237e+01        3.527e+04    =>     35513
+3.0 --> +4.0      4.213e+06       3.710e+01        8.449e+04    =>     84856
+4.0 --> +5.0      5.304e+05       8.005e+01        6.505e+04    =>     65378
+5.0 --> +6.0      6.677e+04       1.421e+02        2.581e+04    =>     26016
+6.0 --> +7.0      8.406e+03       2.074e+02        6.107e+03    =>     6206
+7.0 --> +8.0      1.058e+03       2.423e+02        9.522e+02    =>     991
+8.0 --> +9.0      1.332e+02       2.680e+02        1.330e+02    =>     147
+9.0 --> +10.0      1.677e+01       2.680e+02        1.675e+01    =>     11
+10.0 --> +10.1      2.663e-01       2.680e+02        2.659e-01    =>     0
```

FIGURE 2.1: On-screen output of a CLUMPY run producing the fullsky map shown in figure 1.3 (right). The second column shows the total number of clumps in the mass decade given in the first column. The last column gives the number of clumps effectively drawn for this CLUMPY run, where the user-defined precision requirement was 1%.

feature of ΛCDM structure formation and must be accounted for. Assuming the minimum and maximum mass for a Galactic subhalo to be $M_{\rm min} = 10^{-6}{\rm M}_\odot$ and $M_{\rm max} = 10^{10}{\rm M}_\odot$ respectively, and combining $N_{\rm calib}$ with a halo mass function $dN/dM \propto M^{-1.9}$ (see §1.2.2.1), one finds the total number of substructures in a MW-like halo to be $\sim 10^{14}$, the smaller subhalos being the most numerous. CLUMPY randomly draws substructures from their mass and spatial distributions but drawing 10^{14} objects would take a prohibitive amount of time.

In the early stages of the code development, back in 2012, I have worked at defining a criterion that would allow to draw less clumps while keeping the accuracy of the calculation down to the smallest mass scales. The derivation may be found in Charbonnier et al. (2012) and will not be repeated here. The idea is that, for given integration angle $\theta_{\rm int}$ and subhalo mass, there exists a critical distance $l_{\rm crit}$ above which the subhalos are point-like and so numerous that an average description applies. Assuming the mass and spatial distributions of the clumps obtained from numerical simulations, one may indeed compute the average J-factor of a subhalo population. Below $l_{\rm crit}$, clumps must be drawn. We evaluate this distance for each mass decade, from $M_{\rm min}$ to $M_{\rm max}$. The value of $l_{\rm crit}$, hence the number of clumps to draw, depends on a user-defined precision requirement. The less stringent this requirement is, the more valid is the average description and the less clumps are to be drawn. This is exemplified in figure 2.1 where $\sim 2 \times 10^5$ drawn clumps suffices to reach a 1% precision criterion. This procedure is at the core of the *skymap mode* of CLUMPY and has allowed the fast fullsky maps computation required for the study described hereafter.

2.1.2 Observational sensitivity of CTA to dark clumps

This study was undertaken as part of the PhD thesis of Mortiz Hütten, a DESY PhD student working in the VERITAS and CTA collaborations, with whom D. Maurin and myself have collaborated in the last years. For this project, Moritz (in close interaction with us) has first modified CLUMPY_v1.0 to compute fullsky maps using the HEALPIX pixelization scheme (Górski et al. 2005), a feature now available in CLUMPY_v2.0. Published in Hütten et al. (2016), this work aimed at performing the most comprehensive analysis to properly estimate the impact of all modelling

	Model	VAR0	LOW	VAR1	VAR2	VAR3	VAR4	VAR5	VAR6a	VAR6b	HIGH
Varied parameters	inner profile	NFW	E	E	E	E	E	E	E	E	E
	α_m	1.9	1.9	2.0	1.9	1.9	1.9	1.9	1.9	1.9	1.9
	σ_c	0.14	0.14	0.14	0.24	0.14	0.14	0.14	0.14	0.14	0.14
	$\overline{\varrho}_{subs}$	E-AQ	E-AQ	E-AQ	E-AQ	M-VLII	E-AQ	E-AQ	E-AQ	E-AQ	M-VLII
	$N_{\rm calib}$	150	150	150	150	150	300	150	150	150	300
	sub-subhalos?	no	no	no	no	no	no	yes	no	no	no
	$c(m)$	SP	SP	SP	SP	SP	SP	SP	Moliné	P-VLII	P-VLII
Derived parameters	$N_{\rm tot}$ ($\times 10^{14}$)	6.1	6.1	150	6.1	6.1	12	6.1	6.1	6.1	12
	$f_{\rm sub}$ [%]	19	19	49	19	19	38	19	19	19	38
	$f_{\rm sub}(R_\odot)$ [%]	0.30	0.30	0.77	0.30	0.47	0.59	0.30	0.30	0.30	0.93
	$\widetilde{D}^\star_{\rm obs}$ [kpc]	22^{+32}_{-16}	19^{+27}_{-14}	13^{+27}_{-10}	21^{+33}_{-15}	20^{+22}_{-15}	17^{+26}_{-13}	21^{+30}_{-14}	8^{+18}_{-6}	9^{+14}_{-6}	8^{+11}_{-6}
	$\log_{10}(\widetilde{m}^\star_{\rm vir}/{\rm M}_\odot)$	$9.0^{+0.8}_{-1.4}$	$8.8^{+0.8}_{-1.4}$	$8.5^{+0.9}_{-1.5}$	$8.9^{+0.8}_{-1.4}$	$9.0^{+0.7}_{-1.3}$	$8.9^{+0.9}_{-1.4}$	$9.0^{+0.7}_{-1.4}$	$7.9^{+1.4}_{-1.6}$	$7.9^{+1.4}_{-1.5}$	$8.2^{+1.2}_{-1.5}$
	$\log_{10}\left(\frac{\widetilde{J}^\star}{\rm GeV^2\,cm^{-5}}\right)$	$19.9^{+0.4}_{-0.3}$	$20.0^{+0.5}_{-0.3}$	$20.0^{+0.4}_{-0.3}$	$20.0^{+0.4}_{-0.3}$	$20.1^{+0.4}_{-0.3}$	$20.2^{+0.4}_{-0.3}$	$20.3^{+0.5}_{-0.3}$	$20.3^{+0.5}_{-0.4}$	$20.4^{+0.5}_{-0.3}$	$20.8^{+0.5}_{-0.4}$

TABLE 2.1: Parameters for the different models investigated in this study. The first seven lines correspond (from top to bottom) to: the subhalo density profile, the slope of the subhalo mass distribution, the width of the concentration distribution, the subhalo spatial distribution, the number of objects between 10^8 and $10^{10}\,{\rm M}_\odot$, the flag for sub-subhalos, and the mass-concentration relation. The columns are ordered by increasing flux of the brightest object. 'NFW' stands for a Navarro-Frenk-White profile and 'E' for an Einasto profile with $\alpha_{\rm E} = 0.17$. 'E-AQ' is the Einasto parameterisation fitted to the substructure distribution in Aquarius simulation (Springel et al. 2008), while 'M-VLII' and 'P-VLII' correspond to the Via Lactea II parameterisation of Madau et al. (2008) and Pieri et al. (2011) respectively. The mass concentration relation is 'SP' for the Sánchez-Conde and Prada (2014) parameterisation, or the distance-dependent description by Moliné et al. (2017). Derived parameters in the six bottom rows are the following: $N_{\rm tot}$ is the total number of subhalos in the MW; $f_{\rm sub}$ is the global mass fraction contained in subhalos; $f_{\rm sub}(R_\odot)$ is the mass fraction contained in subhalos at the solar distance from the GC; $\widetilde{D}^\star_{\rm obs}$, $\widetilde{m}^\star_{\rm vir}$, and $\widetilde{J}^\star$ are the median distance from the observer, mass, and J-factor of the brightest subhalo from the 500 realisations of each model.

uncertainties linked to our ignorance of the DM halo key properties and determine how they propagate to the sensitivity analysis for CTA.

2.1.2.1 Evaluating the substructure modelling uncertainty

Using CLUMPY, we generated fullsky maps varying each substructure property (§1.2.2.1) according to table 2.1. This essentially impacts the number of substructures and/or their associated $J-$factors. Five hundred skymap realisations for each modelling (LOW, HIGH, VAR0 to VAR6) have been simulated to access their statistical properties. The bottom half of table 2.1 gives the global properties of each modelling, averaged over the 500 realisations. Compared to the LOW model, only the calibration number $N_{\rm calib}$ and the slope of the mass distribution affect the *total* number of subhalos. However, the number of halos within a given J-factor range will depend on all substructure-related properties.

In order to evaluate the impact of the modelling options X on the J-factor, it is useful to define $\overline{N}_X(>J)$ as the mean number of halos with a J-factor above a certain threshold J, averaged over the 500 realisations. The ratio $N_X(>J)/N_{\rm LOW}(>J)$ is plotted in figure 2.2 (bottom panel), where $X = {\rm VAR}i, \quad i \in [0, 6]$, and gives a useful representation of the various effects at play. From the range of substructures properties tested as deviations from the LOW model, we find the distance-dependent concentration parameterisation (solid and dot-dashed black) to have the larger effect in terms of the number of halos with the largest J-factors. Including sub-subhalos (light green) is also important but only plays a role in the outskirts of the halos and is not significant at CTA angular resolution. The concentration is therefore the most important substructure property to pin

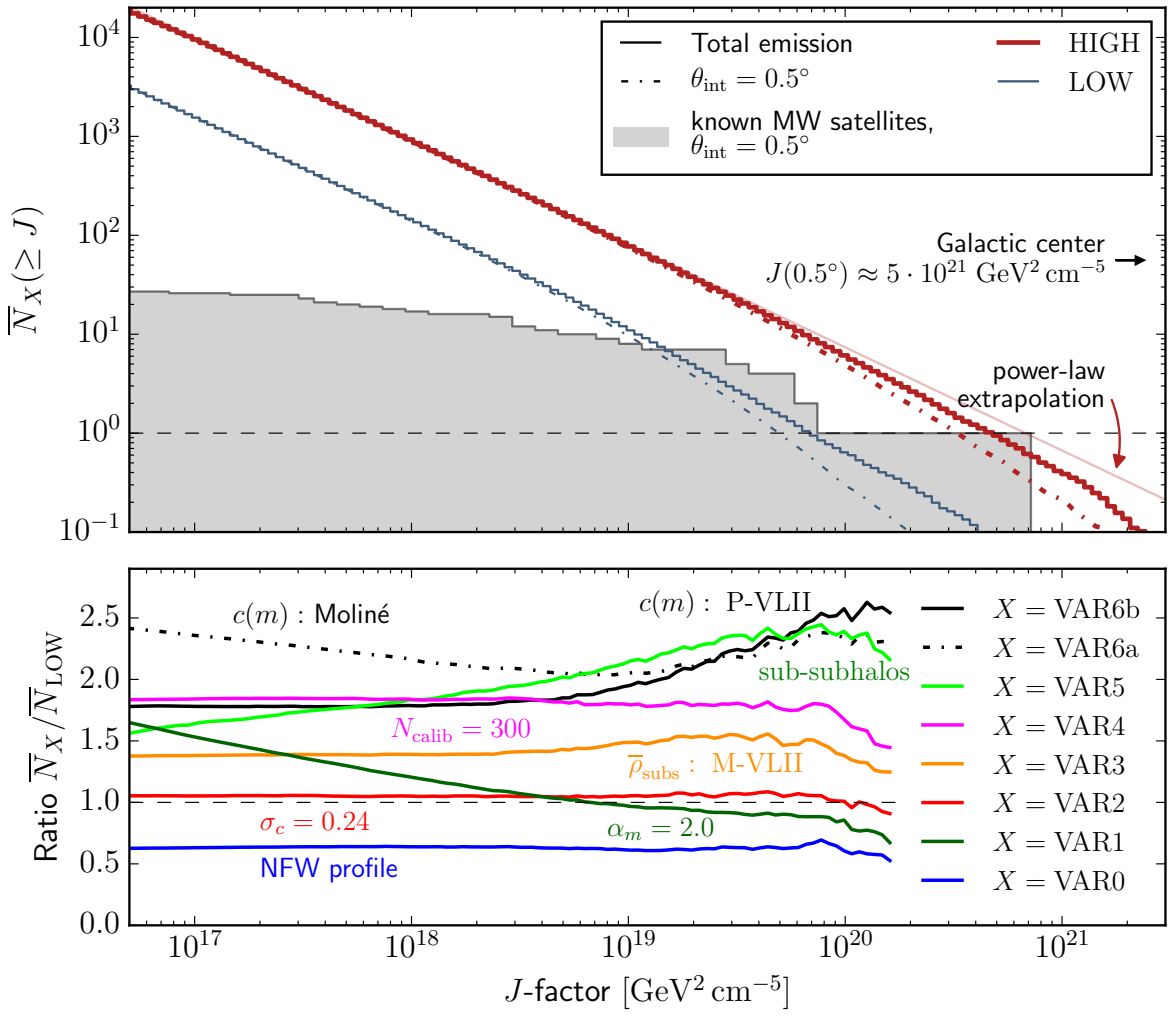

FIGURE 2.2: *Top:* cumulative source count distribution of Galactic subhalos for model LOW and HIGH. The solid lines show the distribution of the total J-factors, while the dashed-dotted lines show the distribution when only taking into account the emission from the central 0.5° of the subhalos. The grey-shaded histogram shows the cumulative distribution of all known dSph galaxy objects J-factor. *Bottom:* ratio of $\overline{N}_X(>J)$ for all models X = VARi, $i \in [0, 6]$ to model LOW. The largest effect comes from including a distance-dependent mass-concentration relation (black) and several levels of substructures (light green).

down in order to make reliable detectability studies. Given the uncertainties regarding the subhalo properties, we made use of the LOW and HIGH models to bracket CTA sensitivity to dark clumps.

We conducted extensive comparison to existing studies to validate the maps obtained from the LOW and HIGH models. Among several approaches, an efficient way to check the global statistical properties of the maps is by the use of the angular power spectrum (APS) of the γ-ray skymaps; this is a powerful tool for DM analyses and has been already computed from numerical simulations such as Aquarius (Ando and Komatsu 2013a), Via Lactea II (Lange and Chu 2015), or MaGICC/g15784 (Calore et al. 2014). Using the HEALPIX implementation in CLUMPY, Moritz Hütten computed the average and variance of the APS over 500 realisations of model LOW and HIGH and found that these models successfully encompass the APS of existing simulations, confirming the validity of the substructure modelling in CLUMPY.

Another test was to compare the cumulative J-factor source count distribution, with that of the known satellites of the MW; this is shown in figure 2.2 (top panel) and indeed, our LOW and HIGH parameterisations do bracket the observations at the high-J end. For lower J values, the number of detected dSph galaxies becomes much lower than the number of subhalos measured from the models. This is what one would expect given that the most numerous low-mass halo would not have retained gas and formed stars to become identified as dSph galaxies. The dSph J-factors used in this figure mostly came from the study done as part of Vincent Bonnivard's PhD thesis (see §2.2, Bonnivard et al. 2015a), but supplemented by some more recently discovered objects I analysed. In particular, the last bin of the dSph histogram that slightly overshoots the HIGH model is due to the Triangulum II object, which has since been ruled out as being a dSph galaxy (see footnote 8); this last bin is therefore not relevant anymore. These tests validated the use the LOW and HIGH parameterisations to compute the CTA sensitivity to these dark subhalos.

2.1.2.2 CTA sensitivity to dark clumps

To go from J-factor skymaps to the actual CTA sensitivity to dark clumps, we relied solely on public CTA information. As a member of the CTA consortium, which neither David Maurin nor myself are, Moritz Hütten really took point on this part of the project, bringing his expertise and knowledge of CTA performances and tools. We considered the experimental setup of the foreseen CTA extragalactic survey, which should uniformly cover 25% of the sky in 400 to 600 hours, with an integrated sensitivity above 100 GeV ranging from 2.5×10^{-12} cm^{-2} s^{-1} to 1×10^{-11} cm^{-2} s^{-1} (for a Crab-like energy spectrum, Dubus et al. 2013). We assumed for simplicity that most of the survey will be performed in a circular region around the Galactic south pole ($b < -30°$) by CTA's southern array. While the primary goal of this survey is non-exotic extragalactic astrophysics, one may nonetheless use it as an opportunity to place limits on dark matter from the (non-) detection of dark clumps, nicely complementing CTA's core DM programme (Galactic centre, dSph galaxies and diffuse exotic emission, Carr et al. 2015).

Using the 500 skymap realisations of the LOW and HIGH models, taking into account CTA's extragalactic survey coverage and a 0.05° integration angle (typical of CTA's angular resolution), the median brightest halo has mass $\log_{10}(M/\mathrm{M}_\odot) = 7.4 \pm 1.4$, is located $d = 7^{+10}_{-5}$ kpc away and has J-factor $\log_{10}(J/\mathrm{GeV}^2\ \mathrm{cm}^{-5}) = 19.7 \pm 0.3$. Such a massive halo would likely have formed stars and be already identified as a dSph galaxy, yielding dedicated pointed observations. Repeating the exercise excluding all halos with masses greater that 10^6 M$_\odot$, to really target *dark* clumps, we find the median brightest halo a factor 2 dimmer within the central 0.05°. This should be kept in mind as no mass cut was considered in the results shown below.

Moritz then used the open-source CTA analysis software `ctools` (Knödlseder et al. 2016) to compute the CTA sensitivity to the median brightest dark subhalo. The sensitivity is obtained from a log-likelihood ratio between a background-only and background+signal hypothesis applied to

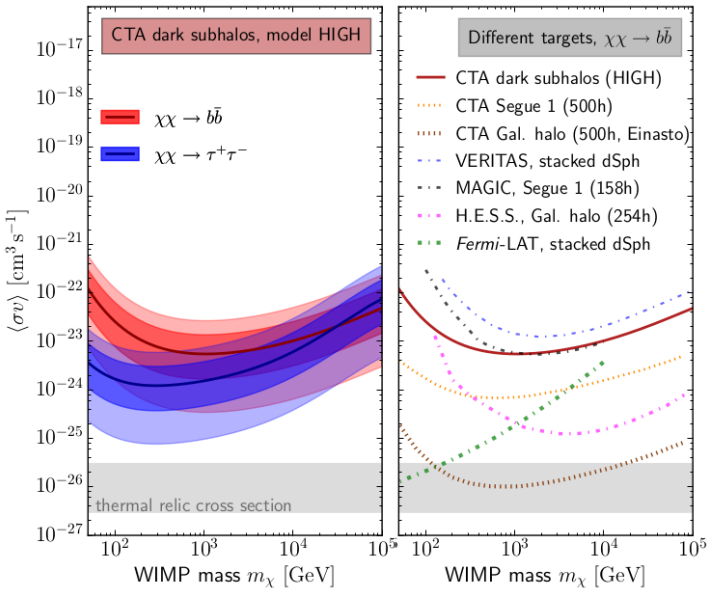

FIGURE 2.3: Sensitivity of the CTA Galactic survey to the brightest subhalo of the HIGH model. *Left:* median (solid lines) and 68% (95%) CI for the $b\bar{b}$ (red) and $\tau^+\tau^-$ (red). *Right:* Comparison to other instruments/targets. Limits from Carr et al. (2015) (CTA), Zitzer (2015) (VERITAS), Aleksić et al. (2014) (MAGIC), Lefranc et al. (2015) (HESS) and Ackermann et al. (2015b) (*Fermi*-LAT).

mock CTA data. The spatial properties of the median brightest halo J-factor is supplemented with a DM particle mass m_χ and a γ-ray spectrum (choice of annihilation channel, see §1.2.2.3), leaving the annihilation cross section $\langle\sigma v\rangle$ the only free parameter for the signal model. Sampling 24 DM masses between 50 GeV$\leq m_\chi \leq$100 TeV, we obtain, for model HIGH, the limits displayed in figure 2.3 (left panel). The analysis is performed for the $b\bar{b}$ (red) and $\tau^+\tau^-$ (blue) channels. The dark and light shaded area correspond to the 68% and 95% statistical uncertainty due to the J-factor variance measured from the 500 skymap realisations. Despite a modest median sensitivity, the 95% CI reaches $\langle\sigma v\rangle \sim 10^{-25}$ cm^3 s^{-1} in $\tau^+\tau^-$ and $\langle\sigma v\rangle \sim$ a few 10^{-25} cm^3 s^{-1} in $b\bar{b}$. Switching to model LOW (not shown) worsens the limits by one order of magnitude.

To put this result in the light of other existing or predicted instrumental results, the right panel in figure 2.3 compares the median limit of the HIGH model to the limits reached by other instruments and/or targets. Dark subhalos searches with a CTA survey is a less powerful probe of DM annihilation than CTA pointed observations of the Galactic halo (dotted brown) and to a lesser extent than dSph galaxies. Our results are less favourable than those previously established by Brun et al. (2011), who concluded that $\langle\sigma v\rangle \sim 4 \times 10^{-26}$ cm^{-3} s^{-1} could be reached from dark halo searches with CTA. This difference can be understood by the combination of choices made in Brun et al. (2011) regarding instrument performance, J-factor estimation and statistical approach, and we are confident our results are more representative of what CTA will be able to achieve [1].

While dark subhalos are not the most constraining objects regarding DM annihilation, the other options are not devoid of systematics. In particular and as we will see in the next section, Segue I, often considered the best dSph target because of its proximity, may not be as promising as originally thought. In any case, dark subhalo searches are complementary to all other routes and undertaking such analysis the CTA planned extragalactic survey will nicely add to the scientific return of the latter.

1. First, our limit is based on the 95% CL whereas theirs was based on 90% CL. Second, Brun et al. (2011) modelled the CTA instrument characteristics extrapolating from HESS, assuming a factor 10 larger effective area and a factor 2 better background rejection. Since then, CTA simulations have shown that the largest improvement in differential sensitivity compared to current instruments will be reached at energies above $\sim$ 1 TeV and extrapolation of HESS performances most likely overestimated the CTA sensitivity to DM. Third, they assumed that the subhalo signal is fully enclosed within the instrumental resolution, which yields another overestimation of the signal.

2.2 Dwarf spheroidal galaxies

With no or very little expected astrophysical γ-ray background and a high mass-to-light ratio, dSph galaxies are prime targets for DM indirect detection. Ground-based IACTs experiments have dedicated a signifiant amount of time to their observations (Acciari et al. 2010; Aleksić et al. 2014; Abramowski et al. 2014b; Zitzer 2015; MAGIC collaboration 2016) and many authors (re)-analyse *Fermi*-LAT data in the direction of these galaxies to place limits on DM annihilation (e.g, Geringer-Sameth et al. 2015b). Another major advantage pushing in favour of these objects is that their DM profiles may be inferred from the kinematics of their member stars, using the so-called Jeans analysis (described in §2.2.1), and removing the need to rely on strong assumptions coming from numerical simulations.

During my postdoc in Leicester and in early stages of my involvement in DM indirect detection, we started thinking that it would be useful to establish a list of the best dSph targets for IACTs and the future CTA. This required robust J-factor estimations, i.e. robust Jeans analyses. In Walker et al. (2011) and Charbonnier et al. (2011), we were the first to use mock dSph kinematical data to validate the Jeans analysis setup we used at the time, by comparing the reconstructed J-factors computed by the first version of CLUMPY to the true value. We showed, using a data-driven approach (i.e., without relying on strong priors, such as assuming that the dSph galaxies had underlying NFW halo profiles), that there was a critical integration angle [2] where the J-factor could be reconstructed optimally. In Charbonnier et al. (2011) we studied the detectability of the eight classical dSph galaxies in the light of these results. We did so by incorporating several effects that had been neglected until then (e.g., taking into account the spatial extension of the dSph galaxies) or relaxing some assumptions that were routinely made (e.g. assume NFW or core profiles) to revisit (and worsen) detectability prospects of ground-based and space-borne γ-ray instruments. From this work, we identified Ursa Minor, Sculptor and Draco to be the most promising objects among the classical dSph galaxies. The idea was to rapidly extend this analysis to the ultrafaint dSph galaxies discovered in the SDSS data.

These studies came five years later, along with an updated estimation for the classical dSphs (Bonnivard et al. 2015a,b,c), and were at the core of Vincent Bonnivard's PhD thesis (supervised by David Maurin at LPSC), with whom I collaborated. At that time, I was extremely busy with *Planck* data analysis, which was the bulk of my work, so that my contribution to these later DM indirect detection analyses have mostly been through our regular discussions, providing suggestions and a critical eye to intermediate results, and the writing of papers. It is these later results that I present below, starting by the extensive study on the limitations and systematics linked to the Jeans analysis in §2.2.2 and the J-factors of all known dwarf spheroidal galaxies summarised in §2.2.3.

2.2.1 CLUMPY: implementation of the Jeans analysis

The Jeans equation relates the dynamics of a collisionless tracer population (i.e. stars in a dwarf spheroidal galaxy or galaxies in a galaxy cluster) to the underlying gravitational potential, hence to the mass profile. Observationally, the tracer population can only be characterised in terms of the projected radius R from the dSph centre; its fundamental characteristics are i) the surface brightness profile, $I^{\rm obs}(R)$ that can be obtained from photometry measurements and ii) the velocity dispersion projected onto the line-of-sight $\sigma_p^{\rm obs}(R)$ that is obtained from spectroscopic follow-ups

2. This critical angle represents a compromise between maximising prospective flux and minimising uncertainty in the dSph's dark matter distribution.

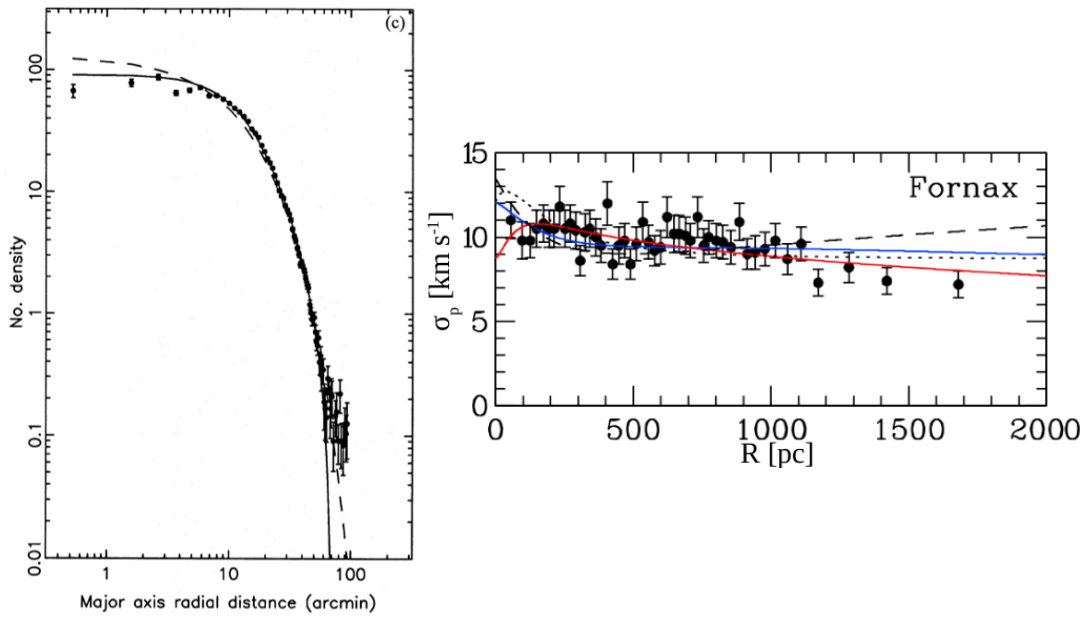

FIGURE 2.4: Surface brightness (left) and velocity dispersion (right) profiles measured in the Fornax dSph galaxy as published in Irwin and Hatzidimitriou (1995) and Walker et al. (2009a) respectively. The lines represent in each case some fit to the data performed by the authors assuming various parameterisations for the light profile (left) or the DM density (right).

of individual member stars [3] (see figure 2.4 for examples of such observational datasets of the Fornax dSph galaxy).

The Jeans equation is obtained after integrating the collisionless Boltzmann equation in spherical symmetry, assuming steady-state and negligible rotational support (Binney and Tremaine 2008) and reads

$$\frac{1}{\nu}\frac{d}{dr}\left(\nu\bar{v_r^2}\right) + 2\frac{\beta_{\rm ani}(r)\bar{v_r^2}}{r} = -\frac{GM(r)}{r^2}, \text{ with } M(r) = 4\pi\int_0^r \rho_{\rm tot}(s)s^2 ds\,, \tag{2.1}$$

where:

- the definition of the enclosed mass $M(r)$ assumes that the mass of the tracer population is negligible compared to the underlying DM halo, i.e. $\rho_{\rm tot} \approx \rho_{\rm DM}$;
- $\nu(r)$ is the 3D number density (or light profile) of the tracer population; it relates to the 2D projection $I(R)$, function of the projected radius R, as

$$I(R) = 2\int_R^{+\infty}\frac{\nu(r)\,r\,dr}{\sqrt{r^2-R^2}}, \text{ and inversely, } \nu(r) = -\frac{1}{\pi}\int_r^{+\infty}\frac{\mathrm{d}I}{\mathrm{d}R}\frac{\mathrm{d}R}{\sqrt{R^2-r^2}}; \tag{2.2}$$

- $\bar{v_r^2}$ is the radial velocity dispersion of the tracers;
- $\beta_{\rm ani}(r) \equiv 1 - \bar{v_\theta^2}/\bar{v_r^2}$ is the velocity anisotropy of the tracers, and depends on the ratio of the tangential to the radial velocity dispersions.

3. The notion of *member* stars is very important and leads to the issue of sample contamination by foreground stars. This will be briefly discussed in the end of this section.

The formal solution to the 3D Jeans equation is

$$\nu(r)\bar{v_r^2}(r) = \frac{1}{f(r)} \times \int_r^\infty f(s)\nu(s)\frac{GM(s)}{s^2}ds, \text{ with } f(r) = f_{r_1} \exp\left[\int_{r_1}^r \frac{2}{t}\beta_{\rm ani}(t)dt\right], \tag{2.3}$$

which projects into observable quantities $\sigma_p(R)$ and $I(R)$ as

$$I(R)\sigma_p^2(R) = 2\int_0^\infty \left(1 - \beta_{\rm ani}(r)\frac{R^2}{r^2}\right)\nu(r)\bar{v_r^2}(r)dr\ . \tag{2.4}$$

The Jeans analysis then goes as follows: i) choose a surface brightness profile parameterisation for $I(R)$, fit it to the measured surface brightness $I^{\rm obs}(R)$ and de-project the result to obtain $\nu(r)$ using Eq. (2.2); ii) given parameterisations for the DM density $\rho_{\rm DM}(r)$ and the velocity anisotropy $\beta_{\rm ani}(r)$, use the Jeans equation Eq. (2.3) to obtain $\nu(r)\bar{v_r^2}(r)$; iii) combine this result with $I(R)$ in Eq. (2.4) to get $\sigma_p(R)$; iv) fit the latter to the observed $\sigma_p^{\rm obs}(R)$ to constrain the free parameters of $\rho_{\rm DM}(r)$ and $\beta_{\rm ani}(r)$. This last step is done using a *Markov Chain Monte Carlo* approach (MCMC), by repeating steps ii) and iii) as many times as there are points in the chains. Finally, we use the MCMC chains to compute the J-factors and propagate the corresponding credible intervals (CI).

In our early work, the Jeans analysis part of the workflow was performed by our colleague, Matt Walker, who was then forwarding the MCMC chains of the DM profile parameters to us, so we could compute the J-factors. This was less than practical and Vincent incorporated the Jeans analysis into CLUMPY for its second release, the details of which are given in Bonnivard et al. (2016a).

2.2.2 Getting the right J-factor

Real life being what it is, spherical cows remain elusive and the assumptions made in the Jeans analysis are not necessarily met in dSph galaxies. First, observations show rather elliptical light profiles and numerical simulations suggests that all DM halo are triaxial, which weakens the assumption of spherical symmetry. Furthermore, the Jeans analysis assumes dynamical equilibrium, which will not be the case if the object is being tidally disrupted. Finally, the reconstruction depends on user-defined parameterisations of the light profile $I(R)$, the velocity anisotropy profile $\beta_{\rm ani}(r)$ and the DM density profile $\rho_{\rm DM}(r)$. Sometimes overlooked in the literature [4], some of these choices are critical to a robust J-factor reconstruction. This shall not prevent us from performing the Jeans analysis, but it is important to somehow account for these limitations in the overall error budget of the J-factors.

Following in the footsteps of our earlier studies, we made extensive use of mock datasets to study these effects. We supplemented the original 64 spherical mock dSph we used in Walker et al. (2011) and Charbonnier et al. (2011), with 34 more complex models (including 2 triaxial mock galaxies) generated for the Gaia Challenge [5]. This gave us a broad range of fake data, characterised by various DM, light and anisotropy profiles, on which we could test and optimise the setup of the Jeans analysis. Furthermore, each of the mock dSph could be used to mimick a classical or an ultrafaint dSph galaxy by varying the size of the stellar sample used in the analysis.

4. Most of the studies will select one or two DM profiles (e.g, NFW and core), use a given light profile parameterisation (e.g. Plummer) and assume a constant velocity anisotropy.

5. http://astrowiki.ph.surrey.ac.uk/dokuwiki/doku.php

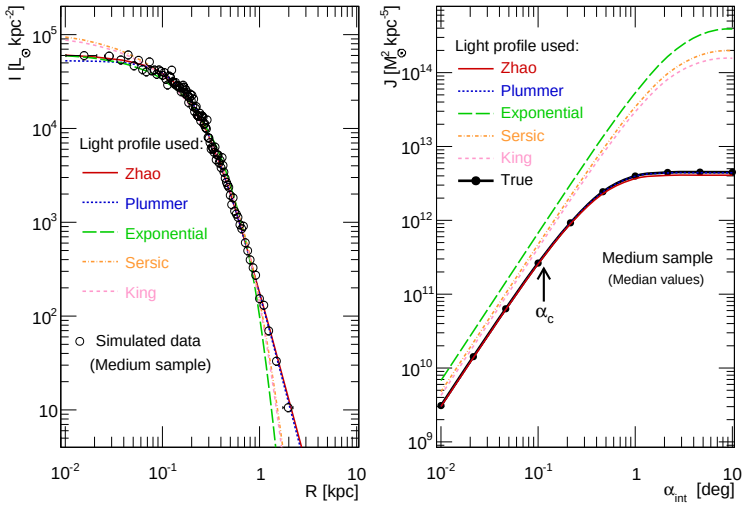

FIGURE 2.5: *Left:* Fit to the light profile of a mock dSph using various standard light profile parameterisations found in the literature (colors). *Right:* Reconstructed J-factors obtained from the Jeans analysis, using the best fit $I(R)$ obtained in the left panel. See text for details.

For the sake of space and legibility, the reader is referred to Bonnivard et al. (2015c) for a detailed description of the possible profile parameterisations that were tested. I simply summarise [6] our findings hereafter:

Light profile The fit of the light profile comes before the Jeans analysis *per se*. We find it to be critical to the subsequent analysis as illustrated in figure 2.5; an underestimation of the light in the outer parts (left panel) yields a drastic overestimation of the total J-factors (right panel). The effect is somewhat mitigated if we restrain the J-factor calculation to the optimal integration angle α_c, but the effect is still a factor of a few, i.e. too large to be ignored. We therefore recommend and use the more flexible Zhao parameterisation (Eq.1.4) to fit the light, prior to running the Jeans analysis.

DM density profile We tested both the Zhao and the Einasto parameterisations (Eqs.1.4 and 1.5) and found that both produce similar reconstruction of the J-factors, whatever the sample size. The Zhao and Einasto profiles have five and three free parameters respectively, and we therefore select the Einasto profile as the default for the Jeans analysis, as less parameters mean faster MCMC runs.

Velocity anisotropy profile Thanks to the Gaia Challenge mock data, we were able to test the effect of assuming a constant anisotropy profile (the most widely used assumption) and show this can lead to a biased reconstruction of the J-factors. This is exemplified in figure 2.6 (left panel), where the J-factor reconstructed using the constant anisotropy (blue) hypothesis overshoots the true value. The safest bet and conclusion is to use a more general form of the velocity anisotropy, namely a Baes & van Hese profile characterised by four free parameters. This bias is only visible for medium and large stellar samples (i.e. classical dSph galaxies) as the large error bars characteristic of the smallest stellar samples (ultrafaint dSph) render that effect irrelevant.

Triaxiality The problem of triaxiality is twofold. First, the J-factor of a given triaxial halo, for which we perfectly know the DM distribution, will not be the same depending on the orientation of the DM halo on the sky. The effect is however relatively small, with a $\sim 30\%$ difference between

6. Table 4 in Bonnivard et al. (2015c) also gives a very concise summary of these findings.

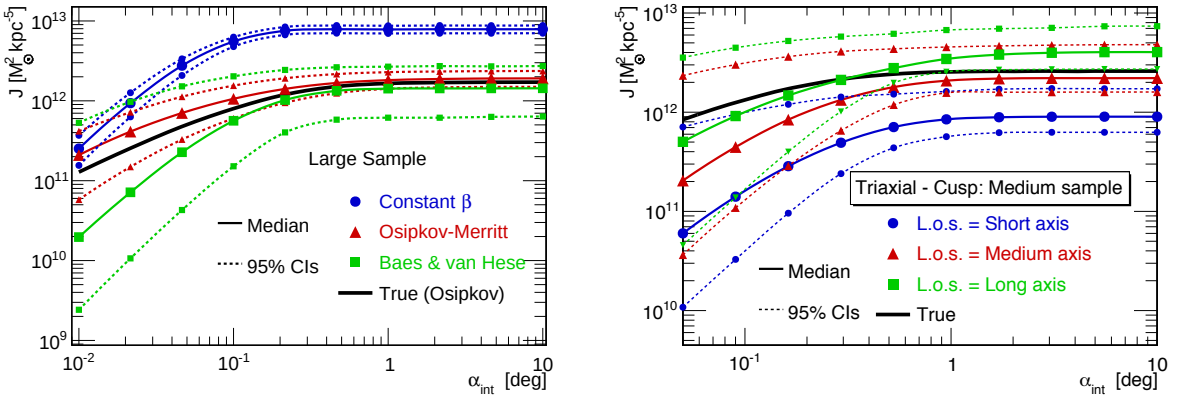

FIGURE 2.6: *Left*: Effect of the velocity anisotropy parameterisation. Median $J(\alpha_{\rm int})$ and 95% CIs of a mock dSph (generated with an Osipkov-Merritt velocity anisotropy) reconstructed using different anisotropy prescriptions (colours). The true $J(\alpha_{\rm int})$ is given in solid black. *Right*: Effect of triaxiality. Median (solid lines) and 95% CIs (dotted lines) J values reconstructed with the spherical Jeans analysis on a mock classical triaxial dSph, for three l.o.s. orientations.

the most extreme orientations. More worrying is the assumption of spherical symmetry made in the standard Jeans analysis. The Gaia challenge provided two datasets from which the velocity dispersion profiles were computed assuming that the line of sight was parallel to the triaxial dSph's small, intermediate and long axis. The spherical Jeans analysis was then performed on each of these datasets and the result shown in figure 2.6, right panel. The reconstruction typically yields a result a factor of $\sim 2-3$ away from the truth, with the error bars not always encompassing the true value (blue). In practice, the orientation of the dSph DM halos is unknown so that the effect should be added to the error budget separately. We note that Sanders et al. (2016) reached similar conclusions and provide analytical formulas to correct the J-factors (obtained using the spherical modelling) for the effect of a flatten morphology.

The above systematics study has also been performed for DM decay and the conclusions reached are roughly the same. We therefore use the same optimal Jeans analysis setup (Einasto DM profile, Zhao light profile, Baes & van Hese velocity anisotropy profile, plus a few justified cuts in the parameter space not discussed here) for both decay and annihilation.

2.2.3 Identifying the most promising dSph targets

We applied the optimal Jeans analysis defined above to all 23 dSph galaxies for which spectroscopic data was available at the time. These include the eight classical dSph galaxies from our earlier works, the 13 ultrafaint dSph galaxies later discovered in the SDSS data (see Belokurov et al. 2006 for an exemple) and the two recently-discovered ultrafaint dSph galaxies identified in the data of the Dark Energy Survey (DES) in 2015 (Koposov et al. 2015). The results were published in Bonnivard et al. (2015a) for 8 classical + 13 SDSS dSph galaxies, in Bonnivard et al. (2015b) for Reticulum II, and in Walker et al. (2016) for Tucana II [7].

Figure 2.7 summarises the results for the J-factors computed for a $\alpha_{\rm int} = 0.5°$ integration angle and compares them to that of other works. A similar figure was produced for the DM decay but is not included here. The overall trend is expected and is the same for all studies, with the closest

7. I was not involved in the Tucana II analysis. Vincent ran the optimal Jeans analysis on the latest data obtained by Matt Walker and was a co-author of the paper.

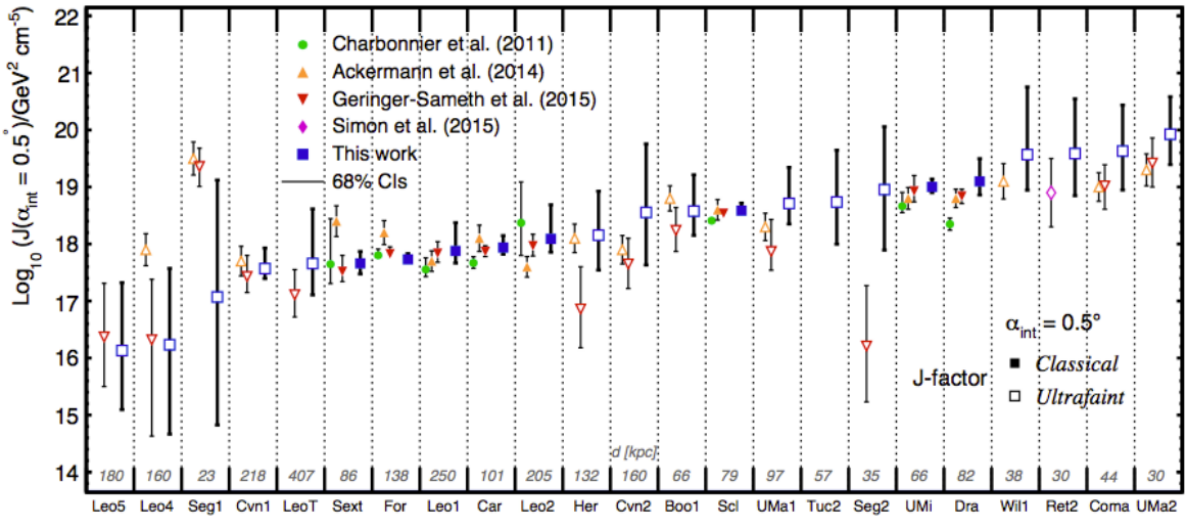

FIGURE 2.7: J-factors and 68% CIs for $\alpha_{\rm int} = 0.5°$ and comparison to other works.

objects having the highest J-factors. From this work, we identified Ursa Major II, Coma and Reticulum II to be the most promising targets [8]. The main differences with other works are as follows:

- For the eight classical dSph, our updated results are slightly larger than that of our original work (Charbonnier et al. 2011). The more flexible light profile and anisotropy parameterisations we are now using, compared to the Plummer profile and constant anisotropy we used previously are responsible for this change.
- Our results display larger error bars than other works. This is understandable given that we use a very flexible Jeans analysis, this flexibility being required to produce unbiased J-factors and a robust error budget. In our data-driven approach, fainter object (smaller stellar samples) will have larger error bars. This was not the case in the third *Fermi*-LAT analysis (Ackermann et al. 2014b) where their error bars remain roughly the same regardless of the nature of the object ('classical' or 'ultrafaint'). This is very likely related to their two-level hierarchical analysis, where the population of MW dSph galaxies is treated as a whole.
- The J-factors of Geringer-Sameth et al. (2015a) tend to be systematically lower than what we find. This is mainly due to the choice of halo radius made by these authors, who use the outermost star location as halo boundary while we use the tidal radius. Their choice is a very conservative one that may lead to an underestimation of the J-factors.
- Finally, we find Segue I to be very discrepant with other studies and a far less promising target than previously thought. Clarifying this issue is very important as ground-based IACTs have been using Segue I as a favourite target, spending significant amount of time for its observation. We believe this behaviour highlights a possible contamination of the kinematic sample by foreground stars and Bonnivard et al. (2016b) have shown, using hundreds of mock data including various levels of contamination, that it may well be the case. Sample contamination is a major problem for these types of analyses (see footnote 8) and various

8. Another object, Triangulum II had a short-lived fame when it was thought to be the most DM-dominated dSph galaxy (Kirby et al. 2015) and a prime target for indirect DM (Genina and Fairbairn 2016), although it was not clear that the system was in dynamical equilibrium (Martin et al. 2016). Kirby et al. (2017) recently showed that the original spectroscopic data was contaminated by a binary star, artificially inflating the velocity dispersion, and that Triangulum II is either a globular cluster or a tidally-stripped dSph galaxy and in any case, not so DM-dominated after all.

methods have been and keep being developed to mitigate against its effects (Walker et al. 2009b; Ichikawa et al. 2017).

In summary, these results highlight the importance of underlying assumptions for the determination of the J-factors. This work has identified the various sources of uncertainties that affect J-factor estimations, following the thorough validation of the method done using mock data. Our data-driven analysis naturally implies larger error bars for dSphs with fewer stars, and vice-versa. Also, thanks to a more flexible parameterisation of the light profile, we find higher J-factors for some targets, which may lower further the upper limits for the DM annihilation cross section.

Dwarf spheroidal galaxies still allow room for improvement. One may expect that many more of them will be discovered by LSST, which will expand our sample of interesting targets (provided some of the new dSphs are located close enough to us). As spectroscopic follow-ups with current instruments is a lengthy process, scaling relations [9] of J-factors are also being explored to provide fast estimates without the full dynamical analysis or spectroscopic datasets (Drlica-Wagner et al. 2015; Pace and Strigari 2018). In the near future, next-generation spectrographs such as the Prime Focus Spectrograph to be mounted on the Subaru telescope (Tamura et al. 2016) or the Maunakea Spectroscopic Explorer project at CFHT (McConnachie et al. 2016), will be able to provide larger spectroscopic samples ($\sim$ 1 order of magnitude larger), yielding better DM profile reconstruction, and less uncertain J-factors. While we may never see a DM signal from these objects, the improved measurements will ensure an improved robustness of future exclusion plots.

9. A $1/d^2$ dependence is the most obvious

3

Focus on the extragalactic scale

Contents

In this chapter, I now turn to the extragalactic targets of interest when searching for DM-induced gamma-ray emission: galaxy clusters (§3.1) and the diffuse γ-ray emission (§3.2).

3.1 Galaxy clusters

Galaxy clusters are the largest gravitationally bound structures in the Universe. Being such large reservoirs of dark matter, they have naturally been considered as interesting targets for DM indirect detection. In 2012, after having completed our study of the eight classical dSph galaxies, we turned our attention to these objects. Given that we know thousands of relatively close-by clusters, we wanted to study the benefits of a stacking strategy for DM annihilation and decay, be it for space (i.e. *Fermi*-LAT) or ground-based instruments (e.g. CTA); the results were published in Nezri et al. (2012) and Combet et al. (2012) respectively. Compared to dSph galaxies, galaxy clusters are more challenging targets as a cosmic ray-induced γ-ray contribution is also expected from these objects. In Maurin et al. (2012), we also investigated whether the same stacking strategy could help disentangling the CR-induced from the exotic γ-ray component. It was also around this time that the community got excited by a possible line emission at 110-130 GeV that was claimed to exist [1] from both the Galactic centre (Weniger 2012) and galaxy clusters (Hektor et al. 2013). The latter were therefore attracting significant attention, especially given the large boost factors that were expected at the time (§3.1.2.1).

It has been a few years since we published these results and we have not pursued further our investigation of these objects in the context of DM indirect detection since. I will first focus on the boost factor and its implementation in CLUMPY in §3.1.1, and follow by presenting the main results of the stacking study we undertook in §3.1.2. Finally, I will also briefly mention in §3.1.3

1. This excess emission was however not confirmed by subsequent analyses.

the work of Antoine Lacroix, a M1 student I supervised in 2016, who worked on applying the Jeans analysis to nearby clusters of galaxies.

3.1.1 CLUMPY: boost factor from DM substructures

Consider a DM halo (e.g. a galaxy cluster) characterised by a smooth DM density $\rho_{\rm sm}$ and a population of substructures with densities $\rho^i_{\rm cl}$. Integrated along the line-of-sight, within a solid angle $\Delta\Omega$, the corresponding J-factor reads

$$J = \int_0^{\Delta\Omega} \int_{l_{\rm min}}^{l_{\rm max}} \left(\rho_{\rm sm} + \sum_i \rho^i_{\rm cl} \right)^2 {\rm d}l\, {\rm d}\Omega \;\equiv J_{\rm sm} + J_{\rm subs} + J_{\rm cross-prod}\;, \tag{3.1}$$

where the rightmost term is a formal expansion of the square bracket. Defining the intrinsic luminosity of a DM clump $\mathcal{L}(M,c)$ as

$$\mathcal{L}(M,c) \equiv \int_{\rm V_{cl}} \rho^2_{\rm cl}(M,c)\, {\rm d}V\,, \tag{3.2}$$

and considering the continuum limit for $N_{\rm tot}$ substructures and with the spatial ($\mathrm{d}\mathcal{P}_V/\mathrm{d}V$), mass ($\mathrm{d}\mathcal{P}_M/\mathrm{d}M$) and concentration ($\mathrm{d}\mathcal{P}_c/\mathrm{d}c$) distributions described in §1.2.2.1, the average J-factor from the clumps can be written as

$$\begin{aligned}\langle J_{\rm subs}\rangle \;&= N_{\rm tot} \int_0^{\Delta\Omega} \int_{l_{\rm min}}^{l_{\rm max}} \frac{{\rm d}\mathcal{P}_V}{{\rm d}V}(l,\Omega)\, {\rm d}l\, {\rm d}\Omega \int_{M_{\rm min}}^{M_{\rm max}} \frac{{\rm d}\mathcal{P}_M}{{\rm d}M}(M) \\ &\times \int_{c_{\rm min}(M)}^{c_{\rm max}(M)} \frac{{\rm d}\mathcal{P}_c}{{\rm d}c}(M,c)\, \mathcal{L}(M,c)\, {\rm d}c\, {\rm d}M\;.\end{aligned} \tag{3.3}$$

The average cross-product term reads

$$\langle J_{\rm cross-prod}\rangle = 2 \int_0^{\Delta\Omega} \int_{l_{\rm min}}^{l_{\rm max}} \rho_{\rm sm} \langle \rho_{\rm subs}\rangle {\rm d}l\, {\rm d}\Omega\;, \tag{3.4}$$

with $\langle\rho_{\rm subs}\rangle$ the spherically-averaged density of substructures (i.e. $\langle\rho_{\rm tot}\rangle(r) = \rho_{\rm sm}(r) + \langle\rho_{\rm subs}\rangle$). From these, the boost factor is then defined as

$$\text{boost} \equiv \frac{J_{\rm sm} + \langle J_{\rm subs}\rangle + \langle J_{\rm cross-prod}\rangle}{J_{\rm no-subs}}\;, \tag{3.5}$$

where $J_{\rm no-subs} = \int \langle\rho_{\rm tot}\rangle^2 {\rm d}l{\rm d}\Omega$. The above description only accounts for a single level of substructures and was implemented as such in the first version of CLUMPY, minus the concentration dependence that Vincent and myself included in the second release. It is this first level of substructures that contributes the most to the boost factor, and we found typical values of $\sim 10-100$ in the cluster mass range ($10^{14} - 10^{15}$ $\mathrm{M}_\odot$) (see §3.1.2, figure 3.2).

Nonetheless, the hierarchical structure formation scenario gives a multi-level view of substructures, with clumps within clumps within clumps, etc. We have therefore also accounted for this effect in CLUMPY's second release using an iterative approach. Not considering any substructure,

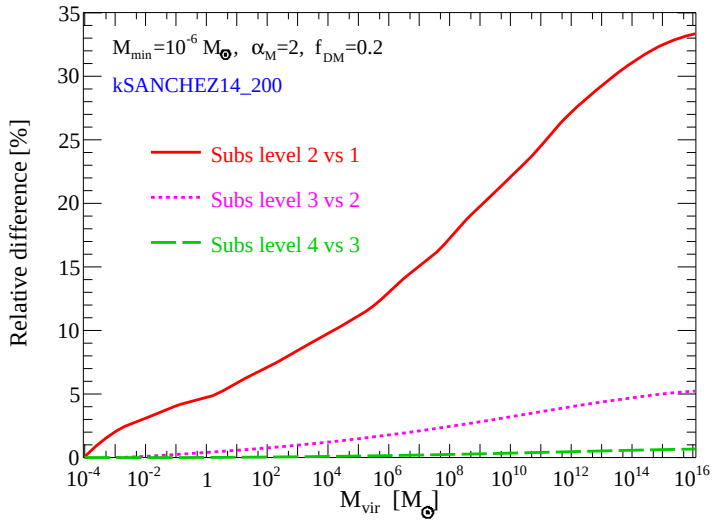

FIGURE 3.1: Relative difference of the J-factors when including one extra level $n+1$ of substructure with respect to the previous level n. Results are shown as a function of the host halo mass. Figure taken from Bonnivard et al. (2016a).

the intrinsic luminosity [2] $\mathcal{L}_0$ of a given DM halo of density $\rho_{\rm tot}$ is directly given by

$$\mathcal{L}_0(M,c) \equiv \int_{V_{\rm cl}} \left[\rho_{\rm cl}^{\rm tot}(M,c)\right]^2 \, {\rm d}V \, . \tag{3.6}$$

From this, a hierarchy of n levels of substructures within this host halo ($n = 1, 2, 3$, etc.), may be iteratively computed from the $n-1$ level as

$$\mathcal{L}_n(M) = \mathcal{L}_{\rm sm}(M) + \mathcal{L}_{\rm cross-prod}(M) \quad + N_{\rm tot}(M) \int_{M_{\rm min}}^{M_{\rm max}(M)} \mathcal{L}_{n-1}(M') \frac{{\rm d}\mathcal{P}}{{\rm d}M'}(M') dM' \, , \tag{3.7}$$

with

$$\mathcal{L}_{\rm sm}(M) \equiv \int_{V_{\rm cl}} \left[\rho_{\rm cl}^{\rm sm}(M)\right]^2 \, {\rm d}V, \quad \text{and} \quad \mathcal{L}_{\rm cross-prod}(M) \equiv 2 \int_{V_{\rm cl}} \rho_{\rm cl}^{\rm sm}(M) \, \langle \rho_{\rm subs}(M) \rangle \, {\rm d}V \, . \tag{3.8}$$

The effect of including $n > 1$ levels of substructures is shown in figure 3.1. In the configuration chosen in this example [3] we find that including a second level of substructure increases the J-factor by $\sim 30\%$ in the galaxy cluster mass range (solid red line). Going to a third level only has a much smaller impact, adding an extra 5% (dotted pink) and any extra-level may be neglected (dashed green). Of course, these results depends on all the substructure properties entering the computation (mass fraction contained in substructures, spatial and mass distributions, choice of the mass-concentration relation, minimum mass for the substructures), but similar conclusions have been reached by others, using different approaches (e.g., Sánchez-Conde and Prada 2014). These extra levels are generally neglected in the literature and in the next section.

2. This is done assuming that the host DM halo is fully encompassed within the integration angle, and far enough to suppose that all substructures and the host halo are at the same distance. In that case, one may consider directly the intrinsic luminosity rather than the J-factor.

3. Here, we consider that 20% of the mass is in the form of substructures, that they reach a minimum mass of $10^{-6} {\rm M}_\odot$, with a mass distribution ${\rm d}\mathcal{P}_M/{\rm d}M \propto M^{-2}$ and a Sánchez-Conde and Prada (2014) mass-concentration relation.

3.1.2 Stacking - an interesting option?

Owing to their large DM content and the possibility of large substructure boosts, galaxy clusters have been largely considered for indirect detection, with analyses performed using both *Fermi*-LAT (Ackermann et al. 2010) and ground-based data (VERITAS, HESS, e.g, Arlen et al. 2012; Abramowski et al. 2012, 2014a). For ground-based observations with IACTs, identifying the most favourable targets is mandatory to make the best possible use of the allocated time. This is not an issue for all-sky survey instruments like *Fermi*-LAT but in that case a stacking analysis could be beneficial.

In Combet et al. (2012) and Nezri et al. (2012), we addressed these questions for DM decay and annihilation respectively in order to i) established a ranking of the best clusters in terms of J-factors [4] and ii) quantify the benefits of a stacking strategy. We did so using the Meta-catalogue of X-ray detected clusters (MCXC, Piffaretti et al. 2011); the latter contains 1743 clusters of galaxies detected in X-rays and assembled from public catalogues available at the time, mainly based on the ROSAT All-Sky Survey or ROSAT serendipitous catalogues. It provides homogenised quantities for each cluster at $\Delta = 500$, including the mass M_{500} within R_{500}, and was therefore the ideal data set on which to perform this analysis.

3.1.2.1 Boost and J-factors of the MCXC galaxy clusters

For the smooth component, we have assumed each MCXC cluster to be described by a NFW DM profile (Eq. 1.4 with $(\alpha, \beta, \gamma) = (1, 3, 1)$), the normalisation ρ_s and scale radius r_s of which being computed assuming the Duffy et al. (2008) mass-concentration (see §1.2.2.1).

Ranking of the best targets On top of this smooth component, we also consider substructures with the following properties: i) $dN_{\rm subs}/dM \propto M^{-1.9}$ with a mass fraction $f = 10\%$ in substructures (Springel et al. 2008), a minimal and maximal mass of $10^{-6}\ M_\odot$ and $10^{-2} M_{\rm cluster}$ respectively, and the Bullock et al. (2001) concentration (down to the minimal mass); ii) the substructure spatial distribution $dN_{\rm subs}/dV$ follows the host halo smooth profile. From this setup, we computed the astrophysical factors with CLUMPY.

Table 3.1 gives the 10 brightest clusters of the MCXC catalog, ordered with decreasing values of the J-factor (third and fourth columns). We also computed the Galactic exotic background $J_{\rm Gal}$ expected at the location of these clusters. The ratio to $J_{\rm Gal}$ can then be used to rank the clusters in terms of contrast to the exotic background (fifth and sixth columns); Virgo and A426 (Perseus) remain the top two targets in both cases, consolidating their status of prime cluster targets for IACTs. The remaining clusters are significantly reshuffled between the two ranking criteria, depending on their position with respect to the Galactic centre.

Boost uncertainty For each galaxy cluster in the MCXC, we compute the boost factors as defined by Eq. (3.5) using a single level of substructures. As mentioned before, the description of the substructures within a host halo depends on a lot of properties that remain quite uncertain; the choices we made for the ranking exercise above provide just one possible configuration. Figure 3.2 shows the histograms of the boosts when varying some of these properties and highlights the theoretical uncertainty that plagues the boost estimation. Our reference model (solid black line) aimed at being conservative. The other histograms (colours) show possible variations of this

4. At low redshifts, cosmology and absorption of γ-rays can be neglected so that reasoning in terms of J-factors is still valid. This will not be the case when considering the overall exotic extragalactic γ-rays, as discussed in §3.2.

Name	d (Mpc)	$\log_{10}\left[J(\alpha_{\rm int})/(M_\odot^2\ {\rm kpc}^{-5})\right]$ (0.1°)	(0.5°)	$\frac{J(\alpha_{\rm int})}{J_{\rm Gal}(\alpha_{\rm int})}$[rank]‡ (0.1°)	(0.5°)
Virgo	15.4	11.1	11.8	20.7 [2]	4.9 [1]
A426	75	10.8	11.5	21.2 [1]	4.5 [2]
A3526	48.1	10.7	11.4	4.7 [30]	0.9 [17]
NGC 4636	13.2	10.6	11.4	6.8 [13]	1.4 [9]
A3627	66	10.6	11.3	1.4 [-]	0.3 [-]
Coma	96.2	10.6	11.3	7.7 [10]	1.6 [8]
NGC5813	21.3	10.6	11.3	2.7 [-]	0.6 [39]
Ophiuchus	116.	10.6	11.2	0.1 [-]	0.02[-]
NGC5044	36.9	10.5	11.2	3.6 [-]	0.7 [-]
AWM7	72.1	10.5	11.2	11.5 [3]	2.3 [3]

TABLE 3.1: Ten brightest galaxy clusters from the MCXC and their contrast $J/J_{\rm Gal}$ for $\alpha_{\rm int} = 0.1°$ and $\alpha_{\rm int} = 0.5°$. The DM Galactic background $J_{\rm Gal}$ is evaluated at the position of the cluster. Whenever the rank is larger than 50, we use [-].

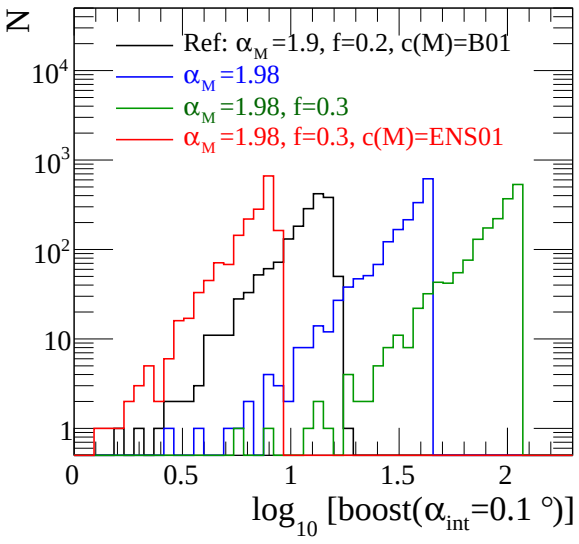

FIGURE 3.2: Histogram of the boost factors computed for each of the MCXC clusters. The different colours correspond to incremental changes of substructure configurations w.r.t. the reference (black): i) steepening the mass function (blue), ii) increasing the substructures mass fraction (green), iii) changing the mass-concentration relation (red). Adapted from Nezri et al. (2012).

configuration, while always staying in the realm of the values/parameterisations published at the time.

Without entering into too much details, this figure shows that for clusters, typical values of the boost lie within 10 – 100. Steepening the mass function (blue) has a large impact as it will increase the number of low mass clumps. The minimum mass of the clumps is also critical but not shown here. Of course, combining a steeper mass function with a larger fraction of substructures can bring the boost to even larger values (green), but the effect can be completely counter-balanced by a different choice of mass-concentration parametrisation (red). We also found that changing the spatial distribution of the clumps had far less impact than the above quantities.

Around the time we undertook this study and in contradiction with our results, it was often claimed that the boost factor in galaxy clusters could reach $\sim 10^3$ (e.g. Pinzke et al. 2011; Gao et al. 2012; Han et al. 2012), making them all the more interesting for indirect detection. The reason behind these high values was that these authors were extrapolating, using simple power laws, the mass-concentration relations established by numerical simulations (i.e. at the high mass range $\gtrsim 10^{11}$ $M_\odot$), down to the DM halo minimum mass, generally taken to be $M_{\rm min} = 10^{-6}$ $M_\odot$.

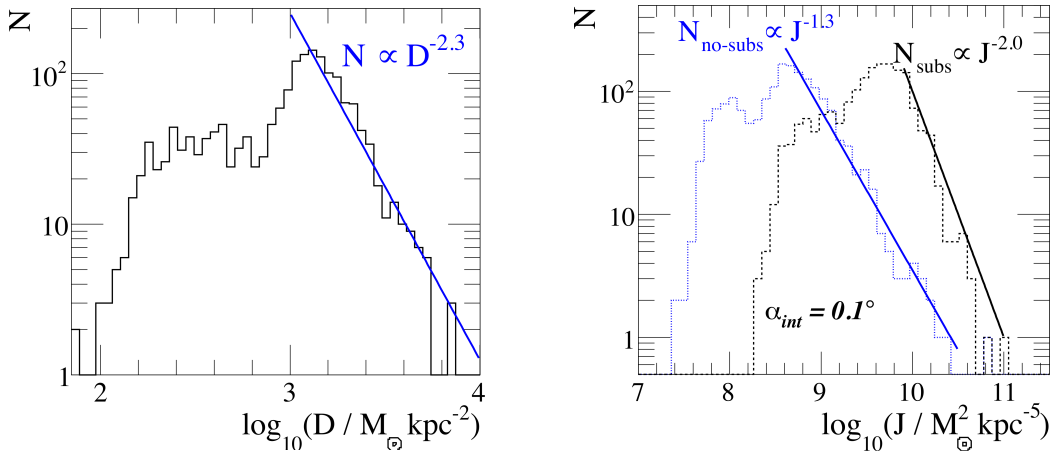

FIGURE 3.3: Distribution of the $\log_{10} N - \log_{10} J$ for decaying (left) and annihilating (right) dark matter. For annihilating dark matter, clusters have been considered as hosting substructures (back) or not (blue). For the former, we have used the reference substructure configuration described in §3.1.2.1. Figures from Combet et al. (2012) and Nezri et al. (2012).

The qualitative behaviour at low mass of the toy model of Bullock et al. (2001) that we have used as our reference is in agreement with results obtained in the low mass range by later numerical simulations (Sánchez-Conde and Prada 2014) [5]. Boost factors of $\sim 10^3$ for galaxy clusters have since also been ruled out by others and are generally not considered anymore.

3.1.2.2 Stacking

As mentioned above, another objective of this work was to evaluate to what level could a stacking strategy be beneficial. To first order, and without considering any instrumental features, one may evaluate the interest of a stacking strategy from the slope $[\log_{10} N - \log_{10} J]$ histograms. Indeed, a slope steeper than -1 means that there are more than ten times more objects being ten times less luminous, so that stacking could be beneficial for all-sky γ-ray survey instruments such as *Fermi*-LAT. These histograms are displayed in figure 3.3 for the decaying (left) and annihilating (right) DM cases. The turnover in the histograms comes from the incompleteness of the catalogue at low X-ray luminosity and will be pushed down to lower J values by future X-ray catalogues (such as promised by the next generation X-ray satellites, eROSITA (medium term) and ATHENA (long term)).

For decaying dark matter, we find $N \propto D^{-2.3}$ which suggests that stacking could be a good option. Assuming an ideal background-free situation, we find that stacking could improve the limits on decaying DM by a factor ~ 100, compared to simply considering the brightest cluster. One must however also consider the corresponding increase of the astrophysical and exotic backgrounds coming from diffuse cosmic-ray propagation and Galactic and extragalactic DM-induced γ-rays. The background increases faster than the signal as a function of the integration angle $\alpha_{\rm int}$ so that some compromise between total flux and signal-to-noise ratio must be considered. In the background-limited regime, we find the SNR to peak after stacking 29, 948 and 971 clusters for $\alpha_{\rm int} = 0.5°,\ 0.1°$, and $0.05°$. In this more realistic case, a stacking strategy yields a factor ~ 5 increase only.

5. The comparison has actually been performed on an updated version of the Bullock et al. (2001) toy model by Macciò et al. (2008), but the behaviour at the low mass end, relevant to our purpose here, was the same in both cases.

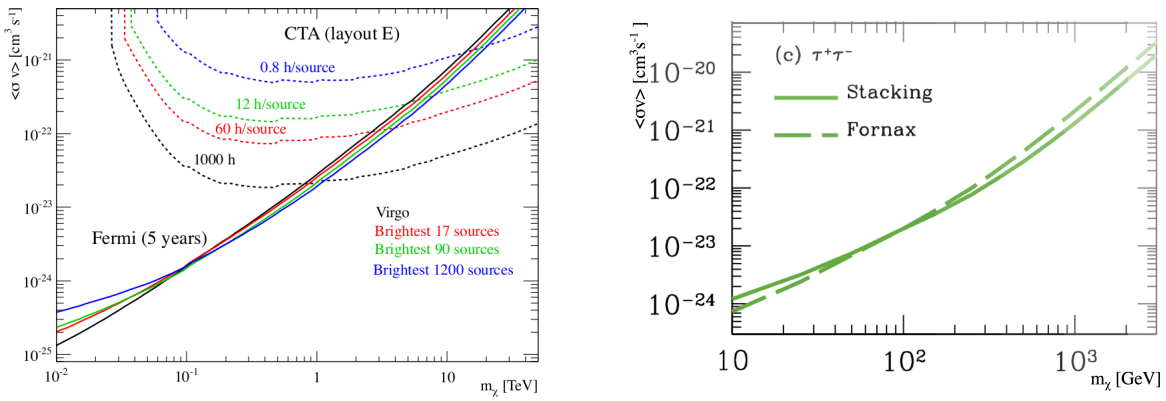

FIGURE 3.4: *Left*: Our forecast limits of a stack analysis using 5 years of *Fermi*-LAT data (dashed lines) or 1000h of CTA observation time (dotted lines). Figure published in Nezri et al. (2012). *Right*: Adapted from Ando and Nagai (2012). Limits obtained by analysing 2.8 years of *Fermi*-LAT data focusing either of the Fornax cluster alone (dashed line) or performing a stacking analysis of 49 bright galaxy clusters. To be compared to our forecast on the left.

In the case of annihilating DM and if substructures were absent, a stacking approach would not bring anything as $N \propto J^{-1.3}$ (fig. 3.3, right panel, blue). Including the boost from substructures, $N \propto J^{-2}$, stacking could be considered. Using similar considerations as above, we predicted a factor ~ 2 improvement from a stacking strategy in the background-limited regime. From a more realistic treatment, using *Fermi*-LAT performances and background models available at the time and assuming a 5 year exposure, we computed the limits in the $\langle\sigma v\rangle - m_\chi$ plane displayed in figure 3.4 (left panel, solid lines). Above 100 GeV, we found a marginal gain in stacking the brightest clusters (coloured lines), compared to focussing on the brightest one (Virgo in this case, black). Interestingly, similar conclusions were reached independently a few months later by Ando and Nagai (2012), who used 2.8 years of *Fermi*-LAT data focussing either on the Fornax cluster alone (dashed green) or performing a stacking analysis of 49 bright galaxy clusters (solid green). Because CTA will rely on pointed observations, any amount of observing time will have to be split between sources. In that case, the best strategy is to observe for as long as possible the brightest clusters rather than spending time on fainter objects. This is shown as the dashed lines in figure 3.4 (left), where the best limit is obtained by observing Virgo only.

Since this work, the multiplication of surveys and the growing interest in cluster cosmology in the last decade have generated a large number of new cluster catalogues since the MCXC, supplementing X-ray catalogues with SZ and optical datasets (e.g., Wen et al. 2012; Wen and Han 2015; Bleem et al. 2015; Tully 2015; Planck Collaboration et al. 2016a; Takey et al. 2016). Given that distance is critical to DM indirect detection, going to the larger redshifts probed by SZ catalogues will not be particularly beneficial for our purpose here [6]. Conversely, catalogues constructed from optical datasets (e.g. the Tully 2015 catalogue based on 2MASS survey) allow to detect much smaller structures (i.e. galaxy groups [7]) located closer to us and are currently being used in stacking analyses using *Fermi*-LAT data, showing promising preliminary results (Quincy Adams et al. 2016, Rodd's and Sharma's presentations at TeVPA 2017). To my knowledge and at the time of this writing, these studies have not been published/accepted for publication yet.

6. This is not the case of cluster cosmology, as we will discuss in chapter 6.

7. Galaxy groups are a loosely defined concept but include small structures, with only a few member dwarf galaxies and masses as small as a few 10^{11} $M_\odot$.

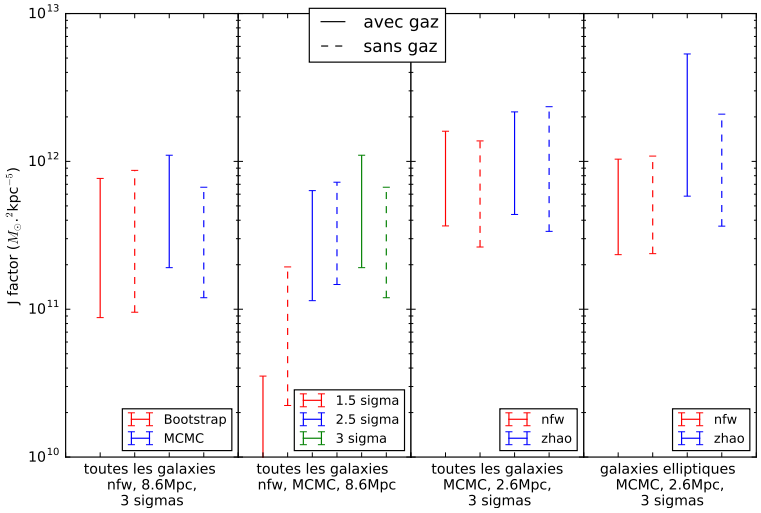

FIGURE 3.5: J-factor of the Coma cluster obtained using the Jeans analysis including gas (solid lines) or not (dashed lines). The various panels and colours correspond to various configurations or data cuts. Figure taken from Antoine Lacroix's end-of-year project report.

3.1.3 Jeans analysis in galaxy clusters

To close this section on galaxy clusters, I will briefly mentioned the work of Antoine Lacroix, whom I supervised for his 4-month Master's end-of-year project. Similarly to dSph galaxies, the mass of galaxy clusters can be estimated using the Jeans analysis from the velocity dispersion of the galaxies within the cluster. Assuming that clusters are spherical and in dynamical equilibrium (which is generally not true), the main difference with the Jeans analysis presented in §2.2.1 is that the intra-cluster gas amounts to a significant fraction of the cluster total mass, so that the assumption $\rho_{\rm tot}(r) = \rho_{\rm DM}(r)$ should be replaced by $\rho_{\rm tot}(r) = \rho_{\rm DM}(r) + \rho_{\rm gas}(r)$.

Antoine's project was to make the necessary modifications into CLUMPY to include a gaseous component in the Jeans analysis and apply it to known close-by clusters of galaxies, such as Coma, for which the galaxy velocities are available in the NASA Extragalactic Database (NED). Similarly to the case of dSph galaxies presented before, this approach allows the propagation of data-driven error bars all the way to the J-factors, but is limited to the few clusters for which sufficient spectroscopic data is available. The results Antoine obtained are summarised in figure 3.5. Apart from when a stringent data cut is applied (red, second panel), we found that including a gaseous component (solid lines) or not (dashed line) gives compatible J-factors, whatever the chosen configuration for the analysis (different panels and colours). The values of the J-factors are also compatible with the one we computed for Coma using the MCXC mass M_{500} obtained from X-ray observations.

3.2 Diffuse extragalactic exotic emission

When restricting ourselves to working at the level of the local Universe, such as in the above studies, the exotic gamma-ray flux could be written as the product of two independent terms, the astrophysical factor J and the particle physics term (see §1.1.2). At these local scales, the gamma-ray source spectrum is neither redshifted nor absorbed so the only dependence with distance is a straightforward $1/d^2$ dilution. However, when one is interested in the extragalactic exotic contribution, coming from the cumulative effect of all DM halos along the line-of-sight, cosmology needs to be accounted for and the formalism becomes more intricate.

3.2.1 Formalism for the extragalactic contribution

Focusing on DM annihilations only, the average isotropic differential intensity observed at Earth (redshift $z = 0$) at energy E_γ, integrated up to redshift $z_{\rm max}$ may be written as

$$I(E_\gamma) = \left\langle \frac{\mathrm{d}\Phi}{\mathrm{d}E_\gamma\,\mathrm{d}\Omega} \right\rangle_{\rm sky} = \frac{\overline{\rho}^2_{\rm DM,\,0}\,\langle\sigma v\rangle}{8\pi\, m_\chi^2} \int_0^{z_{\rm max}} c\,\mathrm{d}z\, \frac{(1+z)^3}{H(z)} \left\langle \delta^2(z) \right\rangle \left. \frac{\mathrm{d}N^\gamma_{\rm source}}{\mathrm{d}E_e} \right|_{E_e=(1+z)E_\gamma} \times e^{-\tau(z,\,E_\gamma)}\,, \tag{3.9}$$

with E_γ the observed energy, Φ the flux, $\mathrm{d}\Omega$ the elementary solid angle, c the speed of light, $\overline{\rho}_{\rm DM,\,0}$ the DM density of the Universe today, and $H(z)$ the Hubble constant at redshift z. The remaining quantities in the equation are as follows:

- As previously introduced in §1.1.2, m_χ and $\langle\sigma v\rangle$ are the mass and velocity-averaged annihilation cross sections of the DM candidate χ, respectively. The differential flux $\mathrm{d}N^\gamma_{\rm source}/\mathrm{d}E_e$ gives the number of γ-ray photons emitted at energy E_e (at the source located at redshift z) per DM annihilation. This is the sum of all possible channels, weighted by their branching ratios.
- These γ-ray photons will not only be redshifted by the expansion of the universe, but may be absorbed along their journey, by interacting with lower energy photons of the Extragalactic Background Light (EBL) or of the CMB to produce e^+e^- pairs. This absorption is parametrised by the optical depth $\tau(z, E_e)$.
- Cosmology comes into play through the Hubble expansion rate $H(z)$, the redshift terms, and the DM density squared $\rho^2_{\rm DM}(z) = \langle\delta^2(z)\rangle \times \overline{\rho}^2_{\rm DM,0}$. For smoothly distributed DM, the clumping factor (or intensity multiplier) $\langle\delta^2\rangle = 1$, whereas for a high density contrast, $\langle\delta^2\rangle \approx \mathrm{Var}(\delta) \gg 1$. The flux multiplier is computed from the halo mass function [8] $\mathrm{d}n(z)/\mathrm{d}M$ and the halo inner density profiles $\rho_h(r|M,z)$ [9] as

$$\delta^2(z) = \frac{1}{\bar{\rho}^2_{m,0}} \int_{M_{\rm min}}^{M_{\rm max}} \frac{\mathrm{d}n}{\mathrm{d}M}(M,z)\mathrm{d}M \int_{V_h} \rho^2_h(r|M,z)\mathrm{d}V\,. \tag{3.11}$$

  Furthermore, the mass function itself depends on the matter power spectrum $p(k,z)$, hence on the underlying cosmological model. With this expression, we are only considering annihilations from DM bound into isolated halos, therefore neglecting any contribution from DM filaments or unbound DM.

3.2.2 Implementation in CLUMPY

Planning for the third release of CLUMPY, I implemented the extragalactic contribution as described above in the code sometime in 2016. Leaving this aside for a while due to my increasing

8. This is the comoving number density of DM halos of a given mass at a given redshift and reads

$$\frac{dn(M,z)}{dM} = \frac{\rho_m}{M}\frac{d\ln\sigma^{-1}}{dM} f(\sigma,z)\,, \tag{3.10}$$

with ρ_m the mean matter density, σ the amplitude of the density fluctuations (and that depends on the matter power spectrum $p(k)$), and $f(\sigma,z)$ the so-called halo multiplicity function that encodes the non linear effects of the growth of structures. It is the parametrisation of the latter term that is referred to when mentioning the various mass functions found in the literature.

9. For a halo of mass M at redshift z and a choice of profile (e.g., NFW or Einasto), the scaling of the DM profile $\rho_h(r|M,z)$ depends on the concentration parameter $c(M,z)$ introduced in §1.2.2.1.

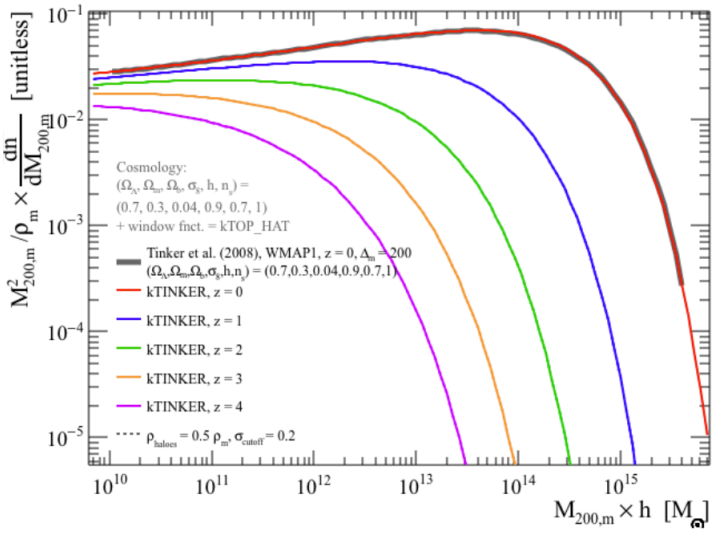

FIGURE 3.6: The Tinker et al. (2008) mass function computed by CLUMPY at different redshifts (colors) from the matter power spectrum produced by CLASS for the set of cosmological parameters quoted on the figure.

involvement in LSST (see part II), this implementation was thoroughly checked [10] by Moritz Hütten during his 3 months visit at LPSC, towards the end of his PhD, in early 2017.

Cosmology and mass functions The matter power spectrum $p(k, z)$ is required to compute the mass function $\mathrm{d}n/\mathrm{d}M$. To do so, I have interfaced CLUMPY with the Boltzmann code CLASS [11] (Lesgourgues 2011) that evolves linear perturbations in the universe from a given set of cosmological parameters and computes CMB and large scale structure observables, among which the matter power spectrum.

The computation of the mass function is largely based on the implementation of Komatsu's very useful Cosmology Routine Library in Fortran [12], from which I translated in C the parts relevant to this work. The formalism of the mass function is well-established, but different authors, running different large scale numerical simulations with different underlying cosmologies, will find different values for the parameters to be used in the mass function.

As has always been our approach with CLUMPY, we provide the user with a variety of mass function parameterisations available in the literature, estimated from early analytical considerations (Press and Schechter 1974), from DM-only numerical simulations (Sheth and Tormen 1999; Jenkins et al. 2001; Tinker et al. 2008, 2010; Rodríguez-Puebla et al. 2016) and more recently from DM and baryons simulations (Bocquet et al. 2016). Figure 3.6 shows the Tinker et al. (2008) mass function as computed by CLUMPY for different redshifts (thin coloured lines) and compared to the mass function given in the original publication at $z = 0$ (thick grey line, behind the red one). The mass function is a direct signature of the bottom-up structure formation, where more massive halos form at later times.

EBL absorption The extragalactic background light is defined as the diffuse emission, typically between 0.1 and 1000 μm, that has been mainly produced by star light and dust emission during the overall evolution of the Universe and that permeates it uniformly. It plays an essential role in high energy astrophysics as γ-ray photons interacting with the EBL will be absorbed to produce e^+e^- pairs. Modelling the EBL absorption is therefore mandatory and several types

10. Those $(1 + z)$ factors... Hours of fun!
11. http://class-code.net/
12. http://wwwmpa.mpa-garching.mpg.de/~komatsu/crl/.

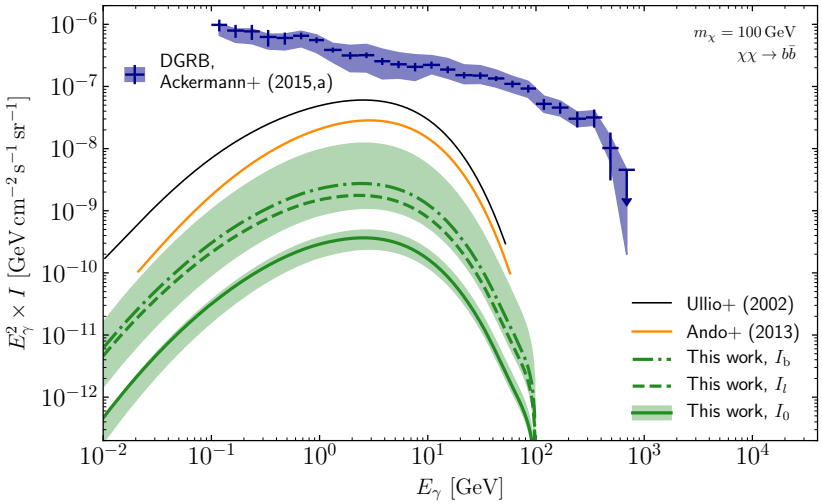

FIGURE 3.7: Isotropic extragalactic intensity from DM annihilation computed by CLUMPY (green) in a variety of configurations. Example of existing results in the literature are also given for comparison (black and orange), along with the measured *Fermi*-LAT diffuse γ-ray background (blue). See text for details. Figure adapted from Hütten et al. (2017).

of models exists in the literature. One approach, called backward modelling, starts from the observed multi-wavelength properties of existing local galaxies and extrapolate to larger redshifts (e.g. Franceschini et al. 2008; Franceschini and Rodighiero 2017). The so-called forward modelling method focuses instead on the mechanisms responsible for the EBL, i.e. emission of stars and dust, and integrate over stellar properties and star formation rate (Finke et al. 2010). Alternatively, semi-analytical models of galaxy formation and evolution can also be used to compute the opacity at any redshift (e.g. Gilmore et al. 2012; Inoue et al. 2013). Given the variety in the modelling approaches, the opacity of each of the works cited above has been implemented in CLUMPY as tables from which $\tau(E, z)$ can be interpolated.

Isotropic exotic extragalactic flux With the cosmology, mass functions and EBL absorption in place, all is ready to compute the exotic extragalactic flux according to Eq. (3.9). Figure 3.7 shows results of the CLUMPY calculation, obtained using the Planck 2015 cosmology, the Rodríguez-Puebla et al. (2016) mass function, the Inoue et al. (2013) EBL absorption, Einasto profiles and the Correa et al. (2015) concentration for the halo description; it assumes a 100 GeV DM candidate that annihilates entirely in the $b\bar{b}$ with a cross section $\langle\sigma v\rangle = 3\times10^{-26}$ cm^3 s^{-1}. For the mass function, we consider the mass range where numerical simulations apply, i.e. $M_\mathrm{min} \gtrsim 10^{10}$ M$_\odot$ (green solid lines), or extrapolating it to lower mass, with $M_\mathrm{min} \gtrsim 10^{-6}$ M$_\odot$ (green dashed line). The latter increases the intensity by an order of magnitude, highlighting the minimum mass of DM halos to be a very important quantity. In this configuration, allowing for 20% of the mass to be in the form of substructures further boosts the signal to the green dot-dashed line.

3.2.3 Results and perspectives

The example given above aimed at presenting the recent developments of the CLUMPY code. We have planned two analyses linked to the extragalactic exotic flux, as described hereafter.

Modelling uncertainties As figure 3.7 already hinted at, the modelling assumptions made to compute the DM-induced extragalactic γ-ray flux may yield significant differences. These include the choice of the mass function and mass range, the assumption when extrapolating to low DM masses, the choice of EBL absorption model, halo dark matter profile and concentration and including or not substructure with these DM halos (and if so, with what mass and spatial distributions and DM inner profile). How these choices may affect the result is further emphasised in figure 3.7 when comparing our results to that of Ullio et al. (2002) and Ando and Komatsu (2013b) (black and orange lines) [13]. The examples given here aimed at highlighting the range of values found in the literature. Our results are however in much better agreement with the more recent estimations of, e.g., The Fermi LAT Collaboration (2015); Moliné et al. (2016), but nonetheless a factor ~ 5 lower than that of the *Fermi*-LAT collaboration (The Fermi LAT Collaboration 2015). Similarly to the approach we took to explore the Galactic dark clump distribution, and thanks to our flexible implementation in CLUMPY, we have systematically explored and quantified the effects of all these assumptions and reported on the corresponding modelling uncertainties (green bands in figure 3.7) in Hütten et al. (2018), now published in JCAP.

Beyond the isotropic average description The above description of the extragalactic contribution to the exotic signal will give a single background value of the flux for the entire sky. To go further, one may consider the fluctuations of the exotic extragalactic flux from one pixel to the next, each line-of-sight considered as a realisation of the underlying statistics. The one-point function (a.k.a., photon count or flux distribution) has been shown to be an interesting approach to statistically constrain populations of γ-ray sources below the detection limit of *Fermi*-LAT (e.g., Malyshev and Hogg 2011; Zechlin et al. 2016). Feyereisen et al. (2015) have applied this approach to compute the expected flux distribution of the exotic extragalactic signal from DM annihilation, and have shown that shape of the γ-ray flux distribution was very sensitive to the exotic component. They concluded that this method could probe annihilation cross sections as low as 6×10^{-26} cm^3 s^{-1}, i.e. twice the thermal relic cross section.

In this context, the next feature that we will be implementing in CLUMPY is the drawing extragalactic halos according to the halo mass function, similarly to what we did at the Galactic scale. For each mass range, there will be a redshift below which halo will be drawn and above which the average description will hold, according to a user defined precision. During Moritz Hütten's visit at LPSC in March 2017, we have written down the algebra and we will be implementing this in 2018. With this final addition to the code, we will be able to address all the caveats that Feyereisen et al. (2015) reported for their analysis: neglecting the scatter and uncertainties in the halo parameters or mass function, considering only NFW DM profiles and assuming that DM halos are all point-like, checking the results against pixel size or DM energy spectrum/channel.

13. In Ullio et al. (2002), the authors used a Moore parametrisation (which diverges at small radii) for the DM halo profiles and a mass concentration according to Bullock et al. (2001), which will both increase the intensity. The prediction of Ando and Komatsu (2013b) is also higher than our estimation. This is understood as they used an effective subhalo boost model typically yielding ~ 20 for halo masses $M = 10^{10}$ M$_\odot$ and ~ 1500 at 10^{15} M$_\odot$. Such large boosts have now been excluded by several works (Sánchez-Conde and Prada 2014; Moliné et al. 2017), including ours, when using physically-motivated mass-concentration relations at low masses.

4
Conclusions

Dark matter indirect detection in the γ-ray channel is a very rich topic. I hope I have managed to convey this message in the previous pages, even if it was mostly presented through the prism of the contributions of my collaborators and I. The approach we have always favoured has been to look closely at the theoretical uncertainties that plague the main indirect detection targets (at the exclusion of the Galactic centre), namely dark Galactic clumps, dwarf spheroidal galaxies, galaxy clusters and more recently the extragalactic exotic background. We have done so through successive developments of the CLUMPY code, the first version of which I started to work on around 2010. A four-bullet points summary of the previous chapters would go as follows:

- For the Galactic clumps, the main source of uncertainty comes from the way the substructures are parametrised and their properties extrapolated to the lowest masses. We typically find an order of magnitude uncertainty on the limits that can be set of the DM annihilation cross section. While a glance at the results suggests these are far less promising than dSph galaxies, considering the error bars on both types of targets actually shows that they would be nicely complementary.
- For the dSphs, we have shown that biases in the J-factor could arise when using too constrained parametrisation in the Jeans analysis, and proposed an optimal setup that yields robust J-factors. Using this optimal setup, we have provided a ranking of the best targets, highlighting that Segue I may not be such a good choice after all and that the best ultrafaint targets come with error bars as large a two orders of magnitude.
- The main uncertainty in the J-factors of the nearby galaxy clusters comes from the evaluation of their boost factor (that typically ranges from 10 to 100), which is linked to the modelling of substructures, similarly to the case of dark Galactic clumps. While stacking clusters could be interesting when focusing on decaying DM, the gain for annihilating DM was found marginal. In any case, clusters appear less promising than dSph galaxies because of their expected astrophysical γ-ray background.

After two previous releases, the next update of CLUMPY will include a flexible treatment of the exotic extragalactic component and will propose, for the first time, a public tool that consistently deals with all exotic γ-ray (and neutrino) signals, from the Galactic to the extragalactic scale. We have already made use of this update to re-evaluate this γ-ray background in the light of the most recent simulation results and carefully assess the corresponding modelling uncertainties. Since the early days, we have planned for CLUMPY to become a public code available to the community, in particular to experimentalists; we are very happy to see it used in both γ-ray and neutrino related studies and collaborations. We are currently interacting with members of the DM working group of the CTA consortium, discussing the possibility of CLUMPY becoming a reference tool for their planned studies of dSph galaxies.

Since I started getting involved in this topic, around eight years ago, the field has significantly evolved and will keep doing so. Observationally, the *Fermi*-LAT instrument has been a game-changer, pushing the limits on annihilation cross section down to the thermal relic value and to the

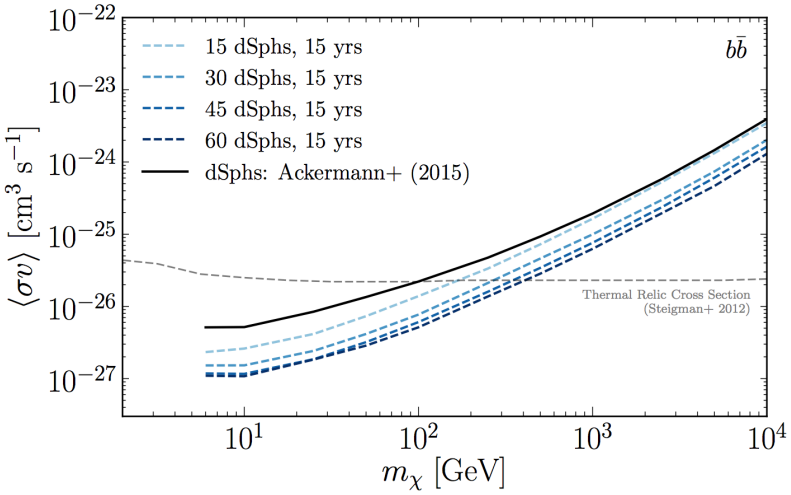

FIGURE 4.1: Projected upper limits on the WIMP annihilation cross section as a function of WIMP mass from the joint analysis of 15 to 60 dSphs, using 15 years of *Fermi*-LAT data. Taken from Charles et al. (2016).

interesting region of the parameter space for 10 – 100 GeV DM candidates. *Fermi*-LAT data also provided a lot of excitement, with e.g. the 130 GeV line episode, the potential signal in the Ret2 dSph or the Galactic centre excess. While the rush for a DM interpretation of these observations was unavoidable, they certainly highlighted even more the necessity to carefully characterise all instrumental effects and to account for all possible astrophysical backgrounds. This will of course be also true for CTA, which promises to bring a similar improvement to the current IACT limits for >TeV DM, especially from observations of the Galactic halo (excluding the central regions dominated by astrophysical sources).

Following in the footsteps of SDSS (that brought the number of known dSphs from 9 to 25), new dSph galaxies are being discovered by ongoing optical surveys such as DES (28 new MW satellites, 11 confirmed as new dSphs); this number should keep increasing with sky coverage, to which LSST will bring a significant addition. Figure 4.1 gives a projection of what could be expected from a 15-year *Fermi*-LAT joint analysis of 15 to 60 dSph galaxies (*Fermi*-LAT most promising targets) and shows the limits to improve by a factor ~ 5; this should univocally confirm or refute the DM interpretation of the Galactic centre excess (Charles et al. 2016). *Fermi*-LAT results will hold for a long time as no successor experiment has yet been approved.

From the modelling point of view, numerical simulations will keep improving their treatment of the baryonic physics and their mass resolution, which should reduce the allowed range of the parameters needed to describe the dark matter and therefore the corresponding theoretical uncertainties. New ways to tackle the problem are also being explored, such as the one-point functions or cross-correlations between γ-rays and cosmic shear (e.g. Shirasaki et al. 2016). Unfortunately and despite our best efforts, DM may remain elusive in γ-rays (or in any other indirect or direct detection experiment).

The only process where DM never disappoints is through the gravitational interaction and some of its fundamental properties may be inferred looking, for example, at i) the census of dSph galaxies in the local volume that will help disentangling cold from warm DM scenarios (Lovell et al. 2014); ii) gaps in stellar streams of the MW that could allow us to probe the population of dark clumps (Erkal et al. 2016); or iii) colliding galaxy clusters where an offset between the

galaxies and the dark matter peaks could indicate that DM is self-interacting (Harvey et al. 2015). These *astrophysical* approaches and many others are being explored by the DM community at large.

Part II

Future work with the Large Synoptic Survey Telescope

5

LSST and DESC: an overview

Contents

With the publication of most of the *Planck* results in 2015, part of the french CMB community has since redirected its efforts towards the main cosmological projects of the next decade, namely the *Euclid* satellite mission and the ground-based Large Synoptic Survey Telescope (LSST) project. After the completion of my *Planck*-related work (component separation and correction of systematic effects in polarisation) and the 2015 data release, I joined LSST-France in early 2016. Being also quite occupied at the time with the study of dark Galactic clumps I presented in §2.1, I really started to get involved in mid-2016. This came after a discussion with Dominique Boutigny and Nicolas Chotard (LAPP) linked to the galaxy clusters science in LSST, a topic that will be discussed in chapter 6. This chapter first provides the reader with a brief overview of the LSST project and objectives (§5.1), and then of the Dark Energy Science Collaboration (DESC) that coordinates all cosmology-related topics (§5.2).

5.1 The Large Synoptic Survey Telescope

5.1.1 The LSST project

The Large Synoptic Survey Telescope (LSST) is a 8m-class wide-field instrument currently being built on top of Cerro Pachón in Chile (figure 5.1). During ten years, it will image the entire visible sky (~20,000 deg^2) every few nights in six optical bands (u, g, r, i, z, y), thanks to a 3-mirror optical setup covering a 3.5° field-of-view and a 3.2-gigapixel camera. From these characteristics, the survey is generally termed *wide-fast-deep* and will consist in 34-second long *visits* (pair of back-to-back 15-second exposures, separated by 4 seconds for readout and shutter opening/closing), each patch of sky being visited twice every night at 15-60 minute intervals, and $\lesssim$1000 times over 10 years. Slewing between patches of sky will be fast, lasting typically 5 seconds, and requires a very stiff and compact mount for a quick dampening of vibrations (figure 5.2, left). Ninety percent of the observing time will be dedicated to the main survey and the remaining 10% to deeper observations of specific fields. The *universal cadence* of observations, meeting the requirements of the various science objectives (§5.1.2) is however yet to be fully defined (LSST Science Collaboration et al. 2017).

FIGURE 5.1: *Left*: Artist rendition of the LSST facility at the top of Cerro Pachón (Chile) under a somewhat exaggerated (and strangely repeating) night sky. The telescope and light reflection on the primary mirror is seen in the dome. *Right*: Construction status of the main building and dome. Picture taken on 7 February 2018. Credits https://www.lsst.org/.

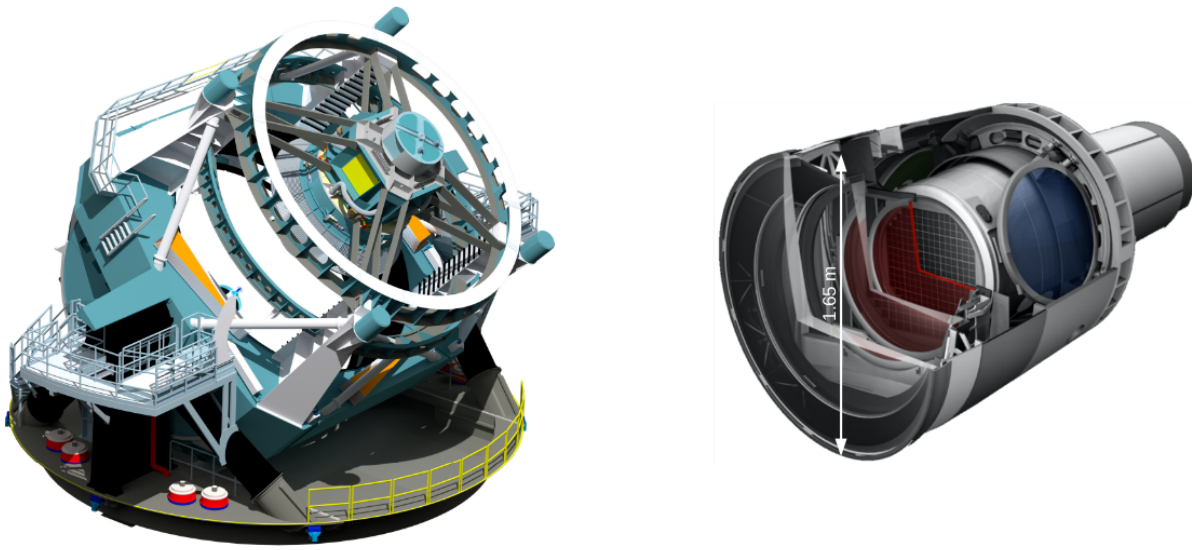

FIGURE 5.2: *Left*: Design of the telescope. The compactness of the mount is required to ensure a quick dampening of the vibrations after slewing. *Right:* Rendering of the camera clearly showing the two (of the three) field corrector lenses and the red filter in front the 3.2×10^9 pixels of the focal plane. Five of the six filters will be loaded on the carousel (only the blue filter is shown in the image), ready to be automatically inserted in front of the focal plane. Credits https://www.lsst.org/.

Each day, LSST will collect ∼ 15 TB of data. At the end of the 10-year survey, the last LSST data release will contain 5.5 million images, and tables of ∼ 37 billions objects (stars and galaxies) and ∼ 30 trillion sources [1]. Besides the instrumental and scientific awesomeness of the project, LSST also represents significant computing challenges; this not only for storing and accessing the data in the foreseen final 15 PB database, but also for ensuring throughout the 10 year survey, efficient daily quality assessment of the data, reliable transient alert system, efficient determination of the orbits of solar system objects, etc.

France, through IN2P3, joined the LSST project in 2007 and is in charge of the construction and delivery of several sub-systems linked to the camera construction. We will also provide half of the computational resources required to process the data. LPSC is more particularly involved in the construction of the filter loader and of the Camera Calibration Optical Bench (CCOB, wide and thin beams). The CCOB wide beam has recently been delivered to SLAC to be used to calibrate the pixels of the camera at the per mil level. Besides the work I will describe further in §6.1, I am also pursuing the development of the CCOB calibration code, that will need to be integrated within the camera software framework under development at SLAC.

5.1.2 Science goals

The scope of what LSST will achieve is tremendous and I only give a brief summary below. For an extensive review of LSST science, I refer the reader to the LSST science book (LSST Science Collaboration et al. 2009).

Cosmology, dark matter and dark energy are the main objectives behind the LSST project. LSST will exploit all possible cosmological probes available at optical wavelengths, namely:

- Weak lensing: it manifests as a statistically coherent deformation of the shapes of background galaxies due to the overall matter distribution along the line-of-sight. It is the prime observable of LSST and will be applied at various scales: large scale structures (cosmic shear, tomography), galaxy clusters (absolute mass calibration, see §6.1) and galaxy scale (galaxy mass profiles, evolution). In particular, cosmic shear is central to LSST cosmological studies. LSST will measure the shapes of billions of galaxies and dramatically improve the statistics of WL-related studies.

- Large Scale Structures: baryon acoustic oscillations (BAO) in the primordial Universe have left their imprint both in the CMB and in the large scale distribution of galaxies. The BAO scale is a standard ruler of the expansion of the Universe and the combination with the CMB provides a large lever arm to constrain cosmological parameters, especially dark energy. Beyond the BAO scale, LSST will measure several LSS-related quantities, e.g., auto- and cross-correlations of galaxy samples, matter power spectrum, galaxy bispectrum, which will supplement our current understanding of the evolution of the Universe (e.g., information on inflation, galaxy bias, etc.).

- Cluster counts: the number of galaxy clusters as a function of mass and redshift – i.e the mass function that was introduced in §3.2 – depends on the expansion history of the Universe, hence on the underlying cosmology (see Allen et al. 2011 for a review). This is the

1. This number is a rough estimate computed as 37 billion objects times 825 observations/object. Source tables are in particular important for studies in the time domain.

topic I have chosen to pursue in the future and more details will be given in §6.1.

- Type Ia supernovae: twenty years ago, SN Ia allowed the discovery of the accelerated expansion of the Universe. This discovery birthed the concept of dark energy, with a cosmological constant being its simple possible form. As standard (or, more accurately, standardisable) candles, they are used to construct a Hubble diagram (luminosity distance versus redshift) that relates to the expansion history of the Universe and the dark energy parameters.

The Solar system: with the opening of the time domain promised by LSST, millions of small moving bodies of the Solar System will be discovered and characterised. In particular, this census will provide a unique window to study trans-neptunian objects, which will bring information regarding the formation of the Solar System and planets. Along the same line, LSST will be very efficient to study *Near Earth Objects* and detect *Potentially Hazardous Asteroids*, whose orbits could bring them (too) close to Earth.

Variable objects: transient and variable phenomena are ubiquitous in the Universe, spanning objects such as variable stars, novae, cataclysmic variables and supernovae, and processes like tidal disruption events by supermassive black holes, gamma-ray burst afterglows or electromagnetic counterparts of gravitational wave events [2]. LSST will dramatically increase the statistics of these events but also send alerts for follow-up observations that will provide new insights into the physics of these various objects.

The Milky Way and local volume galaxies: Galaxy formation is a very broad topic and some insight can be gained by studying stellar populations of the Milky Way and of other nearby galaxies (e.g. Magellanic clouds), in terms of mass function, metallicities, and velocities. A major improvement in our knowledge of the Milky Way is underway, thanks to the *Gaia* space mission that will have mapped, by the end of the mission, the positions and proper motions of $\sim$ a billion stars (down to magnitude $r \sim 20$) with exquisite precision. Less accurate but reaching $r \sim 27$, the LSST will nicely complement the *Gaia* dataset by bringing photometric and astrometric information of ten times more stars, probing not only the disc, but also the entire MW halo.

As seen from above, LSST is a multi-purpose instrument. These science objectives have driven the instrument design and definition data products as described in Ivezic et al. (2008). In particular, LSST Science Collaboration et al. (2017) provides diagnostic metrics to evaluate the various cadence scenarios and maximise the scientific return of the project.

5.2 The Dark Energy Science Collaboration

Distinct and independent of the LSST project (construction, data taking and delivery), science collaborations have been formed to address the topics listed above. There are currently eight active science collaborations: dark energy, solar system, Milky Way, galaxies, AGN, transients, strong lensing and informatics & statistics. Among those, the Dark Energy Science Collaboration (DESC) is by far the largest scientific collaboration aiming at exploiting LSST data. In this small

2. This type of multi-messenger astrophysics became a reality on 17 August 2017, with the neutron star binary merger seen in gravitational waves by LIGO and at all electromagnetic wavelengths, from γ-rays to radio (The LIGO Scientific Collaboration et al. 2017). That was amazing!

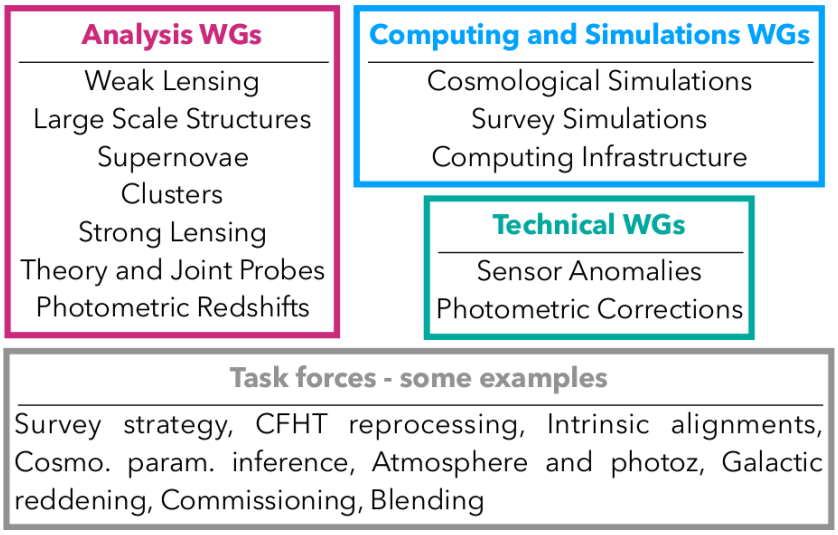

FIGURE 5.3: The various DESC working groups (colour blocks) and examples of a few task forces put in place since 2015 (grey block).

section, I will not describe the overall organisation of the collaboration (management team, advisory board, collaboration council, membership committee, publication board) but simply mention the more science-related aspects. Beyond the science itself, understanding this organisation is a pre-requisite to actually contribute, position, and make oneself useful to the global effort of DESC.

As of 20 September 2017, DESC consists of 677 members and 179 full members [3] and is organised in several working groups (WGs, see figure 5.3). Of course, each of the main probes of LSST has a dedicated working group. Added to those, the *Theory and Joint Probes* group is working at developing the methods and software that will allow the extraction of the cosmological parameters, using the combination of all the available cosmological probes. The determination of photometric redshifts of the billions of galaxies LSST will observe is central, and transverse to all the cosmological observables that will be used; the corresponding WG is very active in developing new approaches to improve and robustly estimate this critical quantity. Computing and simulations (be it simulations of cosmological evolution or of the survey) are essential to the project and three WGs are addressing these questions. Finally, two WGs study critical technical aspects, such as the Sensor Anomaly WG aiming at characterising and correcting some unwanted effects of the CCDs [4]. Task forces are sometimes formed to address a given specific issue that concerns one or several working groups. For example, the newly created *Blending Task Force* aims at studying the impacts of blending [5] on galaxy detection, shape measurements or photo-z estimation, these aspects affecting in turn all DE probes. More generally, the work of the collaboration is organised around the Science Roadmap [6] that identifies key projects and objectives to be met by the time of the first light of LSST.

Beside the regular teleconferences organised by each working groups (typically once or twice a month) to keep track of progress, the collaboration meets twice a year, each collaboration meeting starting with a day of *Dark Energy school*, that is particularly useful for scientists joining the

3. No requirement besides some interest in LSST/DESC is needed to become a DESC member. A member may apply to full membership after having taken part significantly in DESC-related activities in the past and stating intention to keep doing so in the future. I was awarded full membership in August 2017.

4. An example is the brighter-fatter effect (Antilogus et al. 2014).

5. The term blending refers to the fact that two or more galaxies may (partially) overlap along a given line-of-sight.

6. It is available at `http://lsst-desc.org/sites/default/files/DESC_SRM_V1_1.pdf`

project and not yet acquainted with the science of LSST, and finishing by a *hack day*, with the opportunity for everyone to join one of the proposed hacks and possibly start new collaborations. The collaboration also organises a couple of *Hack/Sprint weeks* every year, where the idea is to put groups of people in a room with little distraction for a week, for them to either get started on a new project, or pursue an existing effort and get as much done as possible during those five days. I find these events make the DESC collaboration particularly welcoming to new members, even though arriving in a collaboration of this size with no prior experience is quite daunting.

I spent a few months getting more acquainted with LSST science and the workings of the collaboration, as well as with what was already being covered in the LSST-France community. Galaxy clusters are objects that I have looked into in the past (see 3.1), that are being actively studied at LPSC by colleagues of the NIKA project, and a topic that was starting to get momentum in LSST-France in 2016. I therefore decided to spend my efforts in that direction and settle in the cluster working group. In the next and final chapter of this document, I describe this ongoing work and future efforts.

6

Positioning and perspectives within LSST and DESC

Contents

I started getting involved in cluster-related work around mid-2016, joining my efforts to those of Dominique Boutigny and Nicolas Chotard (LAPP). This final chapter highlights our ongoing work and aims at presenting the direction in which it will likely evolve. In the first section, I give a very brief overview of cluster cosmology simply to provide the reader with the necessary information to grasp the context of our work. The thorough article by Allen et al. (2011) provides an excellent review to the topic.

6.1 Cluster cosmology with cluster counts

Using galaxy clusters as cosmological probes has known increasing interest in the last fifteen years, with the advent of survey instruments at various wavelengths [1] allowing the production of large cluster catalogs (e.g., Böhringer et al. 2004, 2013; Bleem et al. 2015; Planck Collaboration et al. 2016a; Rykoff et al. 2016; Oguri et al. 2017; Banerjee et al. 2018). Cosmological information may be extracted from clusters by a variety of approaches, such as measuring the gas fraction (which constrains the ratio of baryon to total matter density in the Universe), the angular power spectrum of the thermal SZ effect, peculiar velocities using the kinetic SZ effect, or counting clusters in mass and redshift bins. This latter technique is the most widely used and will be at the core of LSST cluster studies; it is the one discussed hereafter.

1. e.g., ROSAT then XMM in X-rays, SDSS and now DES and HSC in the optical, Planck, ACT and SPT at millimetre wavelength.

6.1.1 Method

Using the halo mass function [2] $dn(M,z)/dM$, the number of DM halos $N(M_i, z_j)$ in the opening angle $\Delta\Omega$, in the mass bin M_i and redshift bin z_j is written as

$$N(M_i, z_j) = \frac{\Delta\Omega}{4\pi} \int_{z_j}^{z_{j+1}} dz \frac{dV}{dz} \int_{M_i}^{M_{i+1}} \frac{dn}{dM} dM \ . \tag{6.1}$$

This number is sensitive to cosmology (both in terms of structure growth and geometry) through the mass function and the comoving volume element dV/dz. At the high mass end, counting clusters in bins of mass and redshift therefore allows us to probe cosmology, and is particularly sensitive to the amplitude and shape of the primordial power spectrum, the matter density but also the equation of state of dark energy. Cluster count cosmology requires the following ingredients:

- A cluster catalog that includes cluster redshifts and a mass proxy; for LSST, the mass observable will be the richness which is linked to the number of galaxies belonging to the cluster. At optical wavelengths, cluster finding algorithms such as `redMaPPer` (Rykoff et al. 2014) which identify clusters as overdensity of red-sequence galaxies, are generally used to build the cluster catalogs (e.g., Simet et al. 2017; Melchior et al. 2017). The selection function of the catalog—providing the purity and completeness as a function of cluster mass, redshift and position on the sky—should also be carefully assessed.
- An accurate mass-observable relation: precision on cluster masses is what currently limits cluster cosmology as cluster masses lie in the tail of the mass function, where the latter decreases sharply (see figure 3.6); even a small error on the mass can translate into a large change in cluster abundances. Therefore, baryonic mass proxies (X-ray luminosity, SZ decrement, or richness in the case of LSST) need to be robustly calibrated and estimation of the mass using weak lensing provides a way to do so (e.g., Applegate et al. 2014; Mantz et al. 2016). This is the topic that will be developed further in §6.1.2.
- On the modelling side, numerical simulations, spanning a sufficiently large volume of Universe and including baryonic physics, are required to provide the theoretical mass function. Up to the most recent analyses, cluster cosmological results have relied on the Tinker et al. (2008) mass function, which was established from DM-only simulations using *WMAP* I cosmology (e.g., Benson et al. 2013; Mantz et al. 2015; Planck Collaboration et al. 2016c; de Haan et al. 2016; Schellenberger and Reiprich 2017). More up-to-date cosmologies and baryonic physics have been included, and keep being included, in more recent efforts (e.g., Bocquet et al. 2016; Despali et al. 2016; Rodríguez-Puebla et al. 2016). Dark matter halos extracted from these simulations are also used to test the so-called modelling bias, i.e. how assumptions made for the weak lensing analysis (e.g., spherical symmetry, pre-defined DM profile, choice of cluster centre) affect the reconstructed mass compared to the 'real' mass directly measure from the simulations.
- Finally, data and model should be included in a coherent statistical framework to extract cosmological parameters and allowing for combination with other cosmological probes. This is exemplified in figure 6.1, where the constraints on a constant (left) or evolving (right) dark energy equation of state are displayed for various cosmological probes, including the clusters of the Weighting the Giants project (Mantz et al. 2015).

The above description highlights a strong interplay between various topics. In the DESC collaboration, cluster cosmology is of course handled by the cluster working group, but with strong links to the cosmological simulations, the weak lensing, and the photometric redshift groups.

2. It has been introduced before to compute the extragalactic contribution to the exotic γ-ray signal.

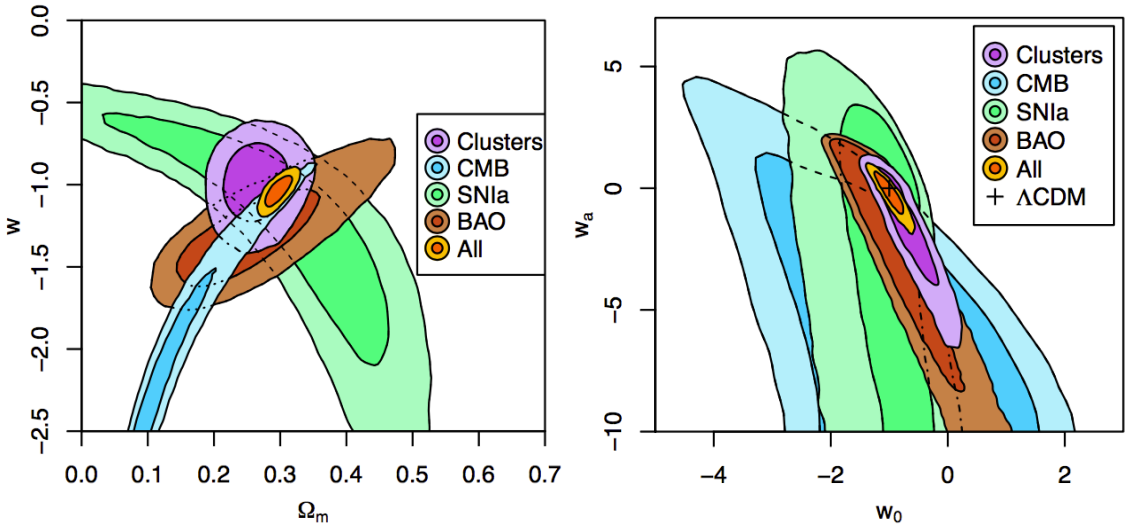

FIGURE 6.1: Constraints on cosmological models assuming a constant (w = cst, left) or evolving ($w = w_0 + w_a(z)$, right) dark energy equation of state using CMB, SNIa, BAO and cluster data. These figures are taken from Mantz et al. (2015) and we refer the reader to this paper for information about the various datasets.

There have been reports of tension between cluster count cosmology and the *Planck* analysis of primary fluctuations in the CMB, independently of the mass observable of the cluster catalogs (e.g., Planck Collaboration et al. 2016c; Medezinski et al. 2018; Miyazaki et al. 2018). While the origin of this issue may lie in several places, an accurate mass calibration appears paramount (Mantz et al. 2015). Furthermore, ongoing discussions in the community place the need for an absolute calibration at the percent level to improve cluster-derived cosmological constraints [3]. Weak lensing measurement of cluster masses are central to this improvement and this is the topic I selected to start my involvement in DESC.

6.1.2 The `clusters` package: WL masses from LSST DM stack catalogs

The light from background galaxies (the sources) passing in the vicinity of a galaxy cluster (the lens) is deviated by gravitational lensing. In the weak regime, the distortions of the shapes and orientations of background galaxies are small and cannot be detected looking at individual background galaxies. However, these distortions are statistically coherent and the cluster WL signal can be measured from the shapes of an ensemble of background galaxies (typically 100 – 1000). The strength of the effect is dependent on the geometry of the source-lens-observer system and on the total mass of the galaxy cluster, independently of the dynamical state of the latter. Weak lensing mass estimation is therefore the method of choice to provide the absolute calibration between mass and mass observable.

In that context, my collaborators and I are working on a project aiming at:

- reprocessing existing images from known galaxy clusters (CFHT or HSC data) using the LSST analysis pipeline (*a.k.a.* the DM stack [4]) to produce catalogues;
- building a cluster analysis pipeline going from these catalogues to the WL mass of the clusters.

3. Current state-of-the-art studies are at the 5-8% level.
4. Here, DM stands for Data Management, not Dark Matter...

This approach serves several purposes. First, it allows us (more specifically Dominique Boutigny and Nicolas Chotard) to exercise the DM stack on real datasets and provide much appreciated feedback to the developers, as only a few people in the DESC collaboration actually use the DM stack at this stage. Second, developing an analysis pipeline is a good way to tackle the steep learning curve inherent to work in any new field, while at the same time providing a hopefully useful tool to the working group and collaboration. This analysis pipeline is wrapped in the `clusters` python package [5] we have developed.

As of today, the various steps implemented in the pipeline are the following:

1. Use the DM stack to read in the catalogs produced by the latter, apply some basics cuts and store them in `astropy` tables.
2. Evaluate the Galactic extinction at each of the catalog objects location and store the magnitude corrections accordingly.
3. Compute the photometric redshifts of each object in the catalogs using existing codes wrapped into the pipeline. To date, we have included two public codes, `LePhare` (Ilbert et al. 2006) and `BPZ` (Benítez 2000), both using a template fitting approach. These codes return not only the best redshift estimate and confidence intervals but the full probability density distribution (*pdf*).
4. Identify the background galaxies to be used for the WL mass estimation based on the *pdf* of the redshift of each object.
5. Finally, estimate the mass of the clusters from the shapes of the background galaxies. The mass code we use is the `pzmassfitter` code developed for the WtG project, which uses a MCMC approach and a likelihood using the full photo-z *pdf* information (Applegate et al. 2014). This was implemented in the pipeline in collaboration with Douglas Applegate during the November 2016 LSST/DESC hack week.

Output examples of the pipeline are given in figure 6.2 for the cluster MACSJ2243.3-0935. This is one of the WtG clusters for which CFHT-Megacam data in the 5 bands (u, g, r, i, z) are available, allowing for reprocessing using the DM-stack. Furthermore, the original catalog from the WtG analysis has been made available for this work, allowing us to repeat the analysis on the original dataset. The left panel in figure 6.2 shows the convergence (i.e. mass) map as reconstructed from the shear measurement; the convergence is indeed the largest at the cluster position (green cross). The posterior distribution for the mass of the cluster, obtained from the MCMC, is displayed in the right panel when using either the catalogs produced by the WtG collaboration (blue) or the one obtained from the DM-stack reprocessing of CFHT data (red). These distributions are compatible and the former case reproduces, as expected, the published results of the WtG collaboration (green).

This result is a first encouraging step towards us contributing to the absolute mass calibration of galaxy clusters, but of course several improvements are still required (§6.2.1). Nicolas and myself have been presenting the clusters pipeline at DESC collaboration meetings and the work has been well received. The pipeline is now also being used by a PhD student from Brown university (USA): he is processing simulated images of cluster WL to determine the shear calibration and checking whether the mass of the input clusters can be satisfactorily reconstructed from the shape measurements performed using the DM stack.

5. https://github.com/nicolaschotard/Clusters

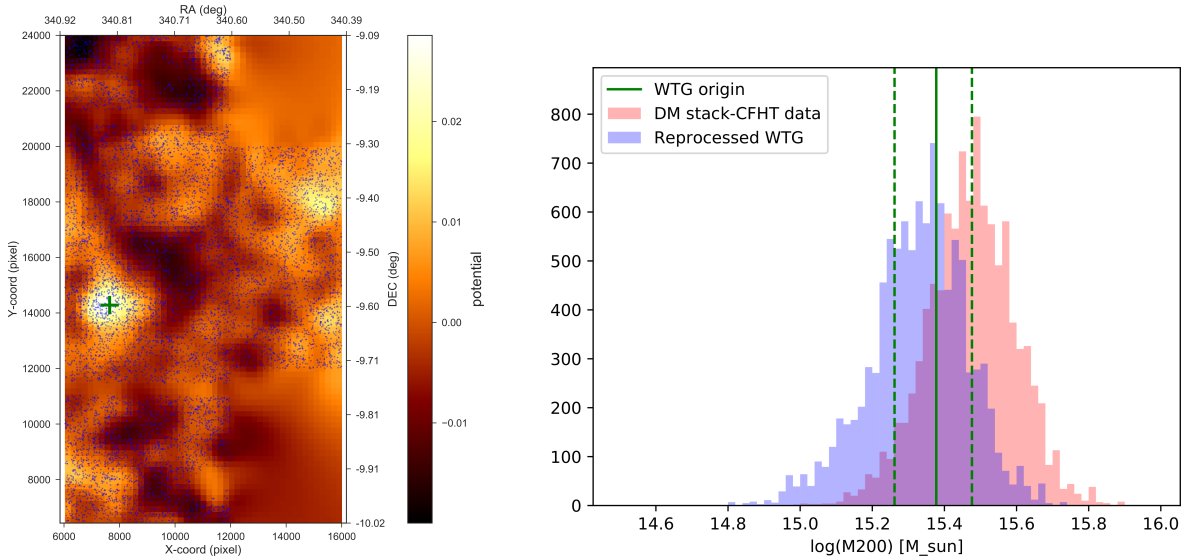

FIGURE 6.2: Example of data reprocessing using the pipeline on the cluster MACSJ2243.3-0935. *Left:* Convergence map (arbitrary units) computed from the shear of background galaxies. The largest values are found at the cluster's location (green cross). *Right:* WL mass M_{200} (estimated within R_{200}) of the cluster from i) the original WtG study (green), ii) the WtG catalogs reprocessed with the pipeline (blue) and iii) DM stack-processed CFHT images of the cluster, the output of which were analysed with the pipeline.

6.2 Directions for future work

6.2.1 On the DESC side

My involvement in DESC has been increasing since I joined the collaboration and, as of today, I find myself mostly interacting with the Clusters WG. Most of the action within DESC takes place in the US and the distance adds an extra difficulty to the already complicated task of joining a large collaboration. The work described above now needs to be extended. The points below give a few possible directions in which to do so.

Cluster-related projects In the early discussions related to the development of the `clusters` pipeline, we identified that flexibility at each of the steps was an important feature to provide. For a given input catalog, how does the subsequent choice of extinction map, photo-z code or mass reconstruction method impact the results? To answer this question, we want the user to be able to very easily switch between various options at each of the steps. For example, we need to add some machine learning-based photo-z codes to our options. Similarly, we only have a single mass reconstruction algorithm available at the moment and this should be extended to using different methods and dark matter profiles (NFW profiles are the default).

These developments are linked to two key projects of the DESC science roadmap, so-called `CLShear` and `CLMassMod` that aimed at quantifying the biases introduced by the shear estimation and WL mass reconstruction methods respectively. The latter will used results from numerical simulations to quantify the bias due to the WL modelling assumptions (e.g., cluster centre, spherical symmetry, NFW dark matter profile, etc.) and is, in spirit, very similar to what we did regarding the Jeans analysis and J-factors of dSph galaxies (see §2.2.2). I am familiar with this kind of approach and find myself very interested in this project. I therefore started getting involved recently, during the *hack day* of the last collaboration meeting.

Beyond this pipeline development and cluster-related activities, but also with this idea of working close to the data and to the DM stack, there are few directions and topics that would bring a significant contribution to the DESC effort and that I will explore.

Data reprocessing using DM-stack, catalog validation In the spirit of what is already undertaken by part of the LSST-France community, it will be very important to stay ahead of the curve regarding the reprocessing of precursor data (at CC-IN2P3) as they become available. To date, and in the context of clusters, we have mainly focused on cluster fields measured in five bands by CFHT. The SXDS deep field of the HSC survey (Aihara et al. 2017a) has also already been reprocessed by Dominique Boutigny. We need to keep building on this already recognised expertise to be ready to analyse the future releases of these precursor datasets, but also provide feedback to the DM-stack team. In that context, I would like to increase my involvement at the catalog validation stage, once the reprocessing is done. Indeed, the DM stack is a constantly evolving software, where new methods for e.g. measuring galaxy shapes or deblending, both crucial to WL studies, will be added with time. Even though any new algorithm will be tested prior to their inclusion in the stack, defining metrics to test their stack-implemented version is compulsory.

Deblending provides a good example: it aims at disentangling objects, e.g. two galaxies at different redshifts, that overlap in the image and is particularly problematic in ground-based observations, where the instrumental PSF will increase the size of the objects. This is also especially critical for deep surveys (like LSST or HSC), where the chance of two or more objects overlapping is increased compared to shallower observations (e.g. DES). Deblending failures (or failures to identify ambiguous blends) will yield badly measured shapes and photometry. In particular, the crowded fields characteristic of galaxy clusters may prove more challenging than elsewhere; this is illustrated in the recent HSC release, where failures of the deblender yielded poor 'standard' photometry and, in turn, prevented cluster finding algorithms to identify some clusters (Aihara et al. 2017b). Any deblender should therefore be carefully assessed in terms of performances and limitations. Using existing cluster data, such assessment could be performed by comparing the catalogs produced by the DM-stack from ground-based (e.g. HSC) and space (i.e. HST) images of the same fields, where the much higher resolution HST images serve as reference [6].

Analysis of DC2 /DC3 simulations The DESC science roadmap is, for a great part, organised around various data challenges, termed DC1, DC2 and DC3. The DC1-era covered the 2016-2017 time period and in 2018, the collaboration enters the DC2-era. The DC2 aims at producing a small LSST-like dataset (catalog simulation over 3,000 sq. deg. and images over 300 sq. deg.), representative of the 10 year-long survey (reaching typical magnitudes $r \sim 27.5$), in all 6 bands and suitable for analysis by all WG across the DESC collaboration (this was not the case for DC1). DC3 should extend on that setup with a mock catalog representative of a 18,000 sq. deg. survey and images over 3,000 sq. deg. These data challenges will be a major piece of work and stepping stone for the collaboration. Getting involved in this effort will be mandatory to get ready for real-life analysis of LSST data. LSST-France will contribute to the DC2 effort, by processing the simulated images at CC-IN2P3 using the DM stack; Nicolas Chotard is actually co-leading the DC2 processing. While a definite strategy is yet to emerge, I hope to contribute to the data production stage through the production control and catalog validation. More importantly, for cluster-specific analyses, we will be in a unique position thanks to the `clusters` pipeline described above, that was developed specifically to handle and process DM stack outputs. Nicolas and I will

6. This type of analysis has already been performed on catalogues produced by the widely-used `SExtractor` software (Dawson et al. 2016).

be largely involved in the project aiming at reconstructing the WL masses of the clusters present in the DC2 simulated images, along with our US colleagues.

6.2.2 On the side of LSST project: commissioning, CCOB

This chapter has mainly discussed science-related topics, linked with the Dark Energy Science Collaboration. However, and on a more instrumental front, we (at LPSC) are involved in part of the commissioning of the LSST camera, through the Camera Calibration Optical Bench (CCOB). I will not enter the details, but simply mention the goal of this device, the timeline and the developments currently underway.

The wide beam (WB) version of the CCOB will provide the camera's "first light" to i) identify dead and bad pixels and ii) measure the pixel-to-pixel relative responses at the 0.5% level in the 6 optical bands. This will allow a *direct* characterisation of the focal plane, with the camera not yet integrated with the full optics (e.g., no field corrector lenses). To perform this calibration, the CCOB-WB provides a very stable and controlled illumination, a challenging task achieved through successive instrumental developments undertaken at LPSC. The CCOB-WB has already been delivered to SLAC and a first series of data taken on a single raft (9 CCDs). I joined the CCOB team recently to provide some extra manpower after the departure of Jean-Stéphane Ricol; I am now in charge of developing the CCOB analysis software, the end-product of which should be the relative response of each of the 3 billion pixels of the camera (189 CCD). After discussion with colleagues at SLAC, the analysis software needs to be ready, at least in a beta version, next autumn; this will be a central part of my work in the coming months. After a few intermediate tests, the CCOB-WB will likely be used over the full focal plane in the second half of 2019.

In the coming year (2018), LPSC will also build the CCOB thin beam (TB); this laser-like beam will illuminate the camera under a variety of incident angles, crossing the entire optics before reaching the CCDs. The current plan is to use it both at SLAC, where the camera will be integrated, but also in the dome in Chile. This will allow us to develop an acute understanding of the fully integrated camera (optical alignment of the system, transmission coefficients, ghost images). With the construction of the CCOB-TB starting very soon, we will shortly start discussing the plans for the corresponding analysis software development.

6.2.3 Conclusions

The cosmological community is using all possible means to constrain the contents and evolution of the Universe; a better understanding of the properties of dark matter and dark energy are the most challenging and central tasks to this endeavour. In this context, the Large Synoptic Survey Telescope will be, with the *Euclid* satellite, a major actor in the coming decade and beyond. Ongoing ground-based optical surveys such as DES or HSC-SSP are already showing very nice results (e.g., The Dark Energy Survey Collaboration et al. 2017; Melchior et al. 2017; DES Collaboration et al. 2017; Medezinski et al. 2018; Miyazaki et al. 2018). The experience gained from these two surveys are fundamental assets to LSST and DESC.

I have listed above, in no particular order, a few directions to investigate within LSST/DESC; they fit into the larger picture as follows: first, developing a good knowledge of the instrument is paramount. In the case of LSST, this means in particular understanding the CCD and working close to the pixels; this will be essential to pinpoint the origins of the systematic effects that will appear down the road. Second, LSST DM stack will process images to produce catalogs of galaxy shapes and photometry in six bands. Careful assessment of the images and catalogs is mandatory to validate the algorithms in place in the DM stack. Third and focussing on cluster cosmology,

these catalog quantities will be translated into shear, redshifts, cluster catalogs, richness, WL masses, mass calibration and eventually cosmological parameters. Each step involves complex and imperfect methods that may introduce biases into the results, this statement being true for all the cosmological probes LSST will cover. Using simulated data is the only way to identify and account for these spurious effects. The next three years will be particularly intense on all these fronts to get ready for LSST's first light, but further developments will of course happen over the entire duration of the project.

Finally, I will conclude this document by circling back to the question of the nature and fundamental properties of dark matter, that is central to the indirect detection approach presented in the first part. While DESC is very dark energy and cosmology-centred, a new discussion started at the July 2017 collaboration meeting around the potential for LSST to directly address or at least contribute to answering this question. One aspect, already mentioned before, is the discovery of new dSph galaxies. Not only new close-by candidates could be interesting targets for indirect detection, but this new census of dSph may be compared to that predicted by ΛCDM (or other) scenarios. Dark clumps orbiting in the halo of the MW could also be characterised from the gaps they leave in stellar streams (11 new streams have already been detected in the recent DES data release, Shipp et al. 2018; $\sim$ 100 new stellar streams are expected to be discovered with LSST). Another example is that of colliding galaxy clusters, which will also be largely present in LSST data. The DM distribution of these systems will be reconstructed by lensing and the spatial offsets between the various components (DM, galaxies, gaz) allow to place limits on the self-interacting cross section of DM. I find these topics, linked to the astrophysical manifestations of DM, of particular interest but lack of time has so far prevented me to act more upon it. However, I intend to closely follow the evolution of these discussions and, as more manpower becomes available in the group [7], this is also a place I envision getting involved into.

7. LPSC colleagues from AMS should eventually join us and we are hoping to recruit one or two PhD students in the next two years (hence this *Habilitation à diriger les recherches*).

Bibliography

Abazajian, Canac, Horiuchi, and Kaplinghat. Astrophysical and dark matter interpretations of extended gamma-ray emission from the Galactic Center. *Phys. Rev. D* 90(2), 023526 (2014).

Abramowski, Acero, Aharonian, et al. Erratum: "Search for Dark Matter Annihilation Signals from the Fornax Galaxy Cluster with H.E.S.S.". *ApJ* 783, 63 (2014)a.

Abramowski, Aharonian, Ait Benkhali, et al. Search for dark matter annihilation signatures in H.E.S.S. observations of dwarf spheroidal galaxies. *Phys. Rev. D* 90(11), 112012 (2014)b.

Abramowski et al. Search for Dark Matter Annihilation Signals from the Fornax Galaxy Cluster with H.E.S.S. *ApJ* 750, 123 (2012).

Acciari, Arlen, Aune, et al. VERITAS Search for VHE Gamma-ray Emission from Dwarf Spheroidal Galaxies. *ApJ* 720, 1174–1180 (2010).

Ackermann, Ajello, Allafort, et al. Constraints on dark matter annihilation in clusters of galaxies with the Fermi large area telescope. *J. Cosmology Astropart. Phys.* 5, 025 (2010).

Ackermann, Albert, Baldini, et al. Search for Dark Matter Satellites Using Fermi-LAT. *ApJ* 747, 121 (2012).

Ackermann, Ajello, Albert, et al. Search for gamma-ray spectral lines with the Fermi Large Area Telescope and dark matter implications. *Phys. Rev. D* 88(8), 082002 (2013).

Ackermann, Ajello, Albert, et al. Search for Cosmic-Ray-induced Gamma-Ray Emission in Galaxy Clusters. *ApJ* 787, 18 (2014)a.

Ackermann, Albert, Anderson, et al. Dark matter constraints from observations of 25 MilkyÂ Way satellite galaxies with the Fermi Large Area Telescope. *Phys. Rev. D* 89(4), 042001 (2014)b.

Ackermann, Ajello, Albert, et al. Updated search for spectral lines from Galactic dark matter interactions with pass 8 data from the Fermi Large Area Telescope. *Phys. Rev. D* 91(12), 122002 (2015)a.

Ackermann, Albert, Anderson, et al. Searching for Dark Matter Annihilation from Milky Way Dwarf Spheroidal Galaxies with Six Years of Fermi Large Area Telescope Data. *Phys. Rev. Lett.* 115(23), 231301 (2015)b.

Adriani, Barbarino, Bazilevskaya, et al. An anomalous positron abundance in cosmic rays with energies 1.5-100GeV. *Nature* 458, 607–609 (2009).

Agnese, Anderson, Asai, et al. Improved WIMP-search reach of the CDMS II germanium data. *Phys. Rev. D* 92(7), 072003 (2015).

Aguilar, Aisa, Alvino, et al. Electron and Positron Fluxes in Primary Cosmic Rays Measured with the Alpha Magnetic Spectrometer on the International Space Station. *Physical Review Letters* 113(12), 121102 (2014).

Aihara, Arimoto, Armstrong, et al. The Hyper Suprime-Cam SSP Survey: Overview and Survey Design. *ArXiv e-prints* (2017)a.

Aihara, Armstrong, Bickerton, et al. First Data Release of the Hyper Suprime-Cam Subaru Strategic Program. *ArXiv e-prints* (2017)b.

Ajello, Albert, Atwood, et al. Fermi-LAT Observations of High-Energy Gamma-Ray Emission toward the Galactic Center. *ApJ* 819, 44 (2016).

Akerib, Araújo, Bai, et al. Improved Limits on Scattering of Weakly Interacting Massive Particles from Reanalysis of 2013 LUX Data. *Physical Review Letters* 116(16), 161301 (2016).

Albert, Alfaro, Alvarez, et al. Dark Matter Limits From Dwarf Spheroidal Galaxies with The HAWC Gamma-Ray Observatory. *ArXiv e-prints* (2017)a.

Albert, André, Anghinolfi, et al. Results from the search for dark matter in the Milky Way with 9 years of data of the ANTARES neutrino telescope. *Physics Letters B* 769, 249–254 (2017)b.

Aleksić, Ansoldi, Antonelli, et al. Optimized dark matter searches in deep observations of Segue 1 with MAGIC. *J. Cosmology Astropart. Phys.* 2, 008 (2014).

Allen, Evrard, and Mantz. Cosmological Parameters from Observations of Galaxy Clusters. *ARA&A* 49, 409–470 (2011).

Ando and Komatsu. Constraints on the annihilation cross section of dark matter particles from anisotropies in the diffuse gamma-ray background measured with Fermi-LAT. *Phys. Rev. D* 87 (12), 123539 (2013)a.

Ando and Komatsu. Constraints on the annihilation cross section of dark matter particles from anisotropies in the diffuse gamma-ray background measured with Fermi-LAT. *Phys. Rev. D* 87 (12), 123539 (2013)b.

Ando and Nagai. Fermi-LAT constraints on dark matter annihilation cross section from observations of the Fornax cluster. *J. Cosmology Astropart. Phys.* 7, 017 (2012).

Antilogus, Astier, Doherty, Guyonnet, and Regnault. The brighter-fatter effect and pixel correlations in CCD sensors. *Journal of Instrumentation* 9, C03048 (2014).

Applegate, von der Linden, Kelly, et al. Weighing the Giants - III. Methods and measurements of accurate galaxy cluster weak-lensing masses. *MNRAS* 439, 48–72 (2014).

Arlen, Aune, Beilicke, et al. Constraints on Cosmic Rays, Magnetic Fields, and Dark Matter from Gamma-Ray Observations of the Coma Cluster of Galaxies with VERITAS and Fermi. *ApJ* 757, 123 (2012).

Atwood, Abdo, Ackermann, et al. The Large Area Telescope on the Fermi Gamma-Ray Space Telescope Mission. *ApJ* 697, 1071–1102 (2009).

Balázs, Conrad, Farmer, et al. Sensitivity of the Cherenkov Telescope Array to the Detection of a Dark Matter Signal in comparison to Direct Detection and Collider Experiments. *ArXiv e-prints* (2017).

Banerjee, Szabo, Pierpaoli, et al. An optical catalog of galaxy clusters obtained from an adaptive matched filter finder applied to SDSS DR9 data. *New A* 58, 61–71 (2018).

Baratella, Cirelli, Hektor, et al. PPPC 4 DMν: a Poor Particle Physicist Cookbook for Neutrinos from Dark Matter annihilations in the Sun. *J. Cosmology Astropart. Phys.* 3, 053 (2014).

Bartels and Ando. Boosting the annihilation boost: Tidal effects on dark matter subhalos and consistent luminosity modeling. *Phys. Rev. D* 92(12), 123508 (2015).

Bechtol, Drlica-Wagner, Balbinot, et al. Eight New Milky Way Companions Discovered in First-year Dark Energy Survey Data. *ApJ* 807, 50 (2015).

Belokurov, Zucker, Evans, et al. A Faint New Milky Way Satellite in Bootes. *ApJ* 647, L111–L114 (2006).

Benítez. Bayesian Photometric Redshift Estimation. *ApJ* 536, 571–583 (2000).

Benson, de Haan, Dudley, et al. Cosmological Constraints from Sunyaev-Zel'dovich-selected Clusters with X-Ray Observations in the First 178 deg^2 of the South Pole Telescope Survey. *ApJ* 763, 147 (2013).

Bertoni, Hooper, and Linden. Examining The Fermi-LAT Third Source Catalog in search of dark matter subhalos. *J. Cosmology Astropart. Phys.* 12, 035 (2015).

Bilenky and Petcov. Massive neutrinos and neutrino oscillations. *Reviews of Modern Physics* 59, 671–754 (1987).

Binney and Tremaine. Galactic Dynamics: Second Edition. Princeton University Press (2008).

Blasi. Origin of the positron excess in cosmic rays. *Phys. Rev. Lett.* 103, 051104 (2009).

Bleem, Stalder, de Haan, et al. Galaxy Clusters Discovered via the Sunyaev-Zel'dovich Effect in the 2500-Square-Degree SPT-SZ Survey. *ApJS* 216, 27 (2015).

Bocquet, Saro, Dolag, and Mohr. Halo mass function: baryon impact, fitting formulae, and implications for cluster cosmology. *MNRAS* 456, 2361–2373 (2016).

Boehm, Dolan, and McCabe. Interpretation of the Galactic Center excess of gamma rays with heavier dark matter particles. *Phys. Rev. D* 90(2), 023531 (2014).

Boezio, Pearce, Picozza, et al. PAMELA and indirect dark matter searches. *New Journal of Physics* 11(10), 105023 (2009).

Böhringer, Schuecker, Guzzo, et al. The ROSAT-ESO Flux Limited X-ray (REFLEX) Galaxy cluster survey. V. The cluster catalogue. *A&A* 425, 367–383 (2004).

Böhringer, Chon, Collins, et al. The extended ROSAT-ESO flux limited X-ray galaxy cluster survey (REFLEX II) II. Construction and properties of the survey. *A&A* 555, A30 (2013).

Bonnivard, Combet, Daniel, et al. Dark matter annihilation and decay in dwarf spheroidal galaxies: the classical and ultrafaint dSphs. *MNRAS* 453, 849–867 (2015)a.

Bonnivard, Combet, Maurin, et al. Dark Matter Annihilation and Decay Profiles for the Reticulum II Dwarf Spheroidal Galaxy. *ApJ* 808, L36 (2015)b.

Bonnivard, Combet, Maurin, and Walker. Spherical Jeans analysis for dark matter indirect detection in dwarf spheroidal galaxies - impact of physical parameters and triaxiality. *MNRAS* 446, 3002–3021 (2015)c.

Bonnivard, Hütten, Nezri, et al. CLUMPY: Jeans analysis, γ-ray and ν fluxes from dark matter (sub-)structures. *Computer Physics Communications* 200, 336–349 (2016)a.

Bonnivard, Maurin, and Walker. Contamination of stellar-kinematic samples and uncertainty about dark matter annihilation profiles in ultrafaint dwarf galaxies: the example of Segue I. *MNRAS* 462, 223–234 (2016)b.

Boylan-Kolchin, Bullock, and Kaplinghat. Too big to fail? The puzzling darkness of massive Milky Way subhaloes. *MNRAS* 415, L40–L44 (2011).

Branchini, Camera, Cuoco, et al. Cross-correlating the γ-ray Sky with Catalogs of Galaxy Clusters. *ApJS* 228, 8 (2017).

Bringmann. Particle models and the small-scale structure of dark matter. *New Journal of Physics* 11(10), 105027 (2009).

Brooks and Zolotov. Why Baryons Matter: The Kinematics of Dwarf Spheroidal Satellites. *ApJ* 786, 87 (2014).

Brun, Moulin, Diemand, and Glicenstein. Searches for dark matter subhaloes with wide-field Cherenkov telescope surveys. *Phys. Rev. D* 83(1), 015003 (2011).

Bulbul, Markevitch, Foster, et al. Detection of an Unidentified Emission Line in the Stacked X-Ray Spectrum of Galaxy Clusters. *ApJ* 789, 13 (2014).

Bullock. Notes on the Missing Satellites Problem. *ArXiv e-prints* (2010).

Bullock, Kolatt, Sigad, et al. Profiles of dark haloes: evolution, scatter and environment. *MNRAS* 321, 559–575 (2001).

Calore, De Romeri, Di Mauro, et al. γ-ray anisotropies from dark matter in the Milky Way: the role of the radial distribution. *MNRAS* 442, 1151–1156 (2014).

Campos, Queiroz, Yaguna, and Weniger. Search for right-handed neutrinos from dark matter annihilation with gamma-rays. *J. Cosmology Astropart. Phys.* 7, 016 (2017).

Carr, Balazs, Bringmann, et al. Prospects for Indirect Dark Matter Searches with the Cherenkov Telescope Array (CTA). *ArXiv e-prints* (2015).

Chan, Kereš, Oñorbe, et al. The impact of baryonic physics on the structure of dark matter haloes: the view from the FIRE cosmological simulations. *MNRAS* 454, 2981–3001 (2015).

Charbonnier, Combet, Daniel, et al. Dark matter profiles and annihilation in dwarf spheroidal galaxies: prospectives for present and future γ-ray observatories - I. The classical dwarf spheroidal galaxies. *MNRAS* 418, 1526–1556 (2011).

Charbonnier, Combet, and Maurin. CLUMPY: A code for γ-ray signals from dark matter structures. *Computer Physics Communications* 183, 656–668 (2012).

Charles, Sánchez-Conde, Anderson, et al. Sensitivity projections for dark matter searches with the Fermi large area telescope. *Phys. Rep.* 636, 1–46 (2016).

Chiappo, Cohen-Tanugi, Conrad, et al. Dwarf spheroidal J-factors without priors: A likelihood-based analysis for indirect dark matter searches. *ArXiv e-prints* (2016).

Ciafaloni, Comelli, Riotto, et al. Weak corrections are relevant for dark matter indirect detection. *J. Cosmology Astropart. Phys.* 3, 019 (2011).

Cirelli, Corcella, Hektor, et al. PPPC 4 DM ID: a poor particle physicist cookbook for dark matter indirect detection. *J. Cosmology Astropart. Phys.* 3, 051 (2011).

Combet, Maurin, Nezri, et al. Decaying dark matter: Stacking analysis of galaxy clusters to improve on current limits. *Phys. Rev. D* 85(6), 063517 (2012).

Conrad and Reimer. Indirect dark matter searches in gamma and cosmic rays. *Nature Physics* 13, 224–231 (2017).

Correa, Wyithe, Schaye, and Duffy. The accretion history of dark matter haloes - III. A physical model for the concentration-mass relation. *MNRAS* 452, 1217–1232 (2015).

Cortina, Goebel, Schweizer, and for the MAGIC Collaboration. Technical Performance of the MAGIC Telescopes. *ArXiv e-prints* (2009).

Dawson, Schneider, Tyson, and Jee. The Ellipticity Distribution of Ambiguously Blended Objects. *ApJ* 816, 11 (2016).

Daylan, Finkbeiner, Hooper, et al. The characterization of the gamma-ray signal from the central Milky Way: A case for annihilating dark matter. *Physics of the Dark Universe* 12, 1–23 (2016).

de Haan, Benson, Bleem, et al. Cosmological Constraints from Galaxy Clusters in the 2500 Square-degree SPT-SZ Survey. *ApJ* 832, 95 (2016).

Del Popolo, Lima, Fabris, and Rodrigues. A unified solution to the small scale problems of the ΛCDM model. *J. Cosmology Astropart. Phys.* 4, 021 (2014).

DES Collaboration, Abbott, Abdalla, et al. Dark Energy Survey Year 1 Results: Cosmological Constraints from Galaxy Clustering and Weak Lensing. *ArXiv e-prints* (2017).

Despali, Giocoli, Angulo, et al. The universality of the virial halo mass function and models for non-universality of other halo definitions. *MNRAS* 456, 2486–2504 (2016).

Diemand, Kuhlen, Madau, et al. Clumps and streams in the local dark matter distribution. *Nature* 454, 735–738 (2008).

Drlica-Wagner, Albert, Bechtol, et al. Search for Gamma-Ray Emission from DES Dwarf Spheroidal Galaxy Candidates with Fermi-LAT Data. *ApJ* 809, L4 (2015).

Dubus, Contreras, Funk, et al. Surveys with the Cherenkov Telescope Array. *Astropart. Phys.* 43, 317–330 (2013).

Duffy, Schaye, Kay, and Dalla Vecchia. Dark matter halo concentrations in the Wilkinson Microwave Anisotropy Probe year 5 cosmology. *MNRAS* 390, L64–L68 (2008).

Einasto and Haud. Galactic models with massive corona. I - Method. II - Galaxy. *A&A* 223, 89–106 (1989).

Erkal, Belokurov, Bovy, and Sanders. The number and size of subhalo-induced gaps in stellar streams. *MNRAS* 463, 102–119 (2016).

Feyereisen, Ando, and Lee. Modelling the flux distribution function of the extragalactic gamma-ray background from dark matter annihilation. *J. Cosmology Astropart. Phys.* 9, 027 (2015).

Finke, Razzaque, and Dermer. Modeling the Extragalactic Background Light from Stars and Dust. *ApJ* 712, 238–249 (2010).

Forero, Tórtola, and Valle. Neutrino oscillations refitted. *Phys. Rev. D* 90(9), 093006 (2014).

Franceschini and Rodighiero. The extragalactic background light revisited and the cosmic photon-photon opacity. *A&A* 603, A34 (2017).

Franceschini, Rodighiero, and Vaccari. Extragalactic optical-infrared background radiation, its time evolution and the cosmic photon-photon opacity. *A&A* 487, 837–852 (2008).

Gao, Frenk, Jenkins, Springel, and White. Where will supersymmetric dark matter first be seen? *MNRAS* 419, 1721–1726 (2012).

Genina and Fairbairn. The potential of the dwarf galaxy Triangulum II for dark matter indirect detection. *MNRAS* 463, 3630–3636 (2016).

Geringer-Sameth, Koushiappas, and Walker. Dwarf Galaxy Annihilation and Decay Emission Profiles for Dark Matter Experiments. *ApJ* 801, 74 (2015)a.

Geringer-Sameth, Walker, Koushiappas, et al. Indication of Gamma-Ray Emission from the Newly Discovered Dwarf Galaxy Reticulum II. *Physical Review Letters* 115(8), 081101 (2015)b.

Gilmore, Somerville, Primack, and Domínguez. Semi-analytic modelling of the extragalactic background light and consequences for extragalactic gamma-ray spectra. *MNRAS* 422, 3189–3207 (2012).

Giocoli, Tormen, and Sheth. Formation times, mass growth histories and concentrations of dark matter haloes. *MNRAS* 422, 185–198 (2012).

Gordon and Macías. Dark matter and pulsar model constraints from Galactic Center Fermi-LAT gamma-ray observations. *Phys. Rev. D* 88(8), 083521 (2013).

Górski, Hivon, Banday, et al. HEALPix: A Framework for High-Resolution Discretization and Fast Analysis of Data Distributed on the Sphere. *ApJ* 622, 759–771 (2005).

Green, Hofmann, and Schwarz. The power spectrum of SUSY-CDM on subgalactic scales. *MNRAS* 353, L23–L27 (2004).

Gunn, Lee, Lerche, Schramm, and Steigman. Some astrophysical consequences of the existence of a heavy stable neutral lepton. *ApJ* 223, 1015–1031 (1978).

Han, Frenk, Eke, et al. Constraining extended gamma-ray emission from galaxy clusters. *MNRAS* 427, 1651–1665 (2012).

Han, Cole, Frenk, and Jing. A unified model for the spatial and mass distribution of subhaloes. *MNRAS* 457, 1208–1223 (2016).

Hartman, Bertsch, Fichtel, et al. The EGRET high energy gamma ray telescope. Vol. 3137 of *NASA Conference Publication* (1992).

Harvey, Massey, Kitching, Taylor, and Tittley. The nongravitational interactions of dark matter in colliding galaxy clusters. *Science* 347, 1462–1465 (2015).

Hayashi, Ichikawa, Matsumoto, et al. Dark matter annihilation and decay from non-spherical dark halos in galactic dwarf satellites. *MNRAS* 461, 2914–2928 (2016).

Hektor, Raidal, and Tempel. Evidence for Indirect Detection of Dark Matter from Galaxy Clusters in Fermi γ-Ray Data. *ApJ* 762, L22 (2013).

Hinton and the HESS Collaboration. The status of the HESS project. *New A Rev.* 48, 331–337 (2004).

Holder, Atkins, Badran, et al. The first VERITAS telescope. *Astroparticle Physics* 25, 391–401 (2006).

Hütten, Combet, Maier, and Maurin. Dark matter substructure modelling and sensitivity of the Cherenkov Telescope Array to Galactic dark halos. *J. Cosmology Astropart. Phys.* 9, 047 (2016).

Hütten, Combet, and Maurin. Extragalactic diffuse gamma-rays from dark matter annihilation: revised prediction and full modelling uncertainties. *ArXiv e-prints* (2017).

Hütten, Combet, and Maurin. Extragalactic diffuse γ-rays from dark matter annihilation: revised prediction and full modelling uncertainties. *J. Cosmology Astropart. Phys.* 2, 005 (2018).

Ichikawa, Ishigaki, Matsumoto, et al. Foreground effect on the J-factor estimation of classical dwarf spheroidal galaxies. *MNRAS* 468, 2884–2896 (2017).

Ilbert, Arnouts, McCracken, et al. Accurate photometric redshifts for the CFHT legacy survey calibrated using the VIMOS VLT deep survey. *A&A* 457, 841–856 (2006).

Inoue, Inoue, Kobayashi, et al. Extragalactic Background Light from Hierarchical Galaxy Formation: Gamma-Ray Attenuation up to the Epoch of Cosmic Reionization and the First Stars. *ApJ* 768, 197 (2013).

Irwin and Hatzidimitriou. Structural parameters for the Galactic dwarf spheroidals. *MNRAS* 277, 1354–1378 (1995).

Ivezic, Tyson, Abel, et al. LSST: from Science Drivers to Reference Design and Anticipated Data Products. *ArXiv e-prints* (2008).

Jenkins, Frenk, White, et al. The mass function of dark matter haloes. *MNRAS* 321, 372–384 (2001).

Kaplinghat, Linden, and Yu. Galactic Center Excess in γ Rays from Annihilation of Self-Interacting Dark Matter. *Physical Review Letters* 114(21), 211303 (2015).

Kaplinghat, Tulin, and Yu. Dark Matter Halos as Particle Colliders: Unified Solution to Small-Scale Structure Puzzles from Dwarfs to Clusters. *Physical Review Letters* 116(4), 041302 (2016).

Kirby, Cohen, Simon, and Guhathakurta. Triangulum II: Possibly a Very Dense Ultra-faint Dwarf Galaxy. *ApJ* 814, L7 (2015).

Kirby, Cohen, Simon, et al. Triangulum II. Not Especially Dense After All. *ApJ* 838, 83 (2017).

Klasen, Pohl, and Sigl. Indirect and direct search for dark matter. *Progress in Particle and Nuclear Physics* 85, 1–32 (2015).

Knödlseder, Mayer, Deil, et al. GammaLib and ctools: A software framework for the analysis of astronomical gamma-ray data. *ArXiv e-prints* (2016).

Koposov, Belokurov, Torrealba, and Evans. Beasts of the Southern Wild: Discovery of Nine Ultra Faint Satellites in the Vicinity of the Magellanic Clouds. *ApJ* 805, 130 (2015).

Kuhlen, Vogelsberger, and Angulo. Numerical simulations of the dark universe: State of the art and the next decade. *Physics of the Dark Universe* 1, 50–93 (2012).

Lange and Chu. Can galactic dark matter substructure contribute to the cosmic gamma-ray anisotropy? *MNRAS* 447, 939–947 (2015).

Lee, Park, and Park. Cluster X-ray line at from axion-like dark matter. *European Physical Journal C* 74, 3062 (2014).

Lefranc, Moulin, and for the H. E. S. S. collaboration. Dark matter search in the inner Galactic halo with H.E.S.S. I and H.E.S.S. II. *ArXiv e-prints* (2015).

Lefranc et al. Dark matter search in the inner galactic center halo with H.E.S.S. *ArXiv e-prints* (2016).

Lesgourgues. The Cosmic Linear Anisotropy Solving System (CLASS) I: Overview. *ArXiv e-prints* (2011).

Lovell, Frenk, Eke, et al. The properties of warm dark matter haloes. *MNRAS* 439, 300–317 (2014).

LSST Science Collaboration, Abell, Allison, et al. LSST Science Book, Version 2.0. *ArXiv e-prints* (2009).

LSST Science Collaboration, Marshall, Anguita, et al. Science-Driven Optimization of the LSST Observing Strategy. *ArXiv e-prints* (2017).

Macciò, Dutton, and van den Bosch. Concentration, spin and shape of dark matter haloes as a function of the cosmological model: WMAP1, WMAP3 and WMAP5 results. *MNRAS* 391, 1940–1954 (2008).

Madau, Diemand, and Kuhlen. Dark Matter Subhalos and the Dwarf Satellites of the Milky Way. *ApJ* 679, 1260–1271 (2008).

MAGIC collaboration. Limits to dark matter annihilation cross-section from a combined analysis of MAGIC and Fermi-LAT observations of dwarf satellite galaxies. *J. Cosmology Astropart. Phys.* 2, 039 (2016).

Malyshev and Hogg. Statistics of Gamma-Ray Point Sources below the Fermi Detection Limit. *ApJ* 738, 181 (2011).

Mantz, von der Linden, Allen, et al. Weighing the giants - IV. Cosmology and neutrino mass. *MNRAS* 446, 2205–2225 (2015).

Mantz, Allen, Morris, et al. Weighing the giants- V. Galaxy cluster scaling relations. *MNRAS* 463, 3582–3603 (2016).

Martin, Ibata, Collins, et al. Triangulum II: A Very Metal-poor and Dynamically Hot Stellar System. *ApJ* 818, 40 (2016).

Maurin, Combet, Nezri, and Pointecouteau. Disentangling cosmic-ray and dark-matter induced γ-rays in galaxy clusters. *A&A* 547, A16 (2012).

Maxwell, Wadsley, and Couchman. The Energetics of Cusp Destruction. *ApJ* 806, 229 (2015).

McConnachie, Babusiaux, Balogh, et al. A concise overview of the Maunakea Spectroscopic Explorer. *ArXiv e-prints* (2016).

Medezinski, Battaglia, Umetsu, et al. Planck Sunyaev-Zel'dovich cluster mass calibration using Hyper Suprime-Cam weak lensing. *PASJ* 70, S28 (2018).

Melchior, Gruen, McClintock, et al. Weak-lensing mass calibration of redMaPPer galaxy clusters in Dark Energy Survey Science Verification data. *MNRAS* 469, 4899–4920 (2017).

Mirabal, Charles, Ferrara, et al. 3FGL Demographics Outside the Galactic Plane using Supervised Machine Learning: Pulsar and Dark Matter Subhalo Interpretations. *ApJ* 825, 69 (2016).

Miyazaki, Oguri, Hamana, et al. A large sample of shear-selected clusters from the Hyper Suprime-Cam Subaru Strategic Program S16A Wide field mass maps. *PASJ* 70, S27 (2018).

Moliné, Schewtschenko, Palomares-Ruiz, Bœhm, and Baugh. Isotropic extragalactic flux from dark matter annihilations: lessons from interacting dark matter scenarios. *J. Cosmology Astropart. Phys.* 8, 069 (2016).

Moliné, Sánchez-Conde, Palomares-Ruiz, and Prada. Characterization of subhalo structural properties and implications for dark matter annihilation signals. *MNRAS* 466, 4974–4990 (2017).

Mollitor, Nezri, and Teyssier. Baryonic and dark matter distribution in cosmological simulations of spiral galaxies. *MNRAS* 447, 1353–1369 (2015).

Navarro, Frenk, and White. The Structure of Cold Dark Matter Halos. *ApJ* 462, 563 (1996).

Nezri, White, Combet, et al. γ -rays from annihilating dark matter in galaxy clusters: stacking versus single source analysis. *MNRAS* 425, 477–489 (2012).

Nichols, Mirabal, Agertz, Lockman, and Bland-Hawthorn. The Smith Cloud and its dark matter halo: survival of a Galactic disc passage. *MNRAS* 442, 2883–2891 (2014).

Nieto Castaño. The search for galactic dark matter clump candidates with Fermi and MAGIC. *International Cosmic Ray Conference* 5, 153 (2011).

Oguri, Lin, Lin, et al. An optically-selected cluster catalog at redshift $0.1 < z < 1.1$ from the Hyper Suprime-Cam Subaru Strategic Program S16A data. *ArXiv e-prints* (2017).

Pace and Strigari. Scaling Relations for Dark Matter Annihilation and Decay Profiles in Dwarf Spheroidal Galaxies. *ArXiv e-prints* (2018).

Padmanabhan and Finkbeiner. Detecting dark matter annihilation with CMB polarization: Signatures and experimental prospects. *Phys. Rev. D* 72(2), 023508 (2005).

Pieri, Lavalle, Bertone, and Branchini. Implications of high-resolution simulations on indirect dark matter searches. *Phys. Rev. D* 83(2), 023518 (2011).

Piffaretti, Arnaud, Pratt, Pointecouteau, and Melin. The MCXC: a meta-catalogue of x-ray detected clusters of galaxies. *A&A* 534, A109 (2011).

Pinzke, Pfrommer, and Bergström. Prospects of detecting gamma-ray emission from galaxy clusters: Cosmic rays and dark matter annihilations. *Phys. Rev. D* 84(12), 123509 (2011).

Planck Collaboration, Ade, Aghanim, et al. Planck 2015 results. XXVII. The second Planck catalogue of Sunyaev-Zeldovich sources. *A&A* 594, A27 (2016)a.

Planck Collaboration, Ade, Aghanim, et al. Planck 2015 results. XIII. Cosmological parameters. *A&A* 594, A13 (2016)b.

Planck Collaboration, Ade, Aghanim, et al. Planck 2015 results. XXIV. Cosmology from Sunyaev-Zeldovich cluster counts. *A&A* 594, A24 (2016)c.

Press and Schechter. Formation of Galaxies and Clusters of Galaxies by Self-Similar Gravitational Condensation. *ApJ* 187, 425–438 (1974).

Profumo. Dissecting cosmic-ray electron-positron data with Occam's razor: the role of known pulsars. *Central European Journal of Physics* 10, 1–31 (2012).

Putze and Derome. The Grenoble Analysis Toolkit (GreAT)-A statistical analysis framework. *Physics of the Dark Universe* 5, 29–34 (2014).

Quincy Adams, Bergstrom, and Spolyar. Improved Constraints on Dark Matter Annihilation to a Line using Fermi-LAT observations of Galaxy Clusters. *ArXiv e-prints* (2016).

Rodríguez-Puebla, Behroozi, Primack, et al. Halo and subhalo demographics with Planck cosmological parameters: Bolshoi-Planck and MultiDark-Planck simulations. *MNRAS* 462, 893–916 (2016).

Rykoff, Rozo, Busha, et al. redMaPPer. I. Algorithm and SDSS DR8 Catalog. *ApJ* 785, 104 (2014).

Rykoff, Rozo, Hollowood, et al. The RedMaPPer Galaxy Cluster Catalog From DES Science Verification Data. *ApJS* 224, 1 (2016).

Sánchez-Conde and Prada. The flattening of the concentration-mass relation towards low halo masses and its implications for the annihilation signal boost. *MNRAS* 442, 2271–2277 (2014).

Sanders, Evans, Geringer-Sameth, and Dehnen. Indirect dark matter detection for flattened dwarf galaxies. *Phys. Rev. D* 94(6), 063521 (2016).

Sawala, Frenk, Fattahi, et al. The APOSTLE simulations: solutions to the Local Group's cosmic puzzles. *MNRAS* 457, 1931–1943 (2016).

Schellenberger and Reiprich. HICOSMO: cosmology with a complete sample of galaxy clusters - II. Cosmological results. *MNRAS* 471, 1370–1389 (2017).

Schoonenberg, Gaskins, Bertone, and Diemand. Dark matter subhalos and unidentified sources in the Fermi 3FGL source catalog. *J. Cosmology Astropart. Phys.* 5, 028 (2016).

Sheth and Tormen. Large-scale bias and the peak background split. *MNRAS* 308, 119–126 (1999).

Shipp, Drlica-Wagner, Balbinot, et al. Stellar Streams Discovered in the Dark Energy Survey. *ArXiv e-prints* (2018).

Shirasaki, Macias, Horiuchi, Shirai, and Yoshida. Cosmological constraints on dark matter annihilation and decay: Cross-correlation analysis of the extragalactic γ -ray background and cosmic shear. *Phys. Rev. D* 94(6), 063522 (2016).

Silk and Bloemen. A γ-ray constraint on the nature of dark matter. *ApJ* 313, L47–L51 (1987).

Silk and Srednicki. Cosmic-ray antiprotons as a probe of a photino-dominated universe. *Physical Review Letters* 53, 624–627 (1984).

Simet, McClintock, Mandelbaum, et al. Weak lensing measurement of the mass-richness relation of SDSS redMaPPer clusters. *MNRAS* 466, 3103–3118 (2017).

Springel, Wang, Vogelsberger, et al. The Aquarius Project: the subhaloes of galactic haloes. *MNRAS* 391, 1685–1711 (2008).

Stecker. The cosmic γ-ray background from the annihilation of primordial stable neutral heavy leptons. *ApJ* 223, 1032–1036 (1978).

Takey, Durret, Mahmoud, and Ali. The 3XMM/SDSS Stripe 82 Galaxy Cluster Survey. I. Cluster catalogue and discovery of two merging cluster candidates. *A&A* 594, A32 (2016).

Tamura, Takato, Shimono, et al. Prime Focus Spectrograph (PFS) for the Subaru telescope: overview, recent progress, and future perspectives. Vol. 9908 of *Proc. SPIE* p. 99081M (2016).

The ANTARES Collaboration. Search of dark matter annihilation in the galactic centre using the ANTARES neutrino telescope. *J. Cosmology Astropart. Phys.* 10, 068 (2015).

The Dark Energy Survey Collaboration, Abbott, Abdalla, et al. Dark Energy Survey Year 1 Results: Measurement of the Baryon Acoustic Oscillation scale in the distribution of galaxies to redshift 1. *ArXiv e-prints* (2017).

The Fermi LAT Collaboration. Limits on dark matter annihilation signals from the Fermi LAT 4-year measurement of the isotropic gamma-ray background. *J. Cosmology Astropart. Phys.* 9, 008 (2015).

The LIGO Scientific Collaboration, the Virgo Collaboration, Abbott, et al. On the Progenitor of Binary Neutron Star Merger GW170817. *ArXiv e-prints* (2017).

Tinker, Kravtsov, Klypin, et al. Toward a Halo Mass Function for Precision Cosmology: The Limits of Universality. *ApJ* 688, 709-728 (2008).

Tinker, Robertson, Kravtsov, et al. The Large-scale Bias of Dark Matter Halos: Numerical Calibration and Model Tests. *ApJ* 724, 878–886 (2010).

Tulin and Yu. Dark Matter Self-interactions and Small Scale Structure. *ArXiv e-prints* (2017).

Tully. Galaxy Groups: A 2MASS Catalog. *AJ* 149, 171 (2015).

Ullio, Bergström, Edsjö, and Lacey. Cosmological dark matter annihilations into γ rays: A closer look. *Phys. Rev. D* 66(12), 123502 (2002).

Walker, Mateo, Olszewski, et al. A Universal Mass Profile for Dwarf Spheroidal Galaxies? *ApJ* 704, 1274–1287 (2009)a.

Walker, Mateo, Olszewski, Sen, and Woodroofe. Clean Kinematic Samples in Dwarf Spheroidals: An Algorithm for Evaluating Membership and Estimating Distribution Parameters When Contamination is Present. *AJ* 137, 3109–3138 (2009)b.

Walker, Combet, Hinton, Maurin, and Wilkinson. Dark Matter in the Classical Dwarf Spheroidal Galaxies: A Robust Constraint on the Astrophysical Factor for γ-Ray Flux Calculations. *ApJ* 733, L46 (2011).

Walker, Mateo, Olszewski, et al. Magellan/M2FS Spectroscopy of Tucana 2 and Grus 1. *ApJ* 819, 53 (2016).

Wechsler, Bullock, Primack, Kravtsov, and Dekel. Concentrations of Dark Halos from Their Assembly Histories. *ApJ* 568, 52–70 (2002).

Wen and Han. Calibration of the Optical Mass Proxy for Clusters of Galaxies and an Update of the WHL12 Cluster Catalog. *ApJ* 807, 178 (2015).

Wen, Han, and Liu. A Catalog of 132,684 Clusters of Galaxies Identified from Sloan Digital Sky Survey III. *ApJS* 199, 34 (2012).

Weniger. A tentative gamma-ray line from Dark Matter annihilation at the Fermi Large Area Telescope. *J. Cosmology Astropart. Phys.* 8, 007 (2012).

Wetzel, Hopkins, Kim, et al. Reconciling Dwarf Galaxies with ΛCDM Cosmology: Simulating a Realistic Population of Satellites around a Milky Way-mass Galaxy. *ApJ* 827, L23 (2016).

Xi, Wang, Liang, et al. Detection of gamma-ray emission from a galaxy cluster with Fermi Large Area Telescope. *ArXiv e-prints* (2017).

Zavala and Afshordi. Universal clustering of dark matter in phase space. *MNRAS* 457, 986–992 (2016).

Zechlin, Cuoco, Donato, Fornengo, and Vittino. Unveiling the Gamma-Ray Source Count Distribution Below the Fermi Detection Limit with Photon Statistics. *ApJS* 225, 18 (2016).

Zhao. Analytical models for galactic nuclei. *MNRAS* 278, 488–496 (1996).

Zhu, Marinacci, Maji, et al. Baryonic impact on the dark matter distribution in Milky Way-sized galaxies and their satellites. *MNRAS* 458, 1559–1580 (2016).

Zitzer. Search for Dark Matter from Dwarf Galaxies using VERITAS. *ArXiv e-prints* (2015).